

## Contents

	Page
<b>Full names and addresses of participating institutions.....</b>	<b>2</b>
<b>Names and e-mail addresses of central personnel.....</b>	<b>3</b>
<b>Preface, by Trond Iversen.....</b>	<b>5</b>
<b>Presentations.....</b>	<b>7</b>
Simulating the last 1000 years with a 3d coupled model, by U. Cubasch, E. Zorita, J. F. Gonzalez-Rouco, H. v. Storch, I. Fast.....	9
An empirically based method for projecting future local snow conditions: Preliminary results, by I. Hanssen-Bauer.....	27
Response in daily precipitation and wind speed extremes from HIRHAM downscaling of SRES B2 scenarios, by J. E. Haugen, T. Iversen .....	35
Technical documentation of the Oslo Regional Climate Model, Version 1.0, by J. Debernard, M. Ødegaard Køltzow.....	51
Simulations with a North Atlantic coupled ice-ocean model, by L. P. Røed, J. Debernard.....	69
Aspects of validation of a North Sea model, by B. Ådlandsvik.....	83
The effect of internal variability on anthropogenic climate projections, by A. Sorteberg, N. G. Kvamstø.....	95
Calculated feedback effects of climate change caused by anthropogenic aerosols, by T. Iversen, J. E. Kristjánsson, A. Kirkevåg, Ø. Seland .....	111

## **Full names and addresses of participating institutions**

met.no : Norwegian Meteorological Institute  
P.O. Box 43 Blindern  
N-0313 OSLO  
NORWAY

Gfi-UiB : Geophysical Institute  
University of Bergen  
Allégt. 70  
N-5007 BERGEN  
NORWAY

IfG-UiO : Department of Geosciences  
University of Oslo  
P.O. Box 1022 Blindern  
N-0315 OSLO  
NORWAY

IMR : Institute of Marine Research  
P.O. Box 1870 Nordnes  
N-5024 BERGEN  
NORWAY

NERSC : Nansen Environmental and Remote Sensing Center  
Edv. Griegsvei 3A  
N-5037 SOLHEIMSVIKEN  
NORWAY

### **For questions regarding the project, please contact:**

Magne Lystad  
Norwegian Meteorological Institute  
P.O. Box 43 Blindern  
N-0313 OSLO  
Phone: +47 22 96 33 23  
Fax: +47 22 69 63 55  
e-mail: [magne.lystad@met.no](mailto:magne.lystad@met.no)

## Names and e-mail addresses of central personnel in RegClim Phase III|

**Project management group:**

**E-mail address:**

**Leaders:**

Trond Iversen, IfG-UiO  
 Sigbjørn Grønås, Gfi-UiB  
 Eivind A. Martinsen, met.no

trond.iversen@geo.uio.no  
 sigbjorn@gfi.uib.no  
 eivind.martinsen@met.no

**Scientific secretary:**

Magne Lystad, met.no

magne.lystad@met.no

**Principal investigators:**

<b>PM1</b>	Eirik Førland	eirik.forland@met.no
<b>PM2</b>	Bjørn Ådlandsvik	bjorn@imr.no
<b>PM3</b>	Nils Gunnar Kvamstø	nilsg@gfi.uib.no
<b>PM4</b>	Jon Egill Kristjansson	j.e.kristjansson@geo.uio.no
<b>PM5</b>	Trond Iversen	trond.iversen@geo.uio.no

**Contact person at NERSC:**

Helge Drange

[helge.drange@nersc.no](mailto:helge.drange@nersc.no)



## Preface

This is number eight in the series of General Technical Reports from the RegClim project. The reports are now far less frequent than in earlier phases of the project, since papers now to a larger extent are directly submitted to the scientific literature than in the beginning when major model developing work took place.

There is still new development underway in RegClim, and not all manuscripts are in the shape for submission, even though they contain work that deserves to be reported. Some of these are therefore contained in the present GTR 8. Several of the papers are intended to be further elaborated and submitted for publication.

A very important address for these RegClim-papers is Co-ordinating Lead Authors of the upcoming 4<sup>th</sup> assessment report of IPCC (AR4). The report will be provided to selected CLAs of the IPCC AR4. They should also be aware that there are considerable published and unpublished results from RegClim that is not included in the present GTR8 that will be provided to IPCC in several ways. The Bjerknes Centre is compiling full scenario runs with their fully coupled Bergen Climate Model, partly as part of RegClim. Furthermore, RegClim staff is participating on the analysis of model-generated data provided to IPCC. Finally, important aspects of aerosol-climate interactions are partly produced by RegClim as a part of the Aerocom intercomparison project.

The work presented in this GTR8 has been presented and discussed during two all-staff meetings in RegClim (May and November 2004). GTR8 also includes a paper kindly submitted by the project's advisor, Professor Ulrich Cubasch of the Free University of Berlin. That interesting paper was presented in the meeting in May 2004.

Oslo 4. March 2005

Trond Iversen  
Project Leader



## **Presentations**



# **Simulating the last 1000 years with a 3d coupled model**

**by**

**Ulrich Cubasch++, Eduardo Zorita\*, Jesus F. Gonzalez-Rouco+, Hans v.  
Storch\* and Irina Fast++**

\* GKSS Research Centre, 21502 Geesthacht, Germany

+Dept de Astrofisica y Fisica de la Atmosfera, Universidad Complutense de Madrid, 28040  
Madrid, Spain

++Metereologisches Institut, Freie Universität Berlin, Carl-Heinrich-Becker-Weg 6-10, 12165  
Berlin, Germany

## **Abstract**

A simulation of the climate of the last millennium with a state-of-the art ocean-atmosphere climate model, which has been forced with solar variability, volcanism and the change in anthropogenic greenhouse gases, shows global temperatures during the Little Ice Age of the order of 1 K colder than present. This is markedly colder than some accepted empirical reconstructions from proxy data. In this simulation temperature minima are reached in the Late Maunder Minimum, (around 1700 A.D.) and the Dalton Minimum (1820 A.D.), with global temperature about 1.2 K colder than today. The model also produces a Medieval Warm Period around 1100 A.D., with global temperatures approximately equal to present values. A combination of model and tree-ring data leads to an improved temperature estimate for Northern Europe, but not for Southern Europe.

## 1. Introduction

A number of reconstructions of the climate of the past 500 - 1000 years have been published, which rely on data from various sources (tree rings, documentary evidence, ice cores, coral data, varved lake sediments, borehole data, etc.) as proxies using (multivariate) statistical calibration methods (Overpeck et al, 1997, Mann et al, 1998, 1999, 2000, Jones et al, 2001, Crowley and Lowery, 2000; Briffa et al, 2001, 2002, Esper et al, 2002; Luterbacher et al, 2002a,b, Mann and Jones, 2003; Luterbacher et al, 2004). More recently, the historic climate has been simulated in climate experiments using models of different complexity (Crowley, 2000; Bauer et al., 2003; Zorita et al., 2003), which are forced with the historical variations of solar flux, volcanism and greenhouse gases (Crowley, 2000, Solanki and Krivova, 2003, Etheridge et al, 1996, Blunier et al, 1995).

Nonclimatic “noise”, potential nonlinearity and nonstationarity of proxy/climate relationships as well as seasonal biases, that are characteristic for proxy data (Jones and Mann, 2004), result in relatively large uncertainties of proxy-based climate reconstructions. Moreover currently available proxy data are regionally limited and the spatial coverage becomes increasingly sparse in more distant past.

The model data, on the other hand, have a global coverage, however, they depend on the quality of the model employed and on the prescribed external forcing, which, except for the last 30 years, is based on proxy data as well.

In the current paper a complex 3d coupled ocean-atmosphere model is employed to simulate the historic climate. After a description of the model and the experimental set-up (chapter 2), the model results are analyzed and compared to observations (chapter 3). In chapter 4 a method to combine proxy data and model data and its application to data from the European region is introduced, followed by a summary (chapter 5).

## 2. The model and the experimental set-up

The climate model consists of the atmospheric model ECHAM4 with a horizontal resolution of 3.75 x 3.75 degrees and 19 vertical levels, 5 of them located in the stratosphere, coupled to the ocean model HOPE-G with a horizontal resolution of approx. 2.8x2.8 degrees with equator refinement and 20 vertical levels. The ocean and atmosphere models are coupled through flux adjustment to avoid climate drift in long climate simulations. This coupled model has been developed at the Max-Planck-Institute of Meteorology and it has been used in many studies of climate variability and climate change (Grötzner et al, 1998)

The model was driven by estimations of past variations of the solar constant, volcanic activity and concentrations of greenhouse gases (derived from air bubbles trapped in polar ice cores (Etheridge et al, 1996, Blunier et al, 1995)). Annual values of net radiative forcing due to solar variability and volcanic activity were estimated by Crowley (2000) from concentrations of  $^{10}\text{Be}$  (a cosmogenic isotope), from historical observations of sun spots and acidity measurements in ice cores. In this simulation, they were translated to variations in an effective solar constant communicated to the climate model, represented by a global annual number, equally distributed over the solar spectrum, with no seasonal or geographical dependence. In the last two centuries the solar component is very close to the Lean data (Lean et al, 1995). Changes in tropospheric sulphate aerosols and ozone concentrations have not been included.

Two experiments have been run: a first one starting in the year 1550 (“Columbus”) and a second one starting in the year 1000 (“Erik”).

### **3. The modelling results**

#### *The near-surface temperature*

The external climate forcing and the simulated global annual near-surface air temperature (SAT), is represented in figure 1. The model simulates a temperature maximum around 1100 A.D., the Medieval Warm Period (MWP) (Jones et al, 2001), with temperatures very similar to the ones simulated for the present period. The existence of the MWP has been recently a matter of considerable debate, since proxy data have not yielded a consistent picture of its existence (Bradley et al, 2001, Broecker et al, 2001). In this simulation the MWP was a global phenomenon, probably caused by the maximum in solar activity in the 12th century. From 1300 A.D. global temperatures decrease and the simulation enters the so called Little Ice Age (LIA) lasting until about 1850 A.D (Jones et al, 2001). Temperatures in the LIA were about 1 K colder than today's values, the cooling peaking in the Late Maunder Minimum (Eady, 1976) (around 1700 A.D.) and the Dalton Minimum (Jones et al, 2001) (around 1820 A.D.), when simulated temperatures are about 0.25 K colder than the LIA mean. Subsequently, global temperatures start increasing almost continuously into the 20<sup>th</sup> century until the end of the simulation. The simulated secular warming trend in the 20<sup>th</sup> century is approached, but not surpassed, by warming trends around 1100 A.D. and in the 18<sup>th</sup> century. The shorter simulation of the last 500 years with a slightly different model version yields similar results.

The simulated temperature evolution is at variance with the most accepted empirical reconstruction (Mann et al, 1999). The empirical reconstructions based on different proxy data have targeted different temperatures, depending on the sensitivity of the proxies used. Thus, the multi-proxy approach of Mann et al (1999), hereafter MBH99, represents a reconstruction of the annual Northern Hemisphere (NH) temperature, whereas the reconstruction by Esper et al. (2002), based on extratropical dendrochronological data, is probably more strongly biased towards the NH extratropical summer temperatures. Instead of re-scaling the reconstruction to a common framework (Briffa and Osborn, 2002), figure 2 shows these two not re-scaled reconstructions, together with the simulated NH annual temperature and the NH extratropical summer temperature. The discrepancies between reconstructions and simulations remain large, although up to 1600 A.D. the simulated values lie within the  $2\sigma$  errors of MBH99. The NH ECHO-G and MBH99 temperatures are reasonably correlated in the period 1000-1990 A.D., even when the long-term linear trends before and after 1900 A.D. are considered ( $r=0.25$  at interannual timescales , 0.37 at decadal and longer timescales), but the amplitude of the variations is clearly different.

The ECHO simulations show a good agreement with a similar simulation of the last 500 hundred years, independently performed at the Hadley Center for Climate Research (Widmann and Tett, 2004). The latter model is not flux-adjusted, indicating that flux adjustment does not greatly distort the variability at long-time scales.

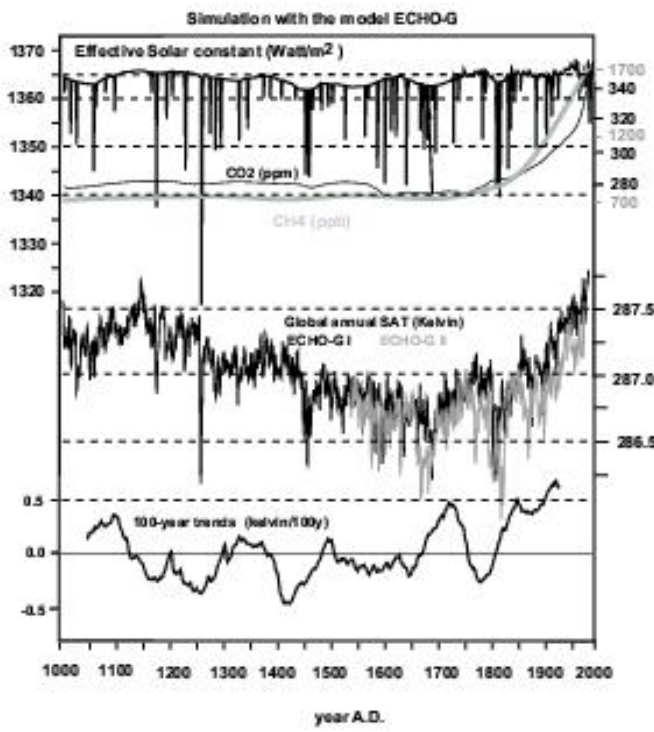


**Figure 1:** External forcing (effective solar constant and greenhouse gas concentration used to drive the climate model ECHO-G; the simulated global annual surface air temperature (SAT) for two ECHO-G simulations and the running 100-year SAT trends for the 1000-year simulation. The spikes in the effective solar constant represent the effect of volcanic aerosols on the radiative forcing. In 1258-9 A.D. an eruption of unknown location, recorded in the acidity measurements of ice cores, causes a temperature drop of about 1K.

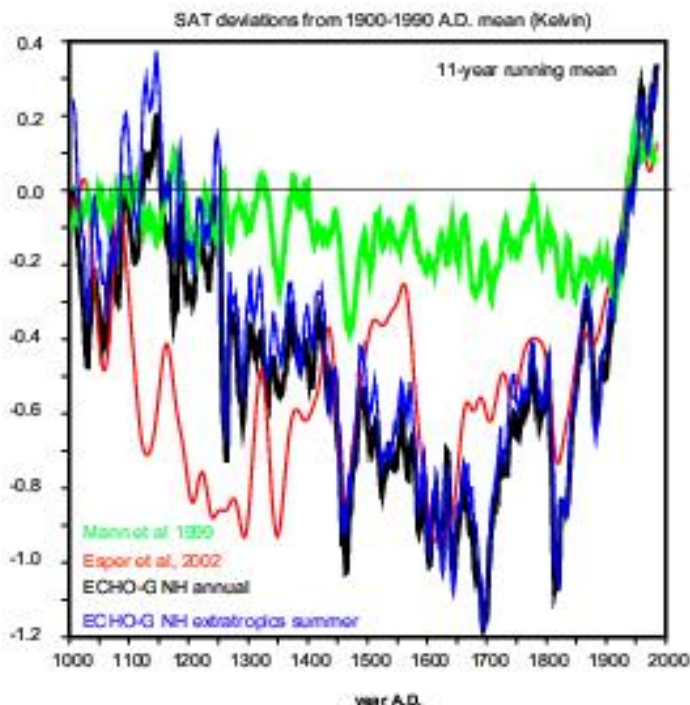


**Figure 2:** Simulated annual and summer extratropical North Hemisphere SAT deviations compared to two empirical reconstructions in the last millennium by Mann et al (2000) and Esper et al (2002).

An assessment about the consistency of the model simulations and empirical reconstructions can be achieved by analysing the temperature evolutions in the 20<sup>th</sup> century, specially in the second half, when a global and complete climate data set of pseudo-observations- the National Centre for Environmental Prediction (NCEP) reanalysis (Kalnay, 1996) is available and solar output underwent strong variability (Lean et al, 1995). The analysis focuses on the NH temperature, which is arguably more reliable than the global mean. Figure 3a shows the NH annual SAT from the NCEP reanalysis together with the evolution of the solar constant. The correspondence between both in the period 1948-1990 A.D. strongly suggests that the solar forcing contributed to a large extent to the North Hemisphere cooling between 1950 A.D. and 1975 A.D. , the subsequent rapid warming (1975-1980 A.D.) and cooling (1980-1990) A.D.), a relationship also previously suggested from sea-surface-temperature data (White et al, 1997).

In the last decade greenhouse warming becomes dominant. The comparison with the Jones et al. (1999) instrumental data set leads to a similar conclusion (figure 3a). It is noted that ensemble simulations with the Hadley Centre model driven only by anthropogenic forcing deviate considerably from observations in this period (Stott et al, 2000).

The inclusion of the effect of volcanic activity would not have changed the overall picture, since in this period volcanic activity, as reflected in ice-core acidity measurements, was regularly distributed over time. The ECHO-G NH temperatures are depicted in Figure 3b. Both show a similar evolution, ruling out internal variability as cause for this behaviour, and suggesting that the model is able to simulate reasonably the effects of a varying solar output. The solar signal in the NH NCEP temperature at 30 mb height (not shown) is not as clear and agrees better than in the simulations, but figure 3b also suggests that a complex stratosphere model may not always be required (Haig, 1996), at least to simulate the NH temperature. Finally, figure 4c shows the MBH99 NH temperature, which in this period displays the smallest variability range.

### ***Climate sensitivity***

One can try to check the consistency of the different SAT data sets through a rough estimation of the sensitivity of the NH temperature to variations of the solar constant, although the climate sensitivity may be depend on the previous pathway and mean state of the climate (Senior et al, 2000; Meehl et al, 2002). By linearly detrending the temperature and solar

constant in the 20th century, the presumably linear warming due to anthropogenic greenhouse gases and the linear increase in the solar constant may be filtered out. The correlation between detrended temperature and detrended solar constant should reflect the sensitivity of temperature to decadal variations of the solar constant, such as the ones of figure 3a. This correlation is represented in figure 4 for the NCEP reanalysis, the Jones et al. instrumental data, the longer ECHO-G simulation and the MBH99 reconstruction. The 20th century regression slopes yield a sensitivity of  $0.13 \text{ K/(W/m}^2\text{)}$  for the NCEP and Jones et al. instrumental data set,  $0.11 \text{ K/(W/m}^2\text{)}$  for ECHO-G temperature, and  $0.08 \text{ K/(W/m}^2\text{)}$  for the MBH99 reconstruction. Previous estimations based on empirical reconstructions yielded a close value of  $0.12 \text{ K/(W/m}^2\text{)}$  (Lean and Rind, 1999). A value of  $0.13 \text{ K/W/m}^2$  corresponds to a sensitivity to net radiative forcing of about  $0.75 \text{ K/W/m}^2$ , assuming a fixed NH reflectivity of 30%, which is closed to the assumed sensitivity to changes in greenhouse gas forcing (IPCC, 2001) and model simulations driven by solar changes (Cubasch et al, 1997). This sensitivity would explain about 0.2K of the NH warming in 1970-1999, approximately one third of the observed NH warming. This is close to a value of 40% estimated from simulations with other models driven by solar forcing alone (Cubasch et al, 1997)

The same sensitivity analysis has been carried out for the ECHO-G simulation and the MBH99 reconstruction in the period 1600-1900 A.D. In this period, greenhouse gases variations should have played a minor role, so that no other external trends are to be expected. This analysis yields a sensitivity of  $0.16 \text{ K/(W/m}^2\text{)}$  for ECHO-G and  $0.02 \text{ K/(W/m}^2\text{)}$  for MBH99. The data from this period are also depicted in figure 4. The sensitivity of the ECHO-G model seems to have been larger in the previous centuries.

Uncertainties in this rough estimate, the different pathway and mean climate in

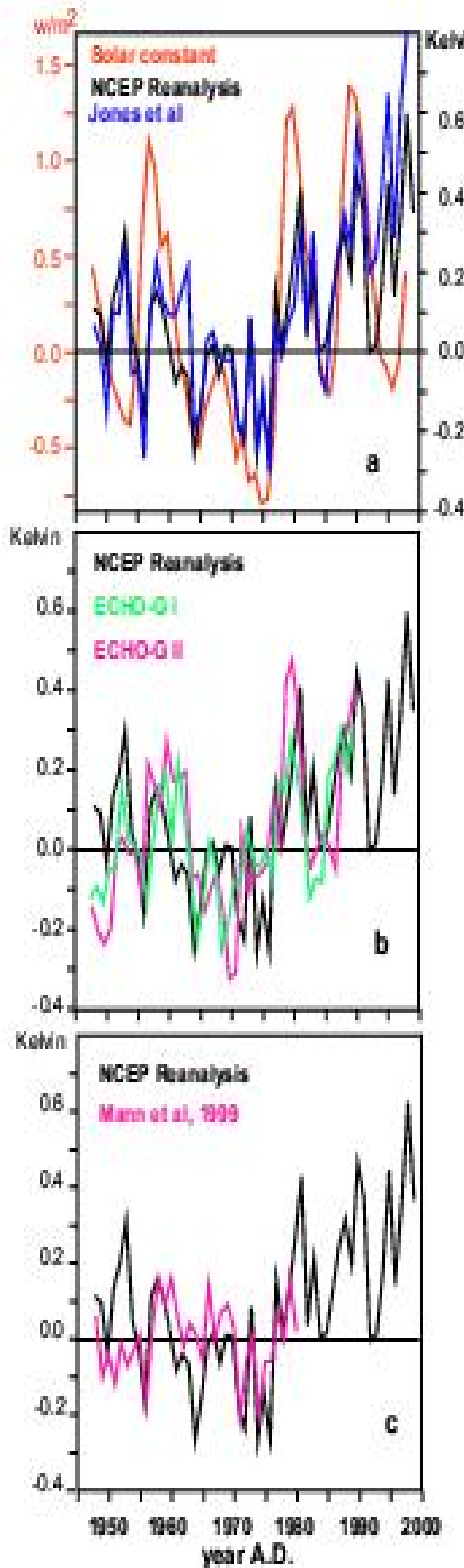


**Figure 3:** Comparison of different North Hemisphere surface temperature average in the period 1900-1999 from the NCEP Reanalysis, the ECHO-G simulations, the Jones et al. (2001) instrumental data set and the MBH99 reconstructions. The evolution of the solar constant as used in the ECHO simulations (derived from the Crowley (2000)) is also included in the upper-left panel. Data are deviations from the 1948-1980 mean.

the LIA (Senior et al, 2000; Mehl et al, 2002), or the presence of stronger volcanic activity could contribute to explain this change. However, the sensitivity derived from the MBH99 reconstruction in the previous centuries is a factor 4 smaller than in the 20th century, possibly indicating that the reconstructions of the solar constant and the empirical temperature reconstructions in the previous centuries are not consistent with their behaviour in the 20th century.

## 4. Synthesis of model and proxy data

As the proxy data become more and more sparse the further one goes back into the past (figure 5), one can try to substitute the missing proxy information by model data. An approach for combining tree-ring data from Europe and the historical climate model simulations is presented in the next chapter.

### 4.1 Methodology and data

The main idea of the approach is the application of statistical climate field reconstruction methods to a *composed* network of proxy and model derived *pseudo-proxy* data (figure 6). Different options are open with regard to the processing and geographical location of pseudo-proxy data, as well as weighting of proxy and pseudo-proxy data.

Following dataset were used to reconstruct the climate over Europe:

- (1) The instrumental dataset CRUTEM2v of gridded monthly mean surface air temperature anomalies relative to the 1961-1990 period (Jones et al, 1999, Jones and Moberg, 2003). The data are available on a  $5^\circ \times 5^\circ$  grid from 1851, although with some notable gaps. 66 grid boxes form the reconstruction area (figure 5a). This compilation of instrumental measurements was chosen to allow for a consistency with other existing temperature reconstructions (e.g. Mann et al, 1998, Briffa et al, 2002).

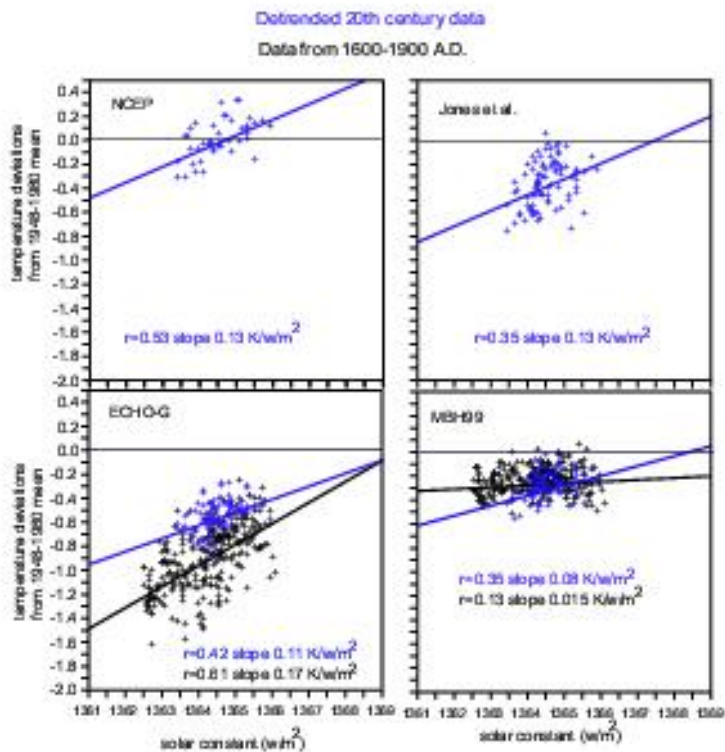


**Figure 4:** Scatter diagrams of annual solar constant, derived from Crowley (2000), and the North Hemisphere annual temperature deviations from the 1948-1990 mean for the NCEP data set, the Jones et al. (1999) instrumental data, the ECHO-G simulations and the MBH99 reconstruction. Black dots include data from the period 1600-1900 A.D, blue dots include linearly detrended data from 1900-1990 A.D. The correlation coefficients and the regression slopes are indicated.

- (2) Gridded measurements of the tree ring density (MLD = Maximum Latewood Density) from the „Schweingruber”-network (Briffa et al, 2001, 2002). The spatial distribution of time-varying data is shown in figure 5a, the temporal changes of availability are presented in figure 5b. In the period of maximal data density (1858-1976) 34 grid boxes of the area are covered with proxy data. Only 7 of these proxy time series are starting at around 1400. An adjustment procedure was applied to the tree-ring data to restore the low-frequency climate variability removed during the standardization.
- (3) Temperature fields from above described historical climate model simulations “Columbus” and “Erik”.

For calibration of proxy networks against instrumental data a partial-least square (PLS)-regression approach (Martens and Nes, 1989) was used. The method is based on the

simultaneous decomposition of predictors and predictands in order to extract components, which explain as much as possible covariance between them. The first few of the extracted components (also called latent vectors) are used in the regression equations instead of the full set of predictors and predictands.

Following to the results of Briffa et al. (2002) MLD network was calibrated against the mean April-September instrumental temperature anomalies. The temporal calibration is based on data from time interval 1897-1976 (calibration period), which is characterized through a better spatial coverage with the measurements. The first 46 years of the instrumental period (1851-1897) have been reserved to validate the derived statistical relationships with independent data.

Monthly averaged simulated temperature fields from “Columbus” and “Erik” runs were interpolated to the observational grid to construct the appropriate pseudo-proxy data from model output. Thereafter the April-September mean temperature anomalies relative to the simulated 1961-1990 means were calculated. Finally the model data were sub-sampled to mimic the time-varying spatial distribution of tree-ring data and averaged across the both simulations.

To take into account a somewhat different nature of proxy and pseudo-proxy data, the PLS-regression was extended to the so-called tri-PLS Regression (Bro, 1998). For this purpose proxies and model derived pseudo-proxies were arranged in a 3-dimensional data matrix.

Prior to the analysis, predictors and predictands were column-wise standardized using corresponding calibration period mean and standard deviation. Due to the changing number of proxy data series during the considered time span the calibration procedure had to be performed several times. In all calibration models the first 4 latent vectors have been retained, which explain 32 to 52% (depending on the number of available proxies) of the interannual temperature variations during the calibration period.

To assess the reconstructive skill of derived statistical models two following statistics were used (*Cook and Kairiukstis, 1990*):

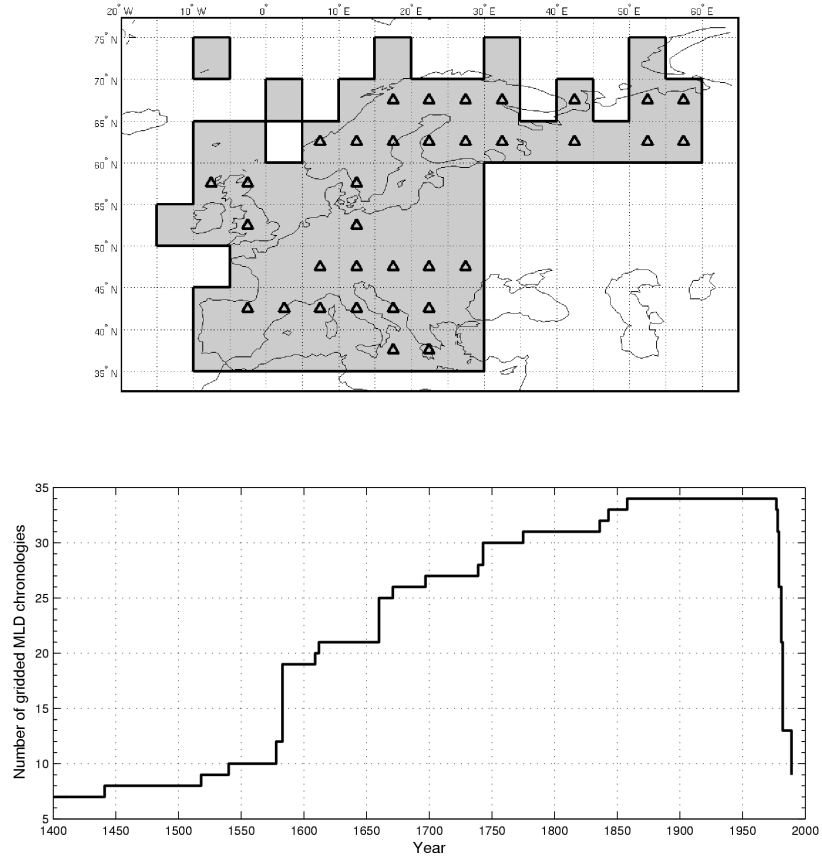


**Figure 5:** (a) European reconstruction domain (shaded) and location of gridded tree-ring data (triangles, maximal coverage); (b) temporal changes of the number of available tree-ring data.

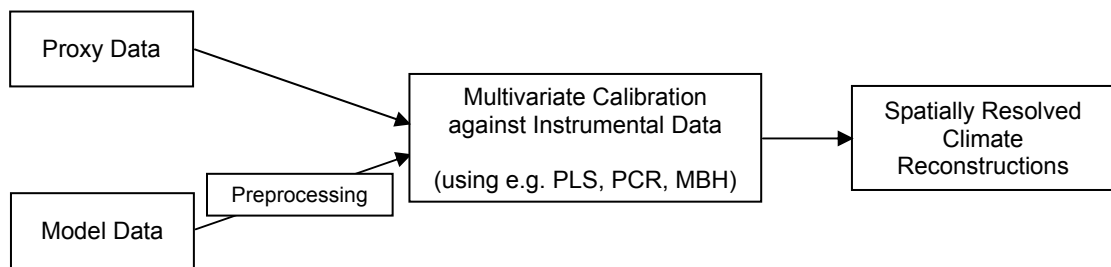


**Figure 6:** Schematic illustration of approach aimed to combine proxy and model information to reconstruct climate variability

(1) Reduction of error (RE), defined as

$$RE = 1 - \sum_{i=1}^n (obs_i - rec_i)^2 \left/ \sum_{i=1}^n (obs_i - \overline{obs}^{cal})^2 \right. ;$$

(2) Coefficient of efficiency (CE), defined as

$$CE = 1 - \sum_{i=1}^n (obs_i - rec_i)^2 \left/ \sum_{i=1}^n (obs_i - \overline{obs}^{val})^2 \right. ,$$

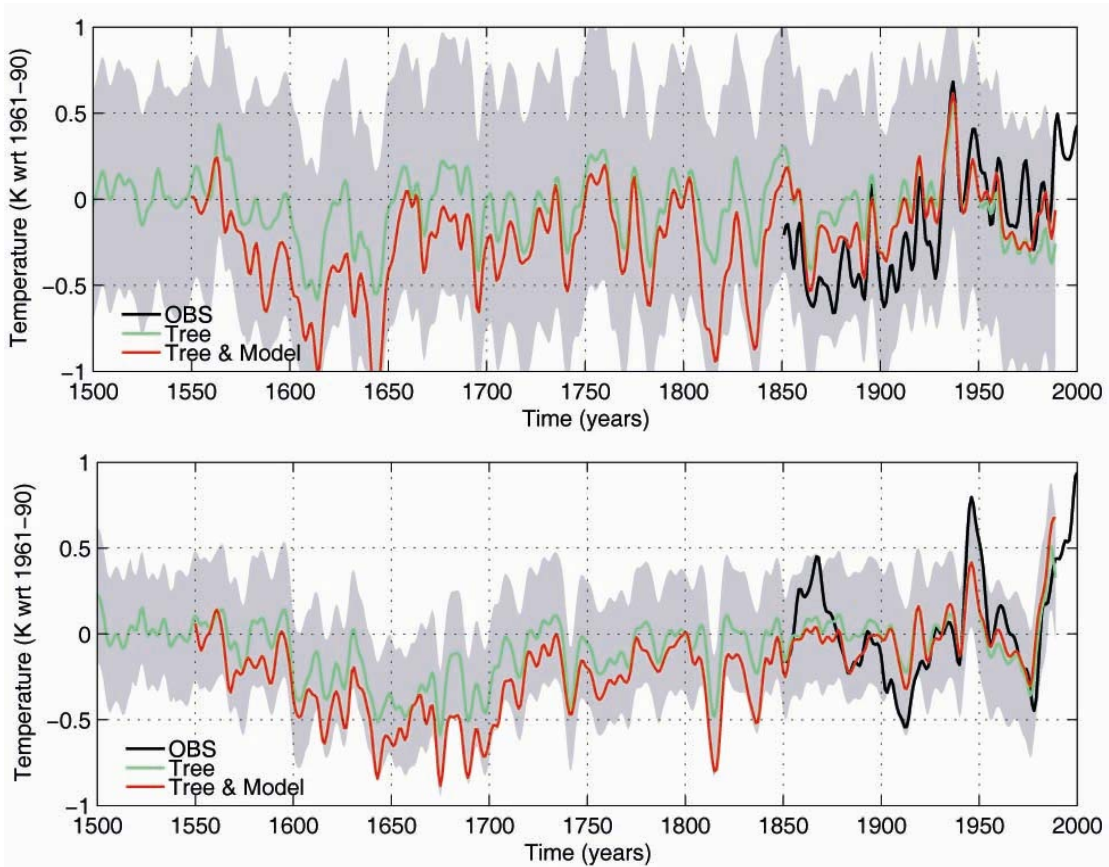
where  $rec_i$  are the reconstructed values,  $obs_i$  are the instrumental measurements and  $\overline{obs}$  is the mean over calibration (validation) period.  $RE = 0$  ( $CE = 0$ ) defines the performance of a simple “climatologic” model, in which a whole series is assigned to its calibration (validation) period mean temperatures. Negative values indicate a unusable reconstruction.

We calculated this statistics for each grid box as well as for 3 regional averaged series: Europe (whole reconstruction area), Northern Europe (north of 53°N) and Southern Europe (south of 53°N).

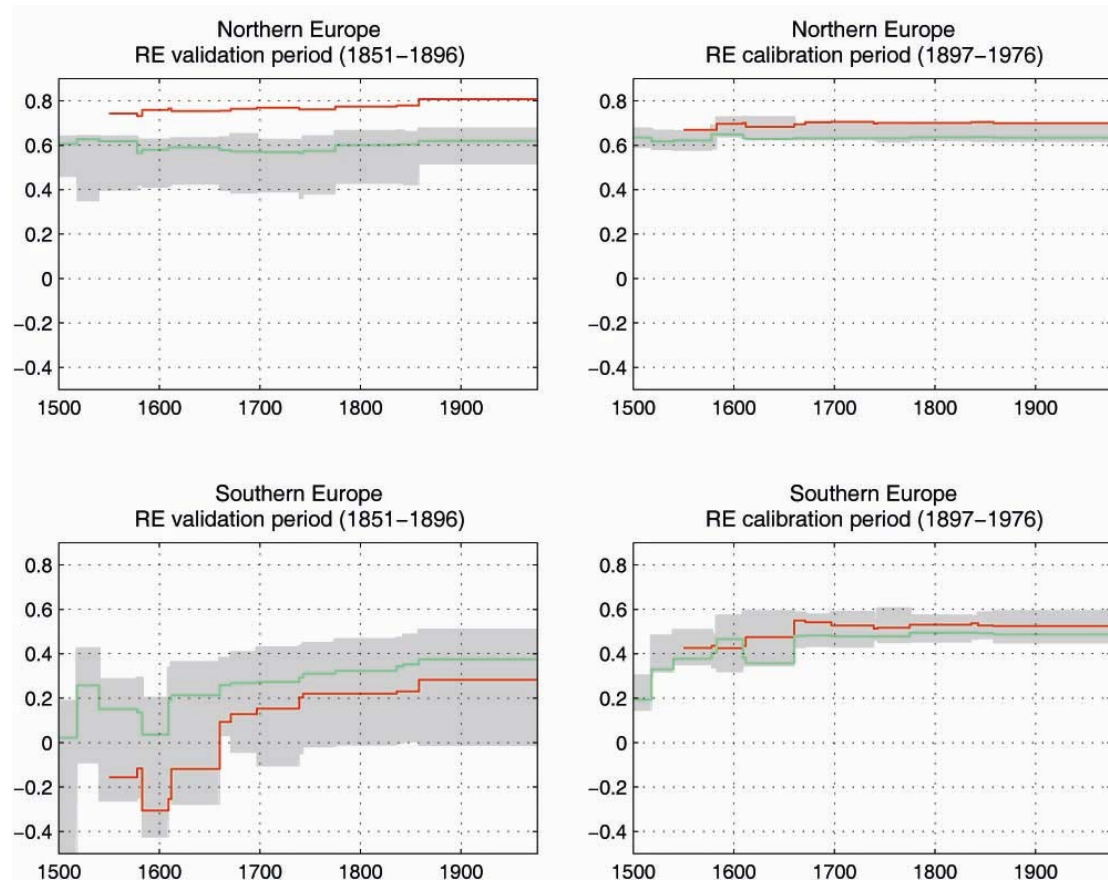
## 4.2 Result

Figure 7 shows regionally averaged reconstructed temperatures anomalies for pure tree-ring based reconstruction (TR) and for joint tree-ring and model reconstruction (TRM). In the Northern Europe one can see an improvement, which is also reflected in the objective reconstruction skill score (RE) (figure 8). In the Southern Europe the model information rather leads to a degradation of reconstructive skill. The distinct difference in the behaviour of southern and northern Europe might indicate a systematic problem either in the tree-rings (are trees responding different to the climate change in different latitudes) or model problems, mainly orography.

A challenging issue is an assessment of the added value of model information comparing to the pure proxy-based reconstruction. This can be addressed via comparison with independent climate reconstructions, which rely on not used proxy data. Another possibility constitutes a form of Monte-Carlo simulation. In order to



**Figure 7:** Reconstructed (TR: green, TRM: red) and instrumental (black) mean April-September temperature anomalies (wrt 1961-1990 mean) for Northern Europe (top) and Southern Europe (bottom) over the last 500 years. The uncertainty range of the tree-ring based reconstruction (estimated as doubled standard error for validation period) is shaded.



**Figure 8:** Reduction of error (RE) for Northern Europe (top) and Southern Europe (bottom) averaged temperature anomalies for pure tree-ring based reconstruction (green), and for tree-ring and model based reconstruction (red). The shaded uncertainty range is estimated by means of Monte-Carlo simulations, which use pseudo-proxies derived from an externally unforced climate simulation.

construct ranges of “by chance changes” a large number of “random” pseudo-proxy time series can be generated from an unforced control model simulation (e.g. by shifting the begin of time series and appending of the cut-off segment at the end or by permutation of years) and used in the above described calibration procedure.

In the case of the improvement of proxy-based reconstruction by model information, which lies beyond the uncertainty ranges from Monte-Carlo simulations, one gains confidence in the consistency of model, proxy and instrumental data.

## 5. Summary

The discrepancies between model simulation and empirical reconstructions are discussed in terms of the climate sensitivity to changes in the solar constant. We find that whereas the model response to changes is roughly constant along the simulation and agrees with the sensitivity derived from instrumental data, the empirical reconstructions show a lower sensitivity in the 20th century, and a much lower one in the past centuries, thus pointing to potential inconsistencies between the reconstructed temperature and solar constant.

It has been tried to use the model data to fill gaps in the proxy-data records. This produces an improved temperature curve for northern Europe. Problems, however arise in southern Europe.

## Acknowledgements

The authors thank S. Legutke and U. Schlese for providing the model and their support in running the simulations. The use of Crowley's, Jones et al. data and data from the NCEP is greatly acknowledged. This work was performed in the frame of the German programme DEKLIM , project REN2000-0786CLI from the Spanish CICYT and the EU project SOAP. Dennis Bray provided editorial assistance.

## References

- Bauer, E., Claussen, M., Brovkin, V. & Huenerbein, A. Assessing climate forcings of the earth system for the past millennium, *Geophys. Res. Lett.* 30 (6), doi: 10.1029/2002GL016639, (2003).
- Blunier , T., Chappellaz, J.A., Schwander, J. , Stauffer, B. & Raynaud, D. Variations in atmospheric methane concentration during the Holocene epoch. *Nature* 374, 46-49 (1995)
- Bradley, S., Briffa, R.K, Crowley,T.J., Hughes, M.K., Jones,, P.D. & Mann M.E. The scope of Medieval warming *Science* 292, 2011-2012 (2001).
- Briffa, K.R. & Osborn, T.J. Blowing hot and cold. *Science* 295, 2227-2228 (2002).

- Briffa, K.R., Osborn, T.J., Schweingruber, F.H., Harris,I.C., Jones, P.D., Shiyatov, S.G. & Vaganov, E.A. Low-frequency temperature variations from a northern tree ring density network. *J. Geophys. Res.* **106**, 2929–2941 (2001).
- Briffa, K.R., Osborn, T.J., Schweingruber, F.H., Jones, P.D., Shiyatov, S.G. & Vaganov, E.A. Tree-ring width and density data around the Northern Hemisphere: Part 1, local and regional climate signals. *The Holocene* **12**(6), 737-757 (2002).
- Bro, R. Multi-way analysis in the food industry: Models, algorithms, and applications. PhD thesis, Royal Veterinary and Agricultural University, Denmark (1998).
- Broecker, W.S. Was the Medieval Warm Period Global?. *Science* **291**, 1497-1499 (2001).
- Cook, E.R. & Kairiukstis, L.A. (eds.) (1990), Methods of Dendrochronology: Applications in the Environmental Sciences, Kluwer Acad., Norwell, Mass.
- Crowley, T.J . Causes of climate change over the past 1000 years. *Science* **289**, 270-277 (2000).
- Crowley, T. J. & Lowery, T.S. How warm was the Medieval Warm Period? A comment on 'Man-made versus natural climate change' *Ambio* **39**, 51–54 (2000).
- Cubasch , U. , Hegerl ,G.C., Voss, R., Waszkewitz, J. & Crowley, T.C. Simulation with an O-AGCM of the influence of variations of the solar constant on the global climate. *Clim. Dyn.* **13**, 757-767 (1997).
- Eady, J.A. The Maunder Minimum. *Science* **192**, 1189-1202 (1976).
- Etheridge, D. , Steele, L.P., Langenfelds, R.L., Francey, R.J., Barnola, J.M. & Morgan V.I. Natural and anthropogenic changes in atmospheric CO<sub>2</sub> over the last 1000 years from air in Antarctic ice and firn. *J. Geophys. Res.* **101**, 4115-4128 (1996).
- Esper, J., Cook, E.R. & Schweingruber, F.H. Low-frequency signals in long tree-ring chronologies for reconstructing past temperature variability. *Science* **295**, 2250-2253 (2002) .
- Goertzner, A., Latif, M., Barnett, T.P.A decadal climate cycle in the North Atlantic Ocean as simulated by the ECHO coupled. *J. Clim.* **11**, 831-847 (1998).
- Haig, D.H. The impact of solar variability on climate. *Science* **272**, 981-984 (1996).
- IPCC 2001. Houghton J.T. *et al.* (eds) *Climate Change 2001: The scientific basis* Cambridge Univ. Press, Cambridge (2001).
- Jones, P.D. & Mann, M.E. Climate over past millennia. *Reviews of Geophysics*, **42**, doi:10.1029/2003RG000143 (2004).
- Jones, P.D. & Moberg, A. Hemispheric and large-scale surface air temperature variations: An extensive revision and an update to 2001. *J. Clim.* **16**, 206–223 (2003).
- Jones, P.D., New, M., Parker, D.E., Martin, S. & Rigor I.G. Surface air temperature and its changes over the past 150 years. *Rev. Geophys.* **37**, 173-199 (1999).
- Jones, P.D., Osborn, T.J. & Briffa, K.R. The evolution of climate over the last millennium. *Science* **292**, 662-667 (2001).
- Kalnay, E. et al. The NCEP/NCAR 40-year Reanalysis Project. *Bull. Amer. Meteor. Soc.* **77**, 437-471 (1996).
- Lean ,J. , Beer, J. & Bradley, R. Reconstructions of solar irradiance since 1610- implications for climate change. *Geophys. Res. Lett.* **22**, 3195-3198 (1995).

- Lean ,J. , Beer, J. & Bradley, R. Reconstructions of solar irradiance since 1610- implications for climate change. *Geophys. Res. Lett.* **22**, 3195-3198 (1995).
- Lean, J. & Rind, D. Evaluating sun-climate relationships since the Little Ice Age. *J. Atmos. Sol.-Terr. Phys.* **61**, 25-36 (1999).
- Mann, M.E. & Jones, P.D. Global surface temperatures over the past two millennia *Geophys. Res. Lett.* **30(15)** CLM 5-1 - 5-4 (2003).
- Mann, M.E., Bradley, R.S., & Hughes, M.K. Global-scale temperature patterns and climate forcing over the past six centuries. *Nature* **392**, 779-787 (1998).
- Mann, M.E., Bradley, R.S., & Hughes, M.K. Northern Hemisphere Temperatures During the Past Millennium: Inferences, Uncertainties, and Limitations. *Geophys. Res. Lett.*, **26**, 759-762 (1999).
- Mann, M. E., Gille, E., Overpeck, J., Gross, W., Bradley, R.S., Keimig, F.T & Hughes, M.K. Global temperature patterns in past centuries: An interactive presentation, *Earth Interact.*, **4** (2000). (Available at <http://EarthInteractions.org>)
- Luterbacher, J. et al. Extending North Atlantic Oscillation reconstructions back to 1500. *Atmos. Sci. Lett.* **2**, 114–124 (2002a).
- Luterbacher, J., Xoplaki, E., Dietrich, D., Rickli, R., Jacobbeit, J., Beck, C., Gyalistras, D., Schmutz, C. & Wanner, H. Reconstruction of sea level pressure fields over the eastern North Atlantic and Europe back to 1500. *Clim. Dyn.* **18**, 545–561 (2002b).
- Luterbacher, J., Dietrich, D., Xoplaki, E., Grosjean, M. & Wanner, H. European seasonal and annual temperature variability, trends and extremes since 1500, *Science* **303**, 1499-1503 (2004).
- Martens, H. & Nes, T. Multivariate Calibration, John Wiley, Chichester (1989).
- Meehl, G., Washington ,W.M., Wigley, T.M.L., Alabaster,, J. & Dai A. Solar and greenhouse gas forcing and climate response in the twentieth century. *J. Climate* **16**, 426-443 (2002).
- Overpeck, J., Hughen, K., Hardy, D., Bradley, R., Case, R., Douglas, M., Finney, B., Gajewski, K., Jacoby, G., Jennings, A., Lamoureux, S., Lasca, A., MacDonald, G., Moore, J., Retelle, M., Smith, S., Wolfe, A. & Zielinski, G. Arctic environmental change of the last four centuries, *Science* **278**, 1251–1256 (1997).
- Senior, C.A. & Mitchell, J.F.B. The time-dependence of climate sensitivity. *Geophys. Res. Lett.* **27**, 2685 - 2688 (2000).
- Solanki, S. K & Krivova, N.A. Can solar variability explain global warming since 1970?, *J. Geophys. Res.* **108(A5)**, 1200 (2003).
- Stott, P. A. , Tett, S.F. B, Jones, G.S., Allen, M.R., Mitchell, J.F.B. & Jenkins, G.J . External control of 20th century temperature variations by natural and anthropogenic forcings. *Science* **15**, 2133-2137 (2000).
- White ,W.B., Lean, J., Cayan, D.R.& Dettinger, M.D. Response of global upper ocean temperature to changing solar irradiance. *J. Geophys. Res.* **102**, 3255-3266 (1997).
- Widmann, M. & Tett, S.F.B. Simulating the climate of the Last Millennium. IGBP Newsletter, 56. 10-13 (2004)
- Zorita, E., von Storch, H., González-Rouco, F.J., Cubasch, U., Legutke, S., Fischer-Brunns, I. & Schlese U. Simulation of the climate of the last five centuries. *GKSS report*, **2003/12** (2003).

# An empirically based method for projecting future local snow conditions: Preliminary results

by

Inger Hanssen-Bauer

Norwegian Meteorological Institute

## Abstract

Local snow conditions largely affect terrestrial biota and human activities. Global climate models have too coarse spatial resolution to give useful information for impact studies concerning projected changes in snow cover and snow depth. In the present study an empirical model is suggested for calculating the local monthly averaged snow depth based upon local temperature and precipitation conditions. The model is developed and tested using data from climate stations in different parts of Norway. Preliminary results indicate that observed long-term trends and inter-annual variability in average snow depth are reproduced satisfactorily in most Norwegian regions. In some regions, though, the model needs further refinement. The model is applied to produce local projections for future snow-depth conditions for selected localities based upon downscaled temperature and precipitation scenarios.

## 1. Introduction

Local snow conditions largely affect terrestrial biota in the Arctic. Global climate models have too coarse spatial resolution to give useful information for impact studies concerning projected changes in snow cover and snow depth. Even in regional models, valleys and mountains are not resolved sufficiently to allow for realistic estimation of local snow conditions, especially in rough terrain. Realistic snow scenarios can be achieved by adjusting daily precipitation and temperature scenarios from regional models to local conditions, and then feed these into a water balance model. This is, however, resource demanding. Scherrer and Appenzeller (2004) suggested a simple model for estimating the influence monthly mean temperature and precipitation on the length of the season with snow cover. In the present study, a similar empirical model is suggested for calculating the local monthly averaged snow depth from monthly data. Both monthly observational data (for model calibrating) and monthly model data (for scenario development) are usually more easily available than daily data. The model may be applied both for gap-filling in historical snow series and for projecting future snow conditions. Data and model development are described in section 2. Preliminary results, and a tentative scenario for changes in snow conditions produced by the model, are presented in section 3.

## 2. Data and snow-model development

Data from the Norwegian Meteorological Institutes database were used for snow-model development and testing. They include monthly series of precipitation, temperature and average snow-depth from 16 Norwegian climate stations. Local temperature and precipitation scenario data for calculation of snow-depth scenarios were taken from the empirical downscaling study by Hanssen-Bauer et al. (2003). The downscaling is based upon the Max-Planck Institute climate model ECHAM4/OPYC3 run with the IS92a emission scenario.

The idea behind the snow-model is that the change in average snow-depth from month  $m-1$  to month  $m$  ( $\Delta SD_m$ ) basically depends on temperature conditions (represented by the average monthly temperature  $T_m$ ) and precipitation (represented by the monthly precipitation sum  $R_m$ ), while the average snow-depth of the previous month ( $SD_{m-1}$ ) is the upper limit for melting. An estimate for the change in monthly mean snow-depth may thus be expressed as:

$$\Delta SD_m = \max \{f(T_m, R_m); -SD_{m-1}\} \quad (1)$$

It is suggested that the function  $f$  may be written on the form:

$$f(T_m, R_m) = a R_m + b T_m R_m + c T_m \quad (2)$$

The coefficients a-c will obviously depend on temperature, as both precipitation phase and melting conditions depend on temperature. Two threshold temperatures (TT1 and TT2) are thus suggested. When  $T_m$  is below TT1 all precipitation is supposed to be solid and no melting is supposed to occur, when  $T_m$  is above TT2 all precipitation is supposed to be liquid:

$$f(T_m, R_m) = \begin{cases} a_1 R_m + b_1 T_m R_m & \text{when } T_m < TT1 \\ a_2 R_m + b_2 T_m R_m + c_2 T_m & \text{when } TT1 \geq T_m > TT2 \\ c_3 T_m & \text{when } T_m \geq TT2 \end{cases} \quad (3)$$

Preliminary threshold temperatures were chosen after inspection of data from a number of Norwegian climate stations. The sensitivity of this choice has not yet been analysed in detail. The model was adjusted to 8 climate stations in Norway by multiple regression analysis of observed data from the period 1961-1990. Preliminary results indicate that the optimal values of the coefficients a and b vary by a factor of 2, dependent on terrain and distance from coast, while the optimum value of c is similar for all stations. Figure 1 shows how the model fits the observations at 3 climate stations in different parts of Norway.

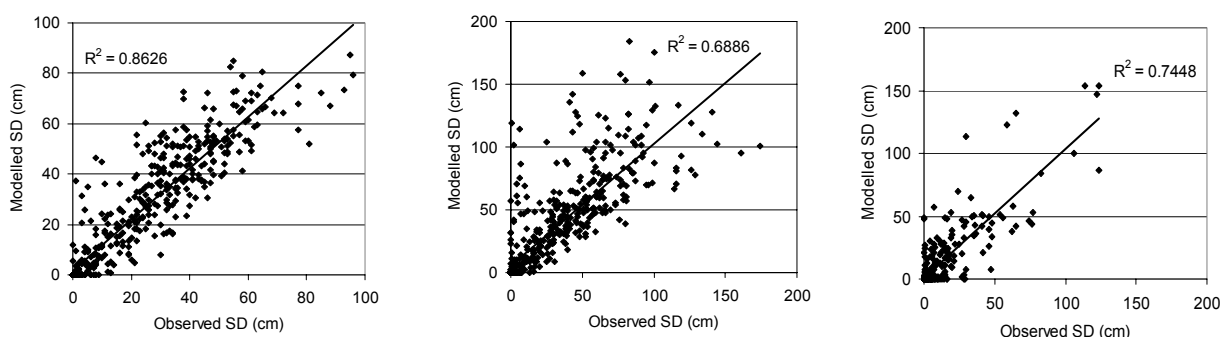


**Figure 1.** Model fit at 3 stations in different parts of Norway. Left: Karasjok in Northern Norway; Middle: Røros in Mid-Norway; Right: Kjevik in Southern Norway.  $R^2$  between observed and modelled snow-depth is given in each plot.

### **3. Preliminary results, reproduction of observed series**

The model has so far been tested at 16 climate stations, of which 8 were used in the model development. Observed and modelled annual mean snow-depth at 3 stations, of which only one (Kjевik) was applied in the model development, is given in Figure 2. The model fit is best at Kjевik, but also good in Tromsø. Both inter-annual variability and long-term trends are satisfactorily reproduced. The negative trend in Kjевik is caused by increasing winter temperature, while the positive trend in Tromsø is caused by increasing winter precipitation. In Sauda, which is situated in the end of a fiord in western Norway, the model fit is worse (Figure 2, lower panel). Though the modelled long-term trend is close to the observed one (about -1.5 cm per decade for annual mean snow-depth), there is a positive bias in the estimated average snow-depth and the observed inter-annual variability is poorly reproduced. The over-estimation of average snow depth seems to be a general feature for stations situated in the inner parts of western fiords, and the model obviously needs to be calibrated specifically for this type of station.

It is possible to use the snow-model to deduce a rough measure for the length of the snow season by counting the number of months with average snow-depth above a threshold (e.g. 1cm). Preliminary results indicate that though the model systematically underestimates the length somewhat (because the last snow – in the model – tends to disappear too fast in the spring), the trend is reproduced reasonably well. An example is given in Figure 3.

### **4. Preliminary results, scenarios**

Local monthly temperature and precipitation scenarios for Norway are available from several global climate models (Benestad, 2002). In the present preliminary snow-projections, only the scenario downscaled by Hanssen-Bauer et al. (2003) was applied. Figure 4 shows local snow-projections for 2 stations calculated from this. For Kjевik, the projected negative trend in snow-depth from 1950 to 2050 is actually slightly smaller than the observed trend from 1947 to 2004. The projected trend in the length of the snow season from 1950 to 2050 is very close to the observed trend during the last 56 years. For Tromsø, the projection indicates that the positive trend we have seen in annual average snow depth will not continue.

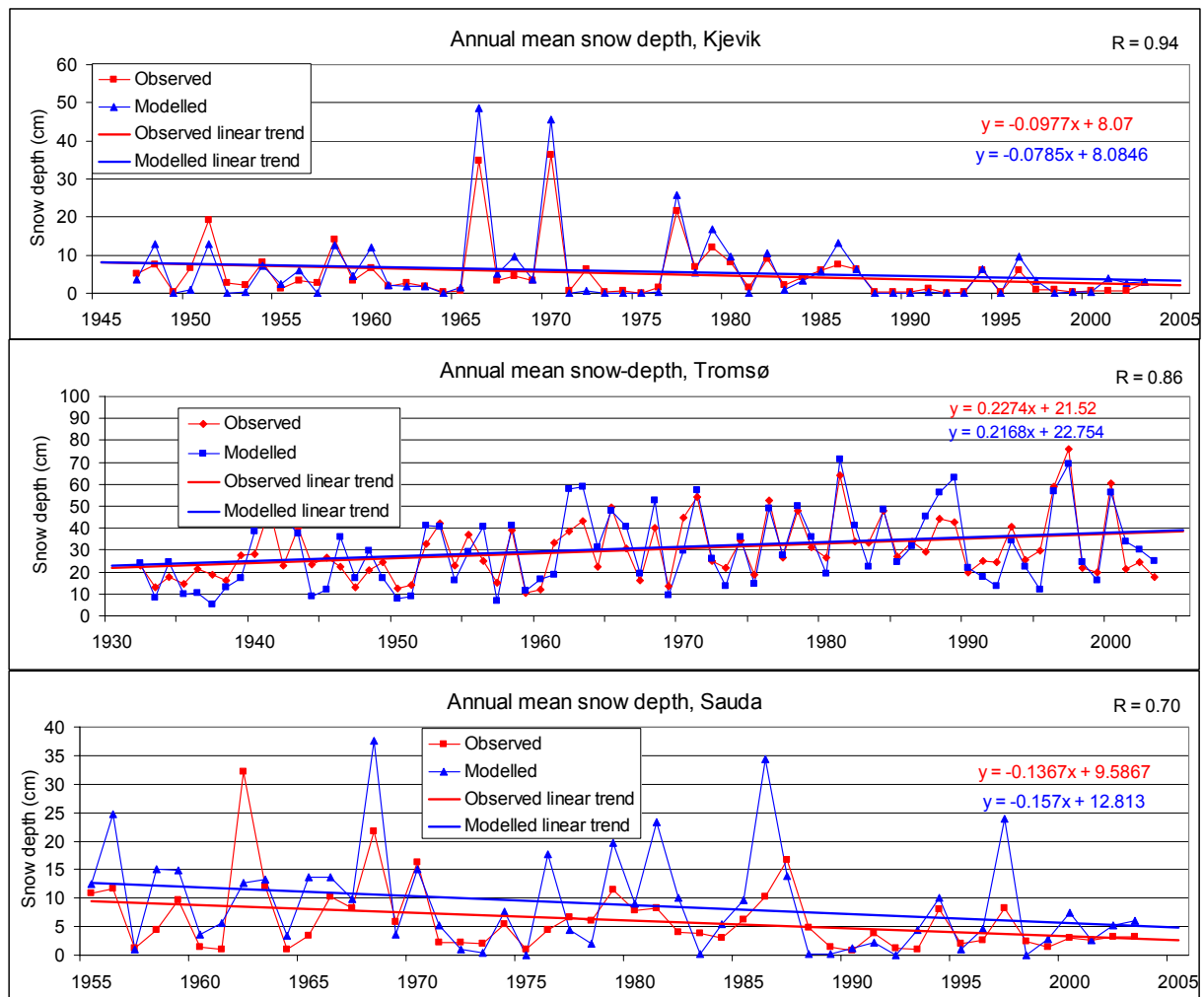


**Figure 2.** Observed and modelled annual mean snow-depth in Kjевik (Southern Norway), Tromsø (Northern Norway) and Sauda (Western Norway). Linear trends are shown.

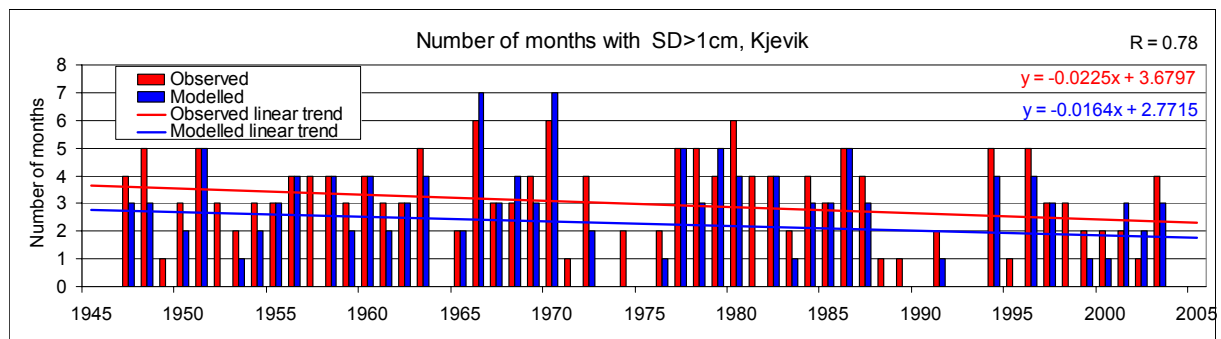


**Figure 3.** Observed and modelled number of months with average snow-dept >1cm at Kjевik. Linear trends are shown.

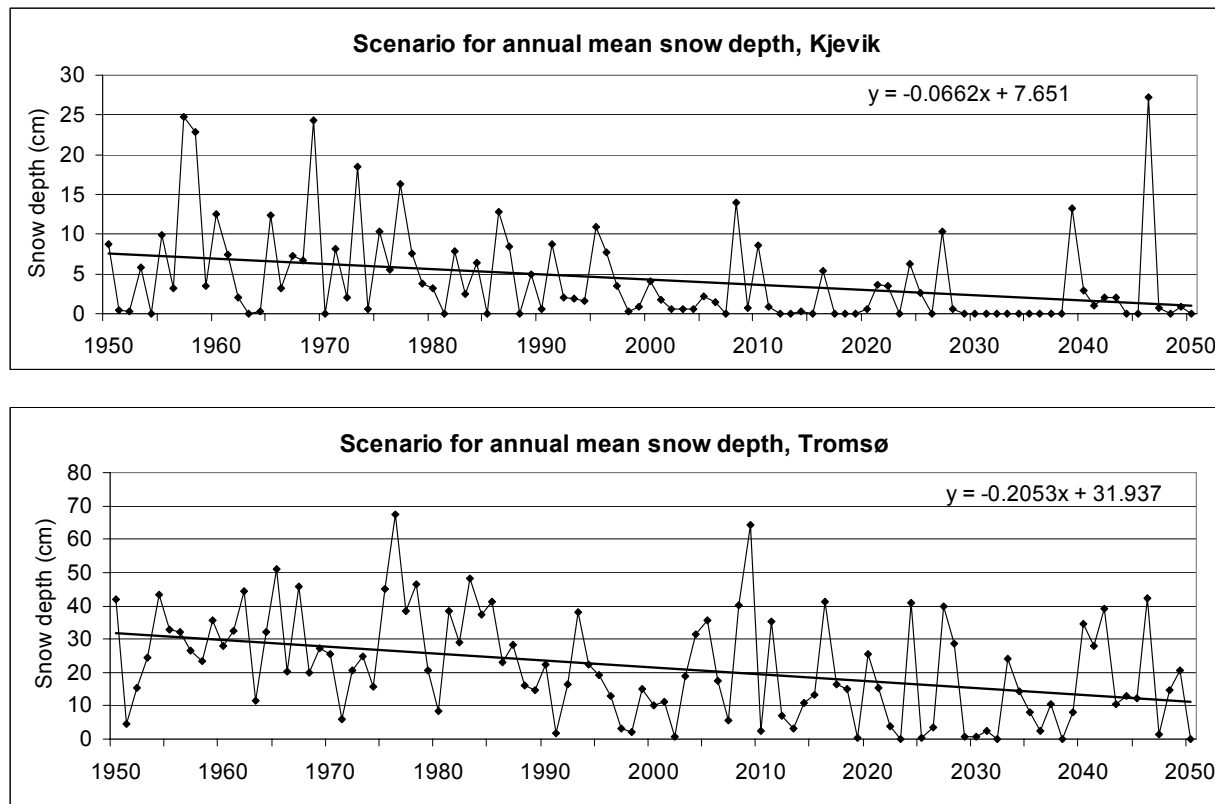


**Figure 4.** A scenario for annual mean snow-depth at Kjевik (Southern Norway), and Tromsø (Northern Norway).

## 5. Preliminary conclusions and further plans

Preliminary results with the empirically based snow-depth model are promising. There are, however, regions where the model does not work satisfactorily, and further adjustment of the model is necessary. Local fitting of the regression model will probably improve the results somewhat, but sensitivity with respect to the choice of threshold-values will also be further investigated. When the model is optimised, it will be possible to produce – in a simple way – ensembles of local snow scenarios based upon temperature and precipitation scenarios downscaled from different climate models.

## References

- Benestad, R.E., 2002: Empirically downscaled multi-model ensemble temperature and precipitation scenarios for Norway. *Journal of Climate*, 15: 3008-3027
- Hanssen-Bauer, I., E.J. Førland, J.E. Haugen, O.E. Tveito, 2003: Temperature and precipitation scenarios for Norway - Comparison of results from dynamical and empirical downscaling. *Climate Research*, 25, 15-27

Scherrer, S.C. and C. Appenzeller, 2004: Trends in Swiss Alpine snow days: The role of local- and large-scale climate variability. *Geophys. Res. Letters*, 31, L13215, doi:10.1029/2004GL020255



# Response in daily precipitation and wind speed extremes from HIRHAM downscaling of SRES B2 scenarios

by

**Jan Erik Haugen<sup>1</sup> and Trond Iversen<sup>2</sup>**

<sup>1</sup>Norwegian Meteorological Institute, Oslo, Norway.

<sup>2</sup>Department of Geosciences, University of Oslo, Norway.

## Abstract

This is a preliminary version of a paper under development. Two time-slices from global climate model (GCM) simulation based on SRES B2 greenhouse gas concentrations have been downscaled with the atmospheric regional climate model (RCM) HIRHAM. The area of downscaling covers central and northern Europe, adjacent sea-areas and Greenland. The GCM data for lateral boundary forcing in the RCM was provided from the Hadley Centre, U.K. (HC) and Max Planck Institute, Germany (MPI), respectively. These were created in two steps; (1) a global low-resolution transient simulation with a coupled atmosphere-ocean-ice model (AOGCM) followed by (2) a global medium-resolution time-slice simulation with an atmospheric model (AGCM) using ocean-ice-state based on (1) or, in the case of the HC, an observation-based correction of (1). The time-slices cover the control period 1961-1990 and the climate scenario period 2071-2100. RCM simulations were carried out with a resolution of 55km.

The present version of the paper does not include a basic analysis of the control period. The main discussion is limited to the response in extreme values of daily precipitation and wind speed. The two modeled estimates of climate response in Europe and adjacent parts of the North-Atlantic Ocean, measured as 110-year trend in climate statistics from the control period to the scenario period, show both similarities and differences. For seasonal values, differences in the regional response for precipitation and wind speed are clearly seen. When taking into account all daily values throughout the year, there seems to be a large degree of agreement in the two simulations, even though qualitative differences are seen. In order to present trends in extreme events and their return periods, the scenarios are analysed both individually and combined. The combined statistics is obtained by lumping together the two sets of time series data from both simulations with equal weight on each. Hence they are treated as equally possible realizations of an ensemble. It turns out that extreme events of daily precipitation and wind speed in the control climate becomes more frequent in the scenario period over large areas in northern Europe, and with a structure similar to the mean climate response of the respective quantity.

## 1. Background

Scenarios for the development of the global climate as a consequence of presumed atmospheric concentration levels of anthropogenic (and natural) greenhouse gases are based on coupled global climate models (GCMs) with coarse atmospheric horizontal grid-resolution (typically  $\sim 280$  km or T42). For most environmental impact studies this resolution is far too coarse. Topography and patchy geographical features, such as coastlines, snow-cover, vegetation, watersheds etc., are too smoothly represented for a direct quantification of impacts in most cases. Furthermore, features associated with atmospheric dynamics and physics are also crudely represented. For extreme weather such as strong winds and heavy precipitation, horizontal resolution is an important issue. Such events are frequently connected with spatially abrupt features like sharp fronts and squall lines, mesoscale vortices, steep mountain slopes and topographical corner effects. Hence, an analysis of potentials for anthropogenic change in occurrence of extreme values of weather elements can not fully rely on raw output of global climate models.

Poor description of processes bound the confidence in climate projections. McAvaney et al. (2001) stated that AOGCM-simulations of the present climate are credible for most variables of interest for climate change over broad continental scales seasonally and annually. These qualities deteriorate for sub-continental scales. In an attempt to dispense with the coarse horizontal resolution of global climate models, different kinds of regional downscaling techniques are being used by the climate modeling community since the last two decades or so (see Giorgi and Mearns, 1991 for an early review). Increased regional skill added to coupled GCM results has been documented by atmospheric downscaling (Giorgi et al., 2001; Denis et al., 2002). Also, weather associated with fine-scale orography is better forecasted than theory for free turbulence suggests (e.g. Boer, 1994; Frogner and Iversen, 2002). Statistical or empirical downscaling (e.g. Wilby and Wigley, 1997) has the major advantage above most other techniques that a large number of global scenarios can be included in the analysis due to the low computational cost. In such analyses, local and regional climate parameters are tied statistically to large-scale patterns resolved in GCMs. Dynamic downscaling is a more physically based approach, which unfortunately is much more resource-demanding. In most applications, this method makes use of numerical models with a considerably finer resolution in a limited domain. Such a regional climate model (RCM) can in principle couple the atmosphere and the ocean, but in most cases an RCM is a pure atmospheric model which only includes interactions with the land surface processes. Also

pure oceanic downscaling models are possible with atmospheric forcing prescribed from the GCM. Dynamic downscaling also embraces use of global atmospheric models with higher resolution than coupled GCMs (typically coarser than ~110 km or T106), which use prescribed oceanic fields. Most present RCMs use horizontal resolution 20-50 km, and even this is regarded of limited usefulness for some types of impact research. In such cases, a combination of dynamical and empirical downscaling may be a way to obtain adequate resolution. In the recent PRUDENCE-project funded by the European Union (EU), the uncertainty in the regional climate change over Europe has been addressed by a common analysis of several coordinated RCM simulations. A continuation and extension of this work takes place in the new EU-project ENSEMBLES.

In the present preliminary version of the paper we concentrate on the response of daily extreme values of precipitation and wind speed in European with adjacent parts of the North Atlantic Ocean. The analysis are based on data from two recent time-slice simulation carried out with the HIRHAM RCM. The size of the domain is sufficiently small for the data imposed on the lateral boundaries to dominate the large-scale climate (see Jones et al., 1995 and 1997 for an analysis). Separate tests performed by interchanging the data for sea-ice and ocean surface temperature from the two driving global models, emphasize this. Hence the RCM-results are mainly fine-scale interpretations of the global data. So far a basic analysis of the quality of the simulations of present-day climate is missing. Statistics for extreme events are so far emphasized, both by individual analyses of the two sets of data and by combining the series and making common statistics in the way recommended by Räisänen and Palmer (2001). Similar discussions based on another RCM were given by Räisänen et al (2004) and with different RCMs and GCMs by Christensen et al. (2001).

As always when dealing with such analysis, it is important to notice that only a subset of possible climate scenarios and climate realizations are included. Two important sources to uncertainty are associated with future atmospheric concentrations of greenhouse gases, and with the multitude of climate realizations caused by natural climate variability due to internal processes in the climate system. A third and very important source is different and uncorrelated imperfections in the different climate model. Since we use only one emission scenario, no spread can be ascribed to emission scenario uncertainty. Two estimates of 110-year trends in thirty-year long climate statistics are certainly not sufficient to cover all natural variability. On the other hand, by choosing data from two models with quite different regional signatures over the Atlantic-European region, a considerable span of variability is covered. Parts of this span stem from inevitable model imperfections, but since we use the same model

for downscaling, this part of the spread is due to the different global models only. This part of the modeled spread in the climate trend statistics in this paper may actually exaggerate the spread due to natural internal variability, to the extent that different model imperfections cause considerable uncorrelated errors. More work will later be allocated to attribute different sources of spread in the climate projections.

## 2. Models and global forcing

The HIRHAM RCM (Christensen et al. 1997; 1998) was imported from Max Planck Institute (MPI), Hamburg, in 1997 and a similar version is at present also used at the Danish Climate Centre, Copenhagen. The main component of HIRHAM is described in Bjørge et al. (2000). The model is running on a rotated spherical grid (approximately 55 km resolution) and with 19 levels in the vertical. The integration domain covers 96x96 grid squares. The physical parameterizations are adapted from the ECHAM4 AGCM (Roeckner et al. 1996).

Data from two AGCMs, HADAM3H and ECHAM4 were supplied from the Hadley Centre (HC), U.K. and MPI, Hamburg (MPI), respectively. The HC-data were originally made available for the PRUDENCE-project, while the ECHAM4-data were kindly supplied by the MPI-staff (D. Jacob, pers. comm.). Both centers have carried out transient coupled atmosphere-ocean-ice AOGCM runs from pre-industrial conditions in 1860 up to the end of this century 2100, using observed greenhouse gas concentrations until model year 1990 followed by IPCC SRES B2 concentrations from 1990-2100. The B2-scenario assumes a gradual increase in CO<sub>2</sub> emissions from ca. 7 Gt(C)/a in 2000 to ca. 13 in 2100. This is amongst the moderate scenarios for CO<sub>2</sub> increase used in IPCC TAR (IPCC, 2001). The range of model-estimated increase in global mean surface temperature from 1990 to 2100 was 1.8 – 3.2 °C.

The actual global forcing for the two RCM simulations were from medium-resolution (T106) AGCM re-runs for the two 30 year time-slices used in the present study, i.e. 1961–1990 and 2071–2100, using prescribed SST and sea-ice distributions (details are not included here). The time-slices are preceded by spin-up periods (1 year in the case of HIRHAM) which are ignored in the analysis.

## 3. Response in mean pressure and temperature

In this section a brief description of the mean behavior of the two B2-simulations is presented. The response in mean sea level pressure (MSLP), annual and winter season means,

is shown in Fig. 1. Looking at the annual response, a common feature in the two simulations is an east-west band of relative small change over central Europe, while the pressure response is larger and negative in northern areas. On a larger scale, the north-south gradient in MSLP is strengthened, which may be associated with an overall increased westerly flow over northern Europe. A rather different response in MSLP during winter season may demonstrate the effect of natural variability in such relatively short time-slices of 30 years, even though model imperfections also may contribute to the differences seen. Incidental and intermittent north-south shift of the major storm tracks certainly influences the analysis of precipitation and wind speed patterns over central and northern parts of Europe. In this case we see that HC increases the occurrence of low pressures over the North Sea, Skagerak and Southern Scandinavia, whilst MPI tends to increase the cyclonic activity over North-east Europe.

### ***MSLP response***

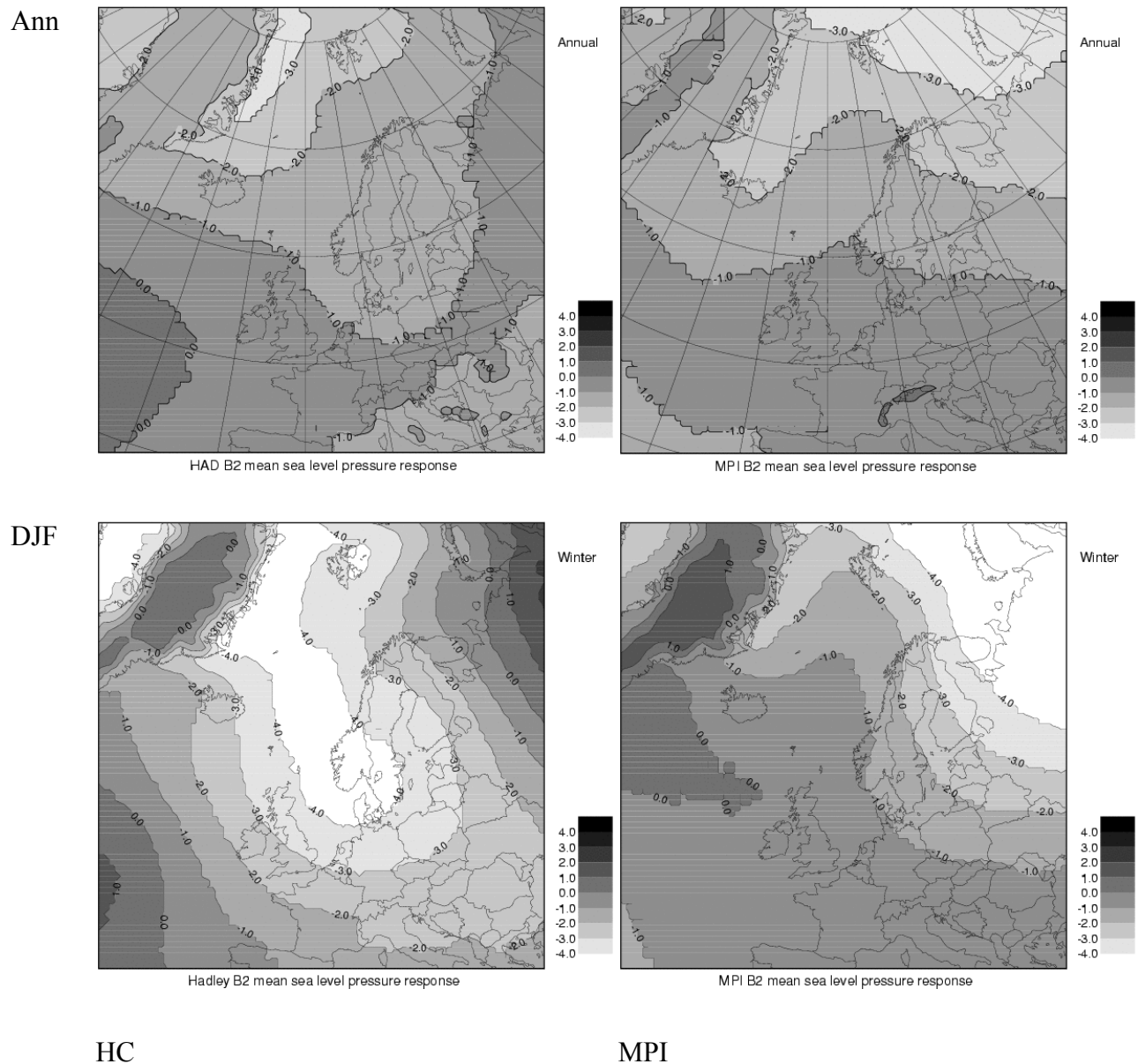


**Figure 1.** Mean sea level pressure response in HIRHAM with B2-forcing from HC (left) and MPI (right), annual (upper) and winter/DJF (lower) 30-year mean values. Contour interval is 1hPa.

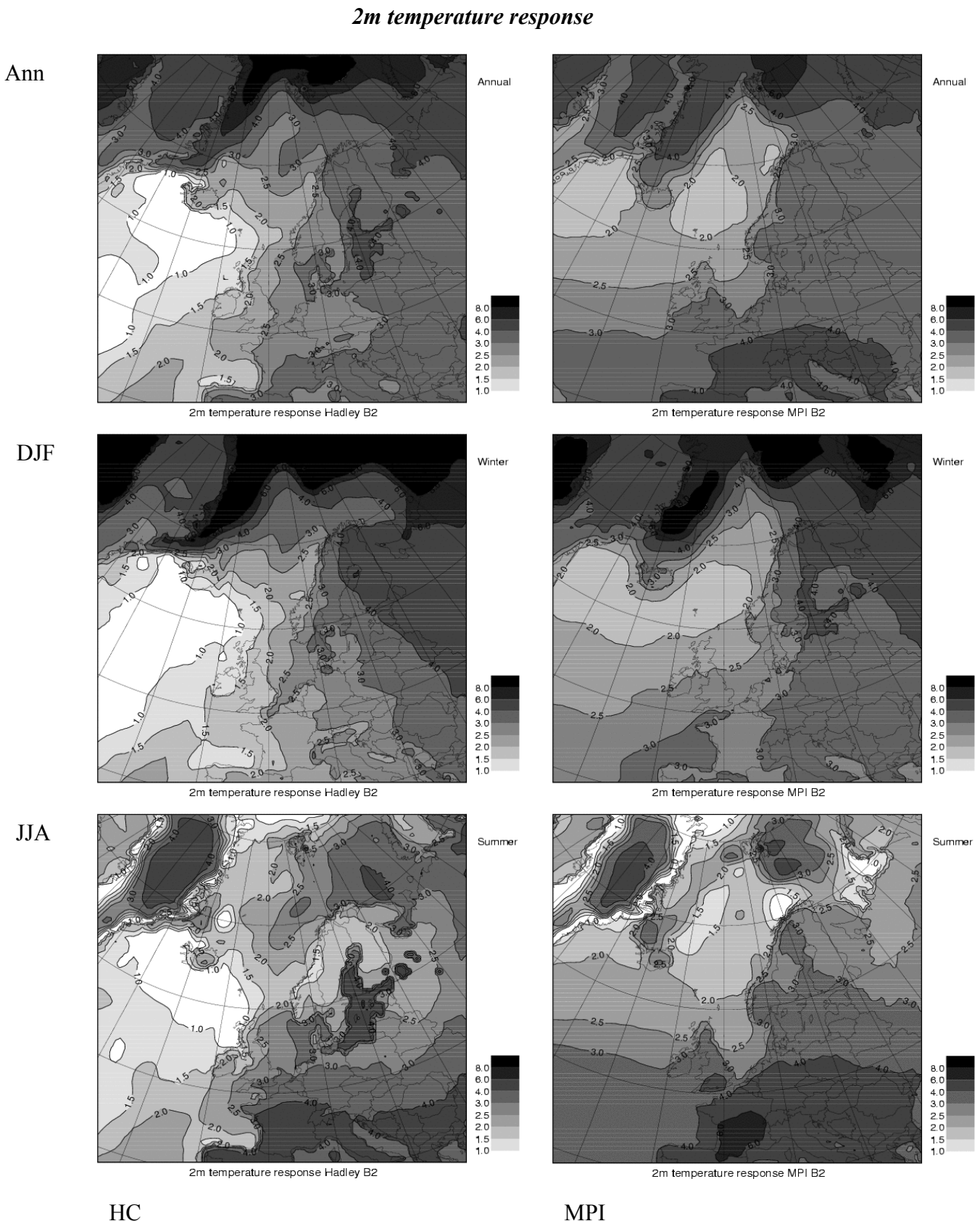


**Figure 2.** 2m temperature response in HIRHAM with B2-forcing from HC (left) and MPI (right), annual (upper), winter/DJF (middle) and summer/JJA (lower) 30-year mean values. Contours with unit degrees C.

The 2 meter mean temperature response (winter, summer and annual) is shown in Fig. 2. On the annual basis there are qualitatively large agreements between the two scenarios, but the overall heating in the MPI data is somewhat stronger than in the HC data. There are two major large-scale features in the results seen from both models: the cold-ocean-warm-land pattern with considerably larger temperature increase over the European continent than over the adjacent parts of the Atlantic Ocean; and the largest warming is experienced in the Arctic during winter. A response in the interval 2.5-4 degrees is present over major parts of the European continent. The 2.5 degree line from Scotland northward along western Scandinavia is seen in both simulations. Over southern Europe the continental warming rate is considerable during summer. Over northern Europe and the Arctic, the heating is stronger in winter than in summer.

One important difference between MPI and HC is seen over the North Atlantic Ocean during the three winter months. HC has a considerably smaller temperature increase over this oceanic area than MPI, which can be associated with differences flow pattern trends diagnosed by e.g. the MSLP.

#### **4. Response in precipitation and wind speed**

In this section precipitation and wind speed response in discussed, both mean values and extremes of daily values. The extremes are presented for annual data only. In this way the analysis is based on the largest possible sample. Furthermore, from the analysis of mean sea level pressure in the previous section we found that the annual mean response was quite similar in the two simulations. This may justify that an analysis based on annual values is feasible, although it may hide the fact that one of the scenarios may dominate the results due to large differences in the response in some period of the year. In addition, we add a combined statistics for the two scenario data-sets in a common analysis (Räisänen and Palmer, 1991). In the combined response statistics the two datasets are given equal weights. The results from both individual and combined analysis are shown. A simple measure of changes in extreme values is the response factor in the scenario period of a certain height percentile computed from the control period. As an example, the highest 0.2778 percentile value in the control period computed from annual values corresponds to one event per year (on average), since  $1/360=0.2778$ . A response factor of  $\frac{1}{2}$ , 1 and 2, respectively, means that these values occur with half, the same and the double frequency (or once every second year, every year and twice per year), respectively, in the scenario period. A statistically more robust

measure, but certainly not very extreme, is the result for the highest 5 percentile, corresponding to an average occurrence of one per 18 days.

## 4.1 Mean values

In Figure 3 we see quite similar results for increases in annual mean precipitation for the two datasets. The annual positive response over major areas is somewhat larger in the MPI results. However, the seasonal results depict differences which may be associated with dominating atmospheric flow regimes relative to major mountain ranges and coastlines. Both HC and MPI projects considerably drier summers in major parts of Europe except for western parts of Scandinavia and in the northern parts of the integration domain. HC is the drier of the two estimates. In winter, precipitation amounts are projected to increase over most regions, but HC produce a larger increase over most parts. In Scandinavia, however, there are considerable differences, which can be ascribed to the response in MSLP and associated flows. With an increased occurrence of cyclonic activity in Southern Scandinavia and the Northern parts of continental Europe, HC projects more precipitation increase in central Europe and the Southern and South-Eastern parts of the Scandinavian mountains, with precipitation decrease over North-Western and Northern Norway. MPI, however, with more cyclonic activity to the North East, major precipitation increase is seen during winter over all westward facing parts of the Scandinavian mountains, whilst considerable shadow effects are seen to the East of these mountains.

As a measure of change in wind speed, the average over the daily maximum values (annually, winter and summer) is presented in Fig. 4. On an annual basis, parts of central Europa and southern Scandinavia are dominated by a slight positive response. In the MPI scenario, this zone is extending to northern land areas, while the the response is negative in southern Europe. This pattern is reversed in the HC results. The increased wind speed during winter in HC is in clear agreement with the MSLP-patterns shown Fig. 1. Maps showing the significance of these changes compared to the variability in the control period have so far not been prepared.

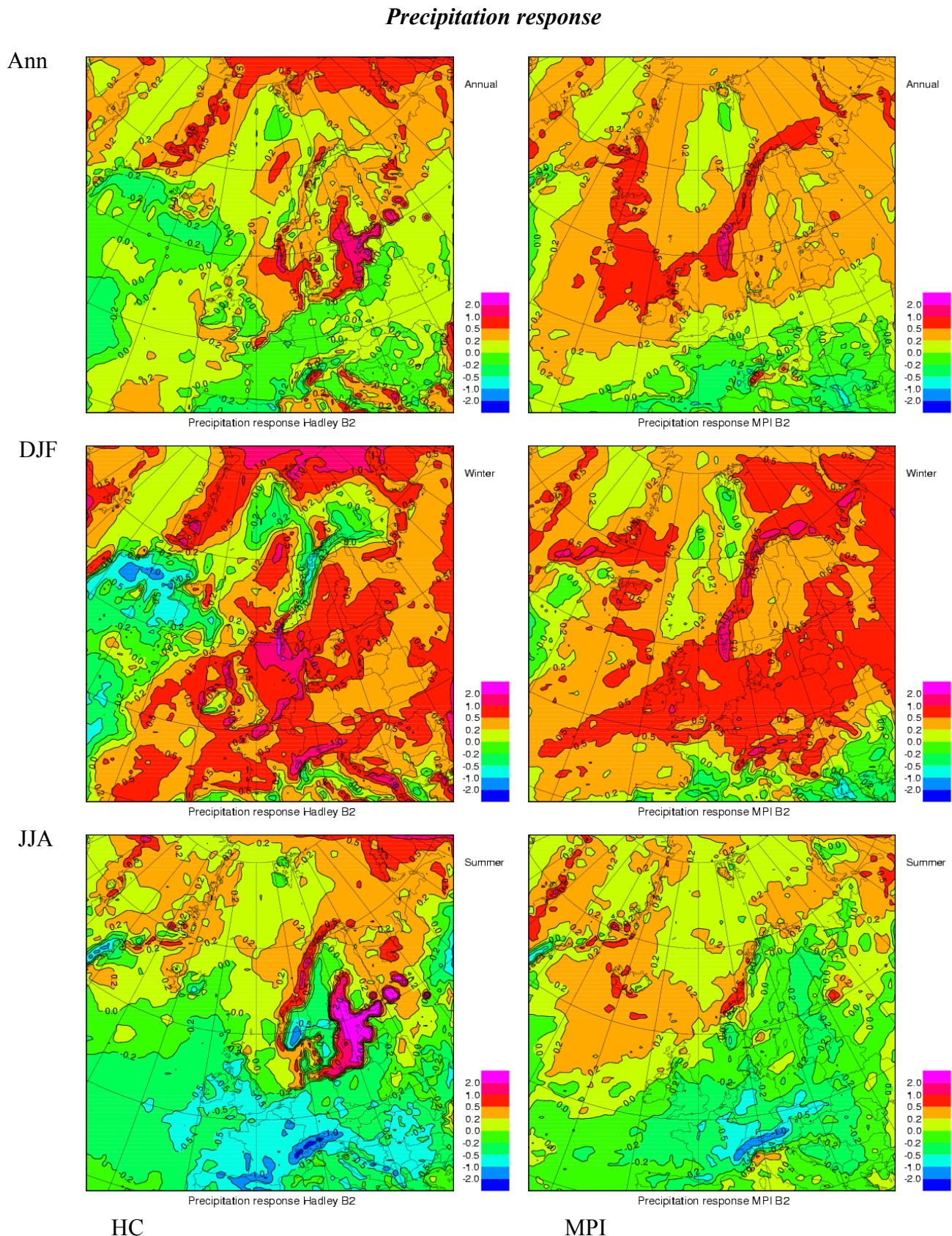


**Figure 3.** Precipitation response in HIRHAM with B2-forcing from HC (left) and MPI (right), annual (upper), winter/DJF (middle) and summer/JJA (lower) 30-year mean values. Contours with unit mm/day.

### Max. wind speed response

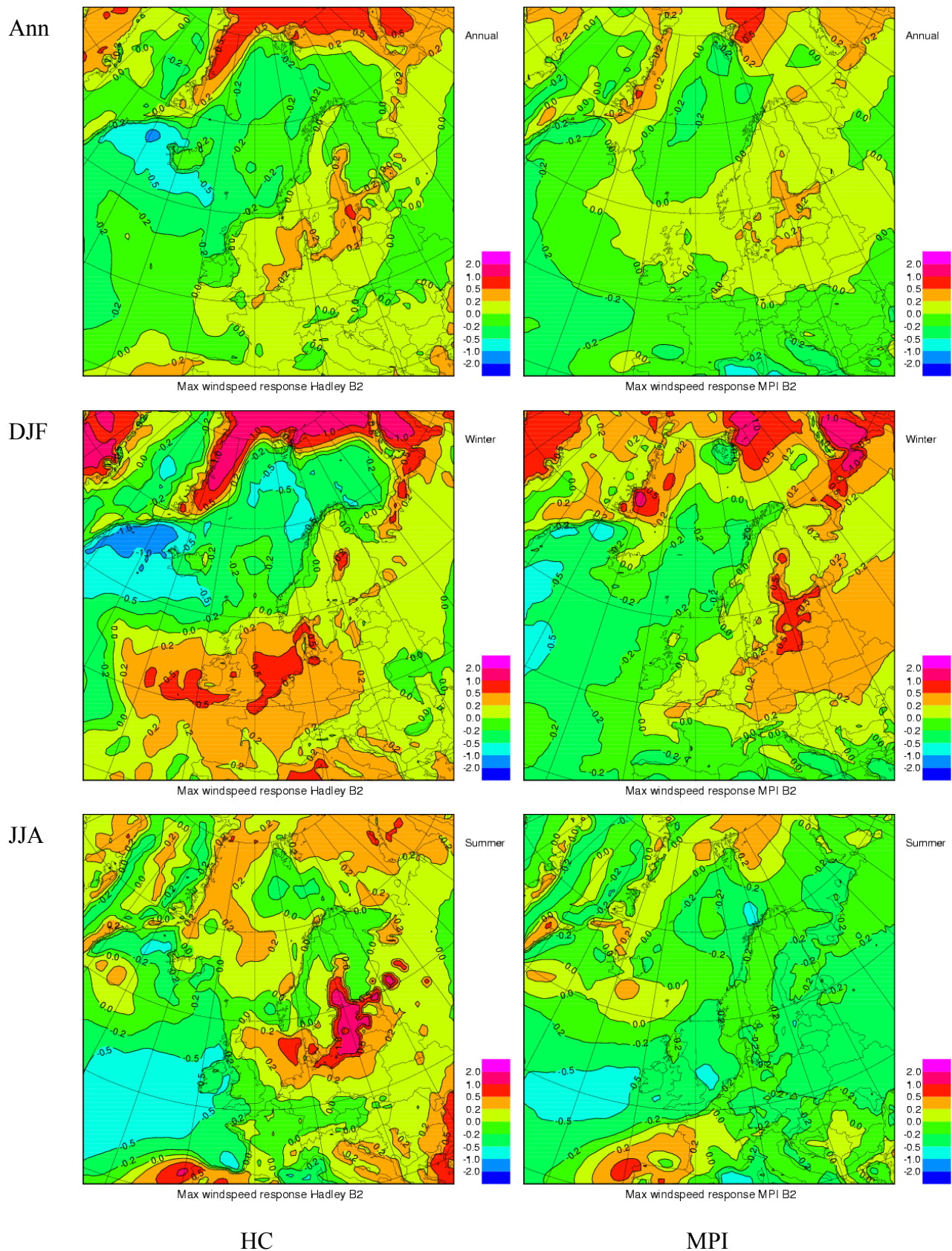


**Figure 4.** Max. wind speed response in HIRHAM with B2-forcing from HC (left) and MPI (right), annual (upper), winter/DJF (middle) and summer/JJA (lower), 30-year mean of daily values. Contours with unit m/s.

## 4.2 Daily extreme values.

In addition to the response in mean fields, the scenario increase in return frequency of events for daily precipitation amounts and daily maximum wind speed, are shown respectively in Figs. 5 and 6. So far we only present statistics based on time series days during the entire year. The results may be compared to the corresponding patterns of response in annual mean fields shown in Figs. 3 and 4. Concerning the factor of increase for the return frequency in the scenario climate of the highest 5%tile values in the control climate, central and northern parts of Europe (land areas and sea areas west of central Europe) are dominated by values larger than 1; 1-1.5 for daily precipitation; and 1-1.25 for daily maximum wind speed. (A factor of 1 means unchanged return frequency and a factor  $> 1$  indicates that the event occurs more frequent in the scenario climate than in the control climate.) In broad terms, the spatial pattern of increased return frequency bears resemblance with the patterns of the mean responses.

For more extreme events: the highest 0.2778 percentiles in the control climate correspond to the highest 30 values during the control period 1961-1990, hence the control climate return frequency is one event per year. Compared to the 5 percentile maps (one event per 18 days in the control climate), there is clearly a larger increase in the return frequency of these rarer events in the scenario climate. Thus for precipitation many areas experience an increase in return frequency in the scenario climate of factors in the interval 1.5-3. The factors are generally slightly larger in the MPI results, while the picture is more patchy and irregular in the HC results. Return frequencies of the most extreme wind speed events are increased with a factor 1.25-2 in the scenario climate over many land areas. Over major parts of the sea areas, however, the return frequency is decreased in the scenario climate. A common maximum area of values above 1.5 is estimated in the north-eastern parts of central Europe.

## 5. Preliminary conclusions

This paper is a preliminary manuscript which will be extended with more results and discussions. The paper discusses selected results from dynamical downscaling over Europe and adjacent sea areas using HIRHAM. Global realizations of the climate response of the SRES B2 emission-scenario for 2071-2100 produced with two different state of the art GCMs have been downscaled.

Concerning response in mean fields, the largest warming during winter occurs in northern Europe. Central and southern Europe experience the largest warming during

## *Return factor precipitation extremes*

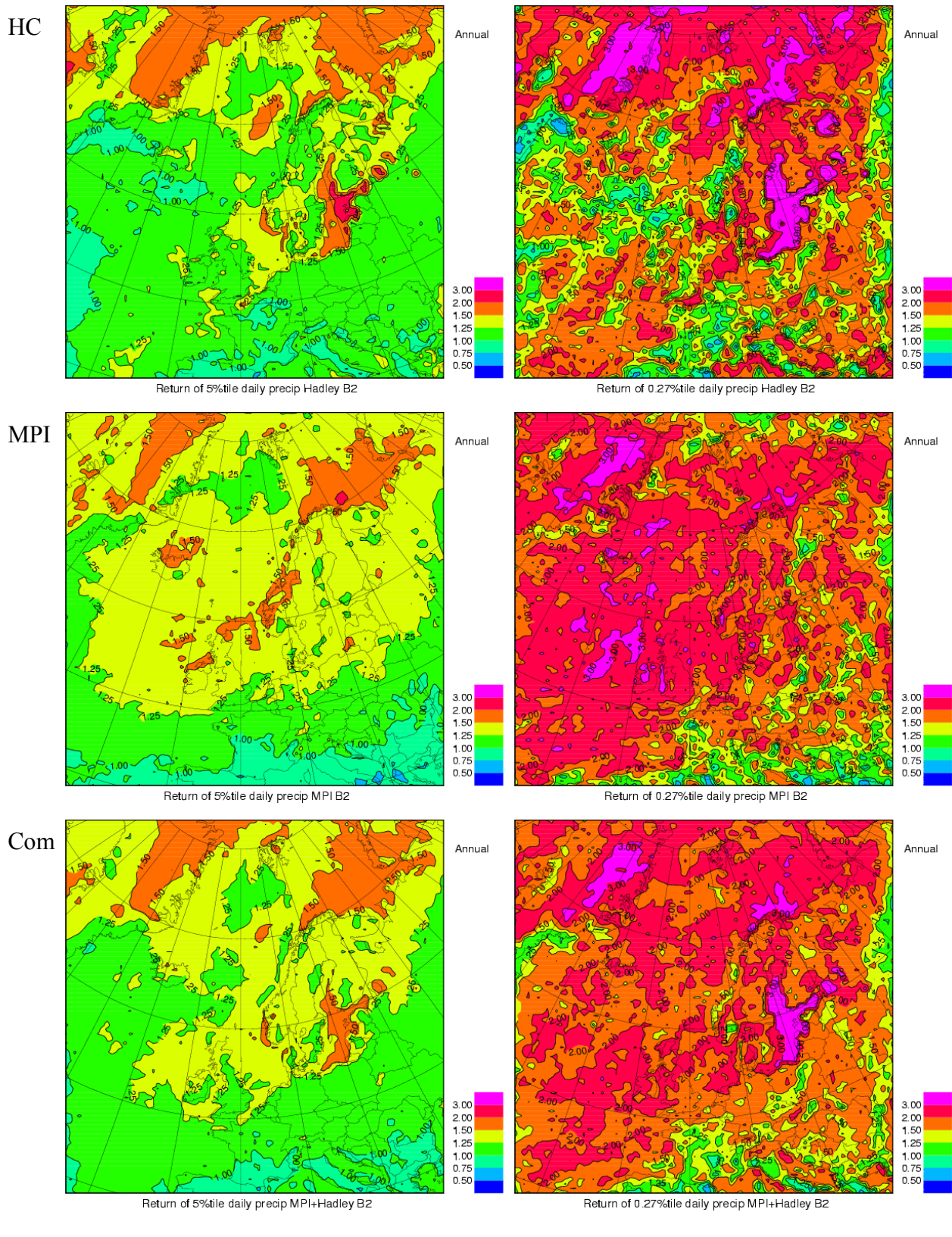


**Figure 5.** Return factors of highest 5%tile (left) and 0.2778%tile (right) daily precipitation in HIRHAM with B2-forcing from HC (upper), MPI (middle). The statistics from combined results in lowest row. A return factor of 2 in 2071-2100 means twice as often compared to the control period 1961-1990

### Return factor max. wind speed extremes

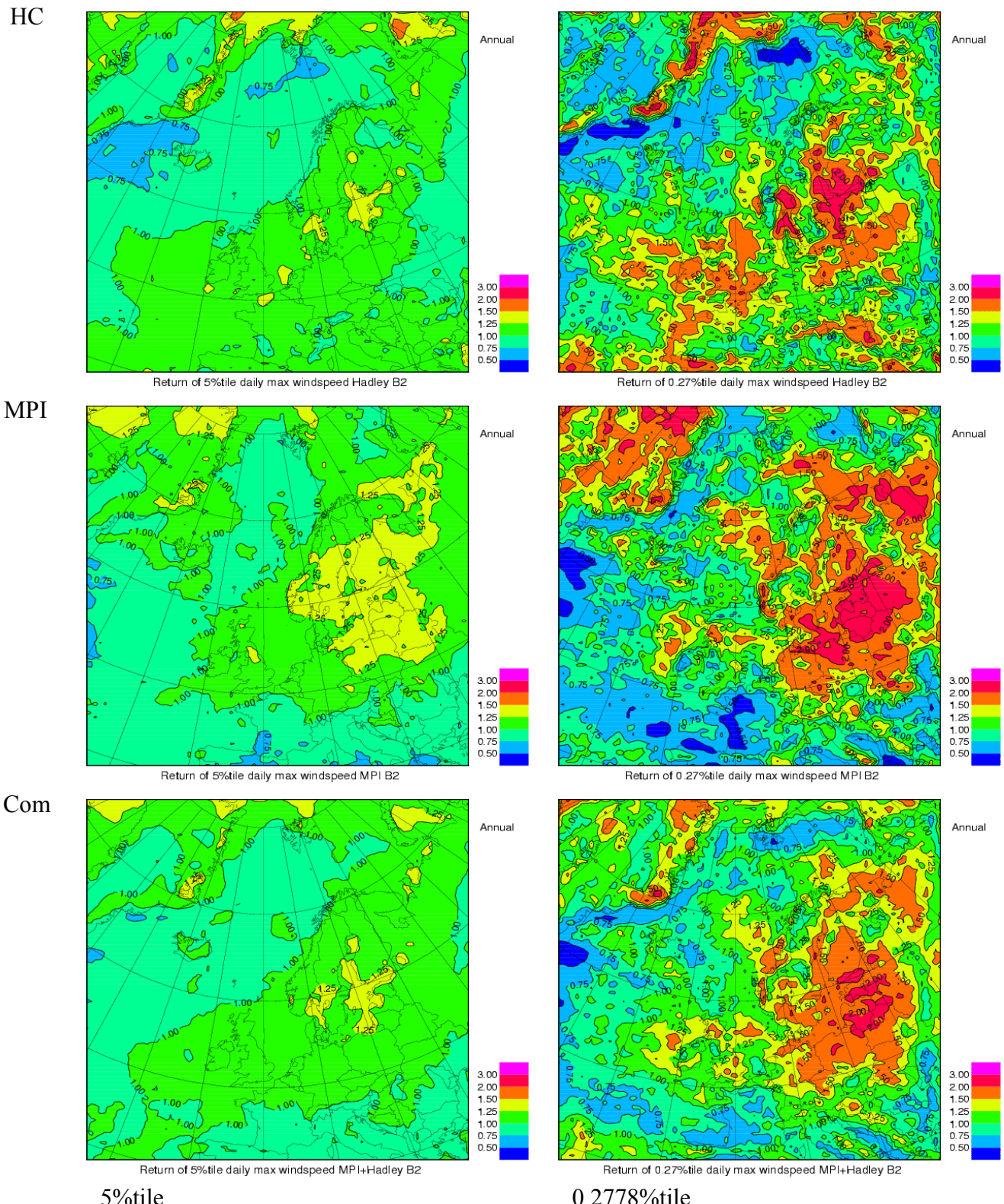


**Figure 6.** Return factors of highest 5%tile (left) and 0.2778%tile (right) daily max. wind speed in HIRHAM with B2-forcing from HC (upper), MPI (middle). The statistics from combined results in lowest row. A return factor of 2 in 2071-2100 means twice as often compared to the control period 1961-1990.

summer, associated with a drier climate. Precipitation response during winter is positive over major parts of Europe, but regional differences are seen, coupled to differences in the atmospheric circulation and wind speed patterns between the scenarios.

The return factor for moderate extreme daily event of precipitation and wind speed follows the patterns seen in mean response to a large extent on an annual basis. The response in return frequency for more extreme events is estimated to be considerably larger.

The two estimates of climate change response implies considerable differences over the Scandinavian mountains. These differences are ascribed to differences in the regional flow patterns predicted by the two models. By combining the results into a common climate change statistics, we obtain more robust results. Parts of the differences may be due to uncorrelated errors in the model results due to model imperfections, however, the differences may also be due to natural internal variability such as the Scandinavian pattern.

## Acknowledgment

The work reported here is funded in part by the Norwegian Research Council, through grant no. 120656/720 to the Norwegian Meteorological Institute/RegClim. Computational costs are covered by a grant from the Research Council's Programme for Supercomputing. The Hadley Centre, the PRUDENCE project at the Danish Climate Centre and the staff at MPI (Dr. Daniela Jacob) is gratefully acknowledged for support of the global data.

## References

- Allen, M. R., P. A. Stott, J. F. B. Mitchell, R. Schnur and T. L. Delworth (2000): Quantifying the uncertainty in forecasts of anthropogenic climate change. *Nature* 407, Oct. 5, 617-620.
- Bjørge, D., Haugen, J. E., and Nordeng, T. E. (2000): Future climate in Norway. DNMI Research Rep. No. 103, 41 pp. Norwegian Meteorological Institute, P. O. Box 43 Blindern, N-0313 Oslo, Norway, ISSN 0332-9879.
- Boer, G. J. (1994): Predictability regimes in atmospheric flow. *Mon. Wea. Rev.*, 122, 2285-2295.
- Christensen, J. H. et al. (1997): Validation of present-day regional climate simulations over Europe: LAM simulations with observed boundary conditions, *Climate Dynamics*, 13, 489-506.
- Christensen, O. B and J. H. Christensen (1998): Very high-resolution climate simulations over Scandinavia. Present Climate. *Journal of Climate*, Vol. 11, No. 12, 3204-3229.
- Christensen, J. H., J. Raisanen., T. Iversen, D. Bjørge, O. B. Christensen and M. Rummukainen (2001): A synthesis of regional climate change simulations – A Scandinavian perspective. *Geophys. Res. Lett.*, 28, 1003-1006.
- Denis, B., Laprise, R., Caya, D. and Coté, J. (2002): Downscaling ability of one-way nested regional climate models: the big-brother experiments. *Climate Dyn.*, 18, 627-646.
- Frogner, I.-L. And Iversen, T. (2002): High-resolution limited-area ensemble predictions

- based on low-resolution targeted singular vectors. *Q. J. R. Meteorol. Soc.*, 128, 1321-1341.
- Giorgi, F. and Mearns, L.O. (1991): Approaches to the simulation of regional climate change: A review, *Reviews of Geophysics*, 29, 191-216.
- Giorgi, F., Hewitson, B., Christensen, J., Hulme, M., von Storch, H., Whetton, P., Jones, R., Mearns, L. and Fu, C. (2001): Regional climate information – evaluation and projections. In: *Climate Change 2001: The Scientific Basis*. (Houghton, J.T. et al., eds.). Cambridge University Press, UK. 881 pp.
- IPCC (2001) *Climate Change (2001): The Scientific Basis*. (Houghton, J.T. et al., eds.). Cambridge University Press, UK. 881 pp
- Jones, R.G., Murphy, J.M. and Noguer, M. (1995): Simulation of climate change over Europe using a nested regional-climate model. I: Assessment of control climate, including sensitivity to location of lateral boundaries. *Q.J.R. Meteorol. Soc.*, 121, 1413-1449.
- Jones, R. G. et al. (1997): Simulations of climate change over Europe using a nested regional climate model. II: Comparison of driving and regional model responses to a doubling of carbon dioxide. *Q. J. R. Meteorol. Soc.*, 123, 265-292.
- McAveney, B.J., Covey, C., Joussaume, S., Kattsov, V., Kitoh, A., Ogana, W., Pitman, A.J., Weaver, A.J., Wood, R.A., Zhao, Z.-C. (2001): Model evaluation. In: *Climate Change 2001: The Scientific Basis*. (Houghton, J.T. et al., eds.). Cambridge University Press, UK. 881 pp.
- Räisänen, J. and Palmer, T.N. (2001): A probability and decision-model analysis of a multimodel ensemble of climate change simulations. *J. Climate*, 14, 3212-3226.
- Räisänen, J. et al. (2004): European climate in the late twenty-first century: regional simulations with two driving global models and two forcing scenarios. *Clim. Dyn.*, 22, 13-31.
- Roeckner, E., K. Arpe, L. Bengtsson, M. Christoph, M. Claussen, L. Dümenil, M. Esch, M. Giorgetta, U. Schlese and U. Schulzweida (1996): The atmospheric general circulation model ECHAM4: model description and simulation of present-day climate: MPI Rep No. 218.
- Wilby, R.L. and T.M.L. Wigley (1997): Downscaling general circulation model output; a review of methods and limitations. *Prog. Phys. Geogra* 21, 530-548.

# **Technical documentation of the Oslo Regional Climate Model, Version 1.0**

**by**

**Jens Debernard and Morten Ødegaard Køltzow**

Norwegian Meteorological Institute, P. O. Box 43 Blindern, 0313 Oslo, Norway

## **Abstract**

The first version of the Oslo Regional Climate Model (ORCM) is technically documented in this report. This is a regional coupled atmosphere – sea ice – ocean model, especially designed for studies over the Arctic Ocean, northern Europe and the northern North Atlantic. This report documents the methods used when the models are coupled. Results from the first 10-year experiments with the model are shortly presented, and they show promising behaviors. However, there are issues that have to be improved. One of them is that the system gives too little sea ice in the Arctic. The same results are earlier seen in simulations with the coupled ice – ocean part of the model. It is argued that tuning or refining the ice model can resolve this.

## 1. Introduction

The present report documents the main technical methods used in the Oslo Regional Climate Model (ORCM), Version 1. The coupled atmosphere-ice-ocean model has mainly been constructed with the Arctic Ocean, northern North Atlantic and Europe as target areas.

One of the important characteristics of the high latitude climate system is the occurrence of snow and sea ice. This has two major effects: First, snow- and ice-covered surfaces are very reflective, and 40-90% of the incoming solar radiation is reflected by the high albedo (Køltzow, 2003). Second, the snow and ice isolate the atmosphere from the warm ocean, and thereby allows the surface temperature over the ice to be very cold (-40 degrees Celsius is not uncommon in the Arctic). However, for drifting pack ice, there will almost always be small regions with open water (leads and cracks), and due to the large temperature contrast between the warm ocean and the cold atmosphere, the ocean-atmosphere heat-flux from these tiny areas might be 2 orders of magnitude larger than the ice-atmosphere heat-flux. Due to the large difference in temperature between the ocean and the ice surfaces, it is not an uncommon situation with strong cooling from sensible and latent heat fluxes at the sea surface, and at the same time heating from sensible heat and ice condensation at the ice surface. Besides the fact that sea-ice changes the surface albedo and isolates the atmosphere from the ocean, it also alters the atmosphere-ocean momentum exchange and acts as a heat reservoir. The ice and coupling modules of MI-IM have both been constructed to utilize the heat reservoir properties of the ice to ensure heat conservation in the communication between the atmosphere, ice and ocean.

From the start of the construction of the ORCM, the main region for application has been the Arctic Ocean and adjacent land areas. Therefore a considerable amount of work has been put into the ice part of the system and the issue of how to handle the interaction between the atmosphere, sea ice and ocean in a coupled system. In this advance the two dominant guiding principles have been 1) heat should be conserved, and 2) the fluxes exchanging heat between the three spheres should be computed only once.

This report starts with a description of the strategy and guidelines that have been used in ORCM, then a detailed description of the coupling interface between the atmosphere and ice/ocean. We will also present some preliminary results from the first 10-year simulation with the system.

## 2. Coupling strategy and method

To establish a coupling strategy for the ORCM the most stringent principle is that the fluxes exchanging energy between the three spheres are calculated only once. At present the ORCM consists of the atmosphere model HirHam, the sea ice model MI-IM and the ocean model MICOM. By studying the documentation of several different coupled climate models, it is decided to base the development on the suggestions given in the two global models NCAR CCSM2.0 (Kauffman and Large, 2002) and BCM (Furevik et al. 2002), and the regional model RCAO (Döscher et al. 2002).

From these studies we have identified the following points that define the coupling strategy:

1. Fluxes are computed only once.
2. Heat and mass should be conserved
3. Fluxes delivered as average values over the coupling time step
4. Fluxes are to be delivered weighted on the atmospheric grid
5. Fluxes and parameters delivered in SI units
6. The ocean mesh is a multiple of the atmospheric mesh

The last item may be viewed as a convenient principle, but actually it makes the task of conserving fluxes much easier. In principle the three meshes could be arbitrary, but this makes it almost impossible to exactly conserve fluxes. The first 3 points, however, are necessary to ensure a heat conservative coupling interface. Based on the experience from other coupled models, it seems obvious that the natural boundary condition to use on interfaces between coupled models is fluxes of heat, momentum and mass (freshwater). To ensure consistency between the fluxes used by the different models, these fluxes should be calculated only once, and then be distributed to the remaining models. The simplest way to ensure global heat and mass conservation is simply to exchange the average or the accumulated value over the complete coupling time step of the flux in question.

Concerning where the fluxes should be calculated, there are several options available. Generally, the horizontal grid in the atmosphere model is coarser than the ice-ocean mesh. Where the fluxes are to be calculated should preferable be based on physical arguments. Concerning stresses (momentum flux) and the surface heat fluxes (turbulent and upward directed long wave radiation), this is normally done in the model that has the most detailed information about the surface state, which in the present context implies MI-IM. However, due to the internal numerical method and coding of the atmosphere model HirHam, it is

difficult to apply these fluxes directly as a boundary condition at the surface without a major recoding of the model. Different approaches are chosen in this respect in the climate models above. In the NCAR CCSM, all surface fluxes are calculated in the ice model or in the coupler at the grid with highest horizontal resolution. The integral of these fluxes over each atmospheric grid cell is then passed to the atmosphere model. On the other hand, in the BCM, all these fluxes are calculated in the atmosphere model on the coarse grid. They are then passed to the coupler and a sub-grid interpolation method is used to distribute the fluxes in the physically most appropriate manner to the ice/ocean grid. The reason for this difference is probably the difficult task of recoding the ARPEGE atmosphere model used in the BCM. The latter option (as in the BCM) is opted here.

Concerning the heat fluxes an implicit numerical method is utilized for the boundary layer physics in HirHam. This routine uses the surface temperature  $T_s$  as a lower boundary condition for several different surface types (land, ice, and sea). Therefore, it may be cumbersome to rewrite these schemes in such a way that they directly make use of a heat flux as the lower boundary condition. Consequently, our approach is again to calculate the turbulent heat fluxes in the atmosphere model, transfer them to MI-IM, and then perform a sub-grid interpolation. Other downward heat fluxes like short-wave solar radiation and downward long wave radiation is naturally calculated in the atmosphere model due to their physical nature, since they depend on vertical integrated properties of the atmosphere. At least for the net short-wave radiation a sub-grid interpolation method should also be used here due to the difference in albedo for ice and water.

The variables transferred between the atmosphere model and MI-IM, are shown in Table 1.

**Table 1:** Fluxes and state variables exchanged in the ORCM

Flux/parameter	Computed where	Unit	Comment
Long wave radiation (up)	Coupler (MI-IM)	W/m <sup>2</sup>	
Long wave radiation (down)	Atmosphere (HIRHAM)	W/m <sup>2</sup>	
Downward short wave radiation	Atmosphere	W/m <sup>2</sup>	
Turbulent heat fluxes	Atmosphere	W/m <sup>2</sup>	
Momentum (stress)	Atmosphere	Pa	
Precipitation (snow, rain)	Atmosphere	m/s	
Evaporation	Atmosphere	m/s	
Runoff	Atmosphere	m/s	
Sea ice concentration ( $A$ )	Coupler (MI-IM)		
Sea ice surface temperature ( $T_{IST}$ )	Coupler (MI-IM)		
Sea surface temperature ( $T_{SST}$ )	Coupler (MI-IM)		
Albedo ( $\alpha$ )	Coupler (MI-IM)		
Cloud fraction (CLF)	Atmosphere		Optionally used in the albedo calculation over water.
2-meter air temperature ( $T_A$ )	Atmosphere		Sub-grid interpolation
2-meter specific humidity ( $q_A$ )	Atmosphere		Sub-grid interpolation
10-meter wind speed ( $u_{10m}$ )	Atmosphere		Sub-grid interpolation

### 3. Sub-grid interpolation and integration of fluxes

The transfers of fluxes between the coarse atmosphere grid and the higher resolved ocean grid is generally of two types, integration from ocean to atmosphere grid and sub-grid interpolation from the coarse to the fine grid. Let  $A$  denote the sea ice concentration, and let the respective contribution to the turbulent fluxes from an open sea be denoted  $Q^o$  and from sea ice  $Q^i$ . The total heat flux to the atmosphere over an atmospheric grid cell with area  $\Omega$  is then defined as the mean flux over the grid cell by the integral

$$(1) \quad \bar{Q}^a = \frac{1}{\Omega} \iint_{\Omega} [A Q^i(x, y) + (1 - A) Q^o(x, y)] dx dy.$$

When the fluxes  $Q^o$  and  $Q^i$  are known, this integral is well defined. More challenging is the problem to find  $Q^o$  and  $Q^i$  for a given  $\bar{Q}^a$ . This is normally done with a sub-grid interpolation method.

As a principle, all fluxes that are sub-grid interpolated with information from the ice model (sea ice concentration, surface temperatures and albedo), are sub-grid interpolated at every thermodynamic time step of the ice model. This is to ensure that best possible information of the surface conditions is always utilized. It also makes it easier to construct a consistent and heat conserving scheme in this way. The computational overhead of the sub-grid interpolation is negligible compared with the rest of the calculations in the ice model.

### 3.1 Solar heat fluxes

For the net short-wave radiation an albedo-weighted sub-grid interpolation is used, that is,

$$(2) \quad Q_{sw}^o = \frac{1 - \alpha^o}{1 - \alpha^{ref}} \bar{Q}_{sw}^a \text{ and } Q_{sw}^i = \frac{1 - \alpha^i}{1 - \alpha^{ref}} \bar{Q}_{sw}^a,$$

Here  $\alpha^i$  and  $\alpha^o$  are the ice/snow and ocean albedo, respectively. The constraint of heat conservation defines the reference albedo equal to the mean albedo of the atmospheric grid cell as

$$(3) \quad \alpha^{ref} = \bar{\alpha} = \frac{1}{\Omega} \iint_{\Omega} [A\alpha^i + (1 - A)\alpha^o] dx dy.$$

The ice ocean albedo is calculated in the ice model and transferred to the atmosphere model where it is combined with the land surface albedo in regions that are partially covered by land. Therefore, the net solar heat-flux in the atmosphere model is a mix of that absorbed in the ice/ocean system and that absorbed at land. However, because the coupler knows exactly what albedo the atmosphere model has used over the ocean areas of a grid-cell, it can recalculate the absorbed solar radiation from downward solar radiation in a consistent and equal way to that used in the atmosphere model. This ensures conservation of solar heat in the system.

### 3.2 Turbulent fluxes

Surface heat fluxes depends strongly on the surface temperature, so a sub-grid interpolation method where the ice and ocean fluxes are approximated with a Taylor expansion in the surface temperature is widely used, that is,

$$(4) \quad Q^o = \bar{Q}^a + \frac{\partial \bar{Q}^a}{\partial T_s} (T_{SST} - T_s^{ref}),$$

and

$$(5) \quad Q^i = \bar{Q}^a + \frac{\partial \bar{Q}^a}{\partial T_s} (T_{IST} - T_s^{ref})$$

Here,  $T_{SST}$  and  $T_{IST}$  are the sea surface and ice surface temperatures, respectively, and  $T_s$  denotes the surface temperature used to calculate  $\bar{Q}^a$ . By inserting these expressions into (5) the requirement of heat conservation gives naturally the reference temperature as the area-averaged temperature, that is,

$$(6) \quad T_s^{ref} = \overline{T}_s = \frac{1}{\Omega} \iint_{\Omega} [AT_{IST} + (1-A)T_{SST}] dx dy .$$

This scheme has been modified somewhat in the present version of the coupled system. Generally, the turbulent heat fluxes between the ice or ocean surface and the atmosphere have the form

$$(7) \quad Q_H = \rho_a c_{pa} c_H u_{10m} (T_s - T_A)$$

for sensible heat and

$$(8) \quad Q_L = \rho_a L c_L u_{10m} (q(T_s) - q_A)$$

for latent heat. Here  $\rho_a$  is the density of air,  $c_{pa}$  is the heat capacity of air,  $L$  is the latent heat of evaporation or sublimation,  $u_{10}$  is the wind speed at 10-meter height (positive),  $q_A$  is the specific humidity in the air, and  $q(T_s)$  is the saturation specific humidity at temperature  $T_s$ . The heat-exchange coefficients  $c_H$  and  $c_L$  are depending on the static stability of the lower atmosphere. This implies that heat exchange over open water where the air is unstable is much larger than over cold ice where the air is usually stable. Therefore, a constant sub-grid interpolation coefficient such as that used in equations (7) and (8) might not be appropriate.

We use a three-step procedure for the sub-grid interpolation of the turbulent fluxes.

1. We copy the fields from the atmosphere-grid to the ice-grid. Optionally, we may smooth the solution, but have to ensure heat flux conservation.
2. The heat flux is sub-grid interpolated with respect to the surface temperature  $T_s$ , to a distribution that resembles the surface temperature information of the fine ice grid.
3. The high resolved fluxes are partitioned into components above ice and ocean.

To aid the partitioning of the fluxes between ice and ocean, we use information from the heat flux parameterizations already existing in MI-IM. These parameterizations distinguish between the ice and ocean surfaces. We define the sensible heat fluxes over ice and ocean with the MI-IM parameterization as

$$(9) \quad Q_H^* = D_H^i (T_{IST} - T_A)$$

and

$$(10) \quad Q_H^{o*} = D_H^o (T_{SST} - T_A) ,$$

respectively, and from these we define the heat exchange factor  $D_H$  as

$$(11) \quad \overline{D_H} = \frac{1}{\Omega} \iint_{\Omega} [D_H^i A + (1-A)D_H^o] dx dy .$$

The fine-grid interpolated heat flux is then defined as

$$(12) \quad Q_H = Q_H^{a,i} + \overline{D_H} (T_s - \overline{T}_s)$$

where we let  $Q_H^{a,i}$  define the atmospheric flux, copied and optionally conservatively smoothed on the high resolving ice grid. (The result of task 1 in the three-step procedure mentioned over). The constraint of heat conservation is forced at the scale of the atmospheric grid cell, such that

$$(13) \quad \overline{Q_H^a} = \overline{Q_H^{a,i}} = \frac{1}{\Omega} \iint_{\Omega} Q_H^{a,i} dx dy$$

The last step in the three-step procedure is to partition the heat fluxes between the ice and the ocean. The strategy here is simply to rescale the fluxes from equation (9) and (10) with a factor such that heat conservation is achieved,

$$(14) \quad Q_H = A Q_H^i + (1 - A) Q_H^o = \gamma_H [A Q_H^{i*} + (1 - A) Q_H^{o*}]$$

with the rescale factor limited such that  $0 < \gamma_H < 10$ . If the calculated factor is outside this range, it is a symptom of inconsistency between the fluxes calculated in the atmosphere model, and the present state of the ice model. The ad hoc solution is then to ensure heat conservation by setting

$$(15) \quad Q_H^i = Q_H^{i*} + Q_H - (A Q_H^{i*} + (1 - A) Q_H^{o*})$$

and

$$(16) \quad Q_H^o = Q_H^{o*} + Q_H - (A Q_H^{i*} + (1 - A) Q_H^{o*}).$$

The latent heat flux is handled similar as sensible heat by using equation (8) and the procedure defined through (9) to (20). Evaporation rates over ice and ocean are calculated consistent with the latent heat fluxes, and rescaled to give conservation of the humidity flux.

### 3.3 Surface stress

At present, the same surface stress is used in both the ocean model and the sea ice model. We have not sub-grid interpolated this with respect to the difference in drag over ice and open water. However, near land, a fix is done to avoid the large stress due to topography that is blended into the stress from HirHam. In all atmospheric grid-cells with a land-fraction  $> 0$ , we calculate a new stress from the wind speed with a drag coefficient consistent with the value used over ice in HirHam. In this way we are not conserving the total stress, but it has been found more important to avoid the unrealistic large topography influenced stress than fully conserve momentum in this regional model.

### 3.4 Runoff

In this version of the coupled system, a proper treatment of runoff is not implemented. Only climatologic river runoffs from some large and important rivers are included in the system. An inclusion of true runoff from the atmosphere model is planned in the near future.

## 4. A challenge with fast varying ice-concentration

During cold conditions a sudden opening of the sea ice exposes the warm ocean surface to the cold atmosphere and this implies a huge flux of heat (sensible, latent and long wave radiation) from the ocean into the atmosphere. If the ice refreezes or closes due to advection during the next coupling time step, the heat flux that the ice model receives from the atmosphere model might be too large to give a realistic ice surface temperature due to the lag in time between when fluxes are calculated in HirHam and when they are used in MI-IM. The  $T_{IST}$  can be far too cold due to the strong cooling. In the next coupling time step, the atmosphere model sees this very cold surface tries to heat the surface again with a large downward heat flux. This might develop into an unstable situation where the thermodynamic inertia of the surface is too low to absorb the changes in heat flux from the atmosphere. This situation might be unstable because the atmosphere model over-compensates the changes in surface temperature of the ice. The situation is most likely to occur when the sea ice is thick and snow covered. Then the ice surface temperature is more or less free to respond to the atmospheric fluxes due to the large insulating effect of the thick ice and snow.

The challenge is to get a realistic ice/snow temperature and at the same time conserve heat. The situation occurs when the heat flux from the atmosphere is inconsistent with that the ice surface can receive. To solve the problem we have opted to relax the point in the coupling strategy requiring that fluxes should only be calculated once. We calculate the ice surface temperature with a sensible heat steering from the 2-meter air temperature over the ice. Then, again, we calculate a new sensible heat flux consistent with this temperature difference. Generally, this gives a difference between the sub-grid interpolated flux from the atmosphere model and the flux used by the ice model. This heat difference must be stored in the ice/ocean system in a proper way to ensure heat conservation.

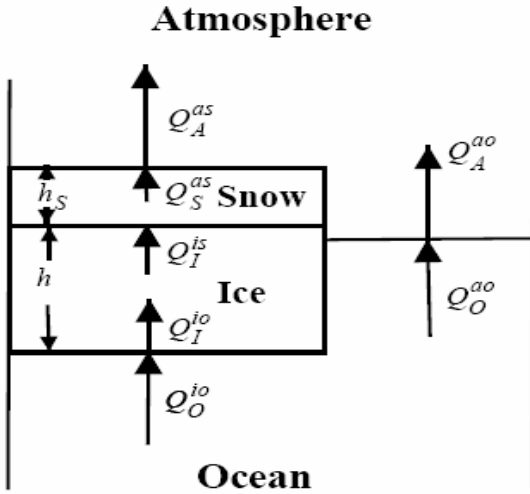


**Figure 1:** Definition of heat fluxes between atmosphere, ice and ocean. The subscript indicates in which medium the flux is valid (A: atmosphere, I: ice, S: snow, and O: ocean). Superscripts denote which interfaces that are relevant for the flux. Thus  $Q_A^{ao}$  is the heat flux from the ocean surface toward the atmosphere and is calculated just above the sea surface, whereas  $Q_O^{ao}$  is the heat flux in the ocean toward the atmosphere-ocean interface and is calculated just below the surface. (*From Røed and Debernard, 2004*).

In MI-IM, internal heat is defined as the energy required melting all the ice in a grid cell. It is formulated as

$$(17) \quad E = \rho_{ice} h_{ice} A q(T, S_{ice}),$$

where  $A$  is the ice concentration,  $\rho_{ice}$  is the ice density,  $h_{ice}$  is the mean ice thickness and  $q(T, S_{ice})$  is the energy required to raise the temperature of an ice parcel to its melting point. It depends on the internal ice temperature  $T$  and ice salinity  $S_{ice}$ , as defined by *Røed and Debernard (2004)*. A conservation law for  $E$  is formulated as

$$(18) \quad \frac{\partial E}{\partial t} + \nabla \cdot (\mathbf{V}_{ice} E) = A(Q_A^{ai} - Q_O^{io}) + (1 - A)(Q_A^{ao} - Q_O^{ao}),$$

where  $\mathbf{V}_{ice}$  is the ice drift velocity and the  $Q$ 's denotes the various heat fluxes as displayed in Figure 1. Note that last term on the right-hand side of (18) is a term for the open ocean portion of a unit cell. Under normal circumstances this term vanishes due to a balance between the two fluxes  $Q_A^{ao}$  and  $Q_O^{ao}$ . If, however, the sea surface temperature ( $T_{SST}$ ) drops below the freezing point of seawater, an imbalance in these fluxes exists and new ice will grow. This in turn contributes to a change in the heat required to melt all the sea ice.

From this definition of the heat content of sea ice it is clear that the excess heat can be stored in the ice in two different ways: In the sea ice, by changing the temperature of the ice, or by changing the ice mass. The first gives a relative low heat capacity for cold or thin ice,

while the latter gives a large heat capacity. In an ice-ocean system there is also possible to store heat in the upper ocean. This has a huge heat capacity and will give a feedback to the ice by changing the freezing and melting rate. In a numerical model, there is also an opportunity to use an artificial heat buffer, which ensures heat conservation over a few coupling time-steps.

In the present implementation, we have opted to store the excess heat in the upper ocean. One argument for this is the ambiguity of the sub-grid interpolation procedure. It is no unique way to do the sub-grid interpolation, and it can be argued that it is a failure in this methodology that gave the inconsistent heat flux to the ice model. The way we transfer the heat difference to the ocean is by modifying the freezing rate over open water or heat flux over open water. In this way, we change the results from the other component of the sub-grid interpolation: the atmosphere-ocean heat flux. This correction is done locally in the ice grid point. If no open water is present ( $A = 1$ ), the ice-ocean heat flux is modified instead.

## 5. Model set-up

### 5.1 Models

HirHam is the atmosphere model in the coupled system and is described in Christensen et al. (1996). The dynamics of the model is taken from the HIRLAM (version 2) model and a leapfrog advection scheme is applied. The physical parameterization is originally taken from the ECHAM4 model with some minor changes. Horizontal resolution is 0.5 degree, while the model in this configuration applies 19 vertical levels. The vertical coordinate is sigma-p, which is terrain following near the surface and following pressure-surfaces in the free atmosphere.

The ice model MI-IM is described in detail in by *Røed and Debernard (2004)*. It has intermediate complexity thermodynamics with one ice layer that includes fully prognostic internal energy, ice concentration and ice mass, while the heat capacity of the snow layer is neglected. The snow is insulating, reflective and has a latent heat contribution to the total heat budget of the model. The momentum equations in MI-IM are discretized with the elastic viscous plastic rheology of *Hunke and Dukowicz (1997)*.

The ocean component of the ORCM is a local *met.no* version of MICOM (Miami Isopycnic Coordinate Ocean Model), which is a dynamic-thermodynamic ocean general circulation model developed by *Bleck et al. (1992, see also references therein)*. The

configuration of the 27 density layers is equal to that used by *Røed and Debernard, 2004* and *Debernard and Røed, 2005*.

## 5.2 Area and grid

HirHam uses a rotated spherical grid of 0.5x0.5 degree resolution covering the Arctic Ocean, most of Europe and the Atlantic Ocean north of approximately 55 degrees north (Figure 2.)

MI-IM and MICOM uses a grid with the same orientation as the atmospheric grid, but with a resolution of 0.25x0.25 degree. The grid is completely overlapping with the atmospheric grid.

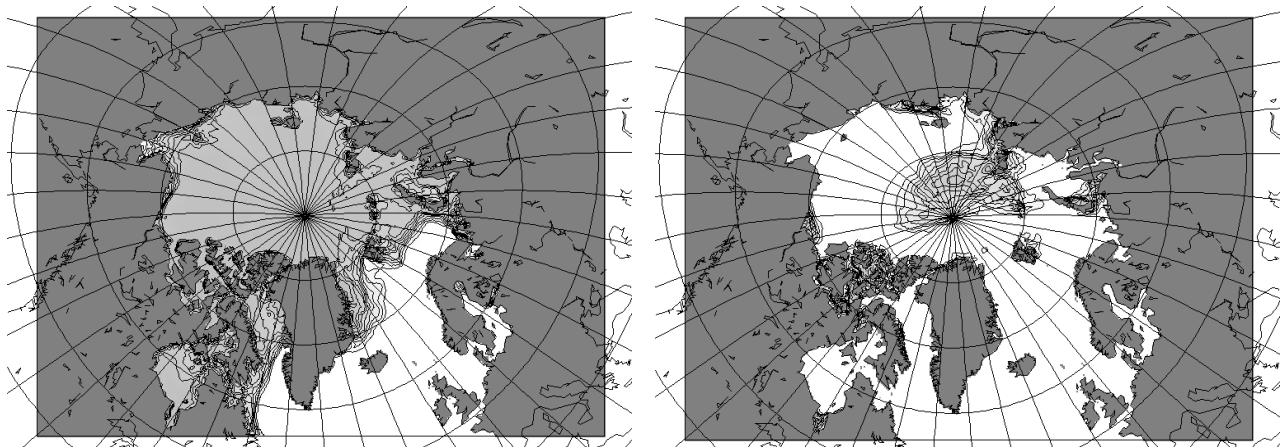


**Figure 2:** Area of the present set-up of the ORCM. Sea ice concentration for March (left) and September (right) 1996 from the first coupled experiment is shown as light gray and with 10% contour intervals. The sea ice and ocean models do not include the Bering Sea, where the atmosphere model relies on surface information from the ERA40 reanalysis (not shown).

## 5.3 Initial and boundary conditions

In the first experiment with the system, HirHam has been forced at open boundaries with 6-hourly fields from the ERA40 reanalysis project for the period 1990-1999. These reanalysis is also used as initial condition in the model.

MI-IM is started from rest, initialized with 90% concentration of 2-meter thick sea ice covered with 5 cm of snow in all regions with SST less than -1 degrees Celsius.

MICOM is also started from rest, with a hydrography specified from the climatology of *Levitus and Boyer (1994)* and *Levitus et al. (1994)*. At lateral boundaries, a small FRS-zone is used, with relaxation of hydrography to the monthly values specified by the climatology, but

with no inflow of water. In this setup the model has a severe underestimation of the barotropic inflow into the Nordic Seas.

## 6. Results from the first 10-year coupled experiment

A 10-year experiment where the ERA40 reanalysis is downscaled is used as a first test of the system. Quite long simulation periods are required to adjust the ice and ocean states to the atmospheric forcing. However, a 10-year period seems to be long enough for sea ice to stabilize. For the ocean a 10-year period is too short to give a full spin up of the currents and hydrography. However, due to the small area used here, and the somewhat crude implementation of the southern open boundary condition, we cannot expect truly realistic ocean response even if we increase the simulation time further. *Debernard et al. 2003* has described a more proper handling of the open boundary in the coupled system, but that method has not been implemented in the present version of the system.

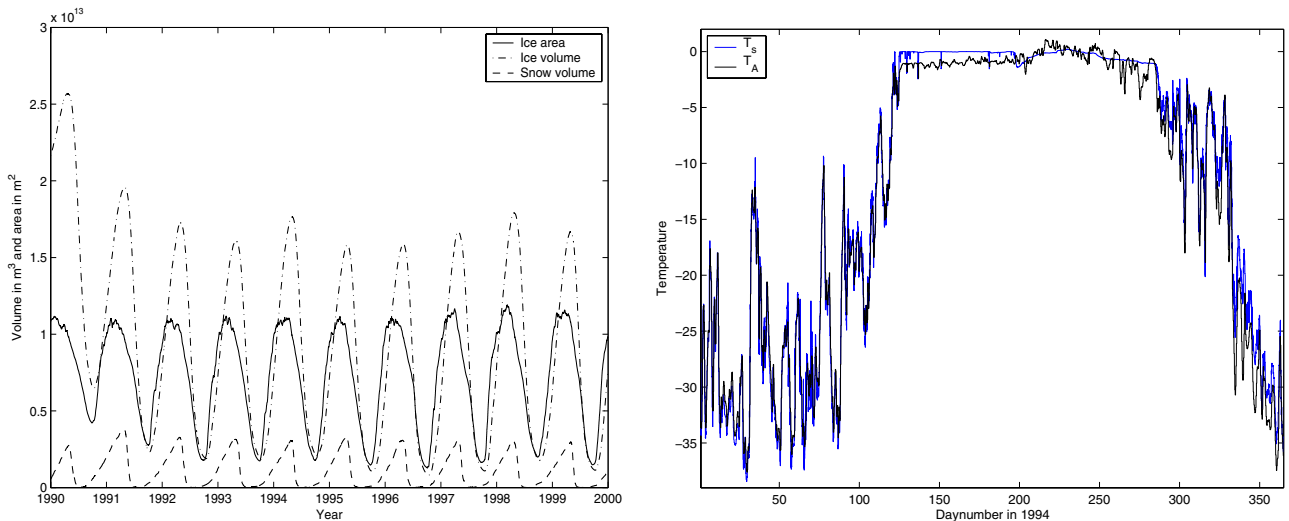


**Figure 3:** Left panel shows the sea ice area (solid line), ice volume (dashed line) and snow volume (dashed-dotted line) for the 10-year coupled integration. Right panel shows the development of the surface temperature  $T_s$  (blue) and 2-meter air temperature  $T_A$  (black) during 1994.

### 6.1. Ice volume

As evident from Figure 3 left panel, the coupled system is loosing sea ice in the present configuration. This is both due to a strong reduction in the ice-covered area in summer (Figure 2) and due to a low ice thickness in winter. A similar picture has been observed in stand-alone simulations with MI-IM coupled to MICOM (*Røed and Debernard (2004)* and *Debernard and Røed (2005)*), but the picture seems to be even worse in the coupled system.

This worsening can at least partly be explained with the coupled heat-conserving properties of the system. A too open or thin ice cover will reduce the global albedo so the ice-ocean system will absorb more heat. The heat penetrating the ocean through leads in the ice will heat the upper ocean, which increases the basal melting of the ice. This decreases the ice-concentration further in a positive feedback loop. This mechanism is evident in both coupled and uncoupled versions of the system. However, in the fully coupled model, more open water and an increase in the ocean temperature will also increase the air temperature, and perhaps more important, in the autumn the ocean mixed layer that has been warmed during summer has to be cooled by the atmosphere before sea ice can start to form. In an uncoupled system, the atmosphere has more or less an infinite heat capacity so this is not a big problem. However, in a coupled system this warm ocean will delay the autumn freezing and trap heat in the upper ocean beneath the sea ice. This will then give too small ice thickness during the winter. The thin ice and low ice concentration in both stand-alone and coupled experiments seems to indicate that refinements or tuning of the ice model might be necessary to give a more realistic ice cover.

## 6.2. Temperature over ice

Figure 3 right panel, depicts time-series of surface temperature  $T_s$  and 2-meter temperature  $T_A$  for a grid-point near the North Pole for the year 1994. The blue and black curves depict the surface temperature and the air temperature, respectively. As evident, during the winter, the two are very closely linked and their difference is relatively small. However, after an abrupt warming during the spring, the surface temperature is stabilizing at 0 degrees Celsius around start of May, while the air temperature is stabilizing near -2 degrees. This seems to indicate that it is radiation, and most likely solar radiation that are the important component of the surface heat budget for starting the melting of the snow and ice. The sensible heat flux is all the time cooling the surface in this situation. During the summer all the ice at this grid-point disappears and then the ocean temperature influences the surface temperature. Solar heat of the ocean then rises the temperature of the ocean mixed layer, and as a consequence of that rises the air temperature above 0 degrees Celsius.

Our first impression is that the snow cover over sea ice is disappearing too early in the summer. This might be due to a too low ice thickness at the end of the winter or a deficiency of the surface heat budget. Stronger sensible cooling, or more heat conduction through the snow and ice might bring the surface temperature below zeros degrees. That will prevent melting and increase the surface albedo.

### 6.3. Comparison with a stand-alone simulation with HirHam and ERA40 reanalysis

**Temperature:** The annual cycle of monthly mean 2-meter temperature from the coupled simulation is depicted in Figure 4 (left) together with results from a stand-alone simulation with HirHam and data from the ERA40 reanalysis. It is evident that both model simulations are warmer than ERA40 during the winter, spring and autumn. Compared with the stand-alone simulation the coupled model is slightly colder during the winter and spring, but considerably warmer during the autumn. This may be a consequence of the storage of heat in the ocean due to the low ice concentration, which delays the autumn freezing in the coupled system. Another effect that may explain the delayed autumn is that the ice thickness in ERA40 and the stand-alone simulation are fixed at values that are constant during the whole winter. This will overestimate the insulating effect of the ice cover in autumn compared with later in the winter.

**Clouds:** The right panel of Figure 4 shows the total cloud cover from stand-alone and coupled simulations (no comparison with ERA40). The coupled model shows more clouds than the stand-alone version. The consequence is a reduced solar insulation in early spring, but also an increased downward radiation during winter. More open water during summer and autumn give more evaporating over the Arctic Ocean during these times of the year, but it is not clear that this should give an increased cloud cover during the whole year.

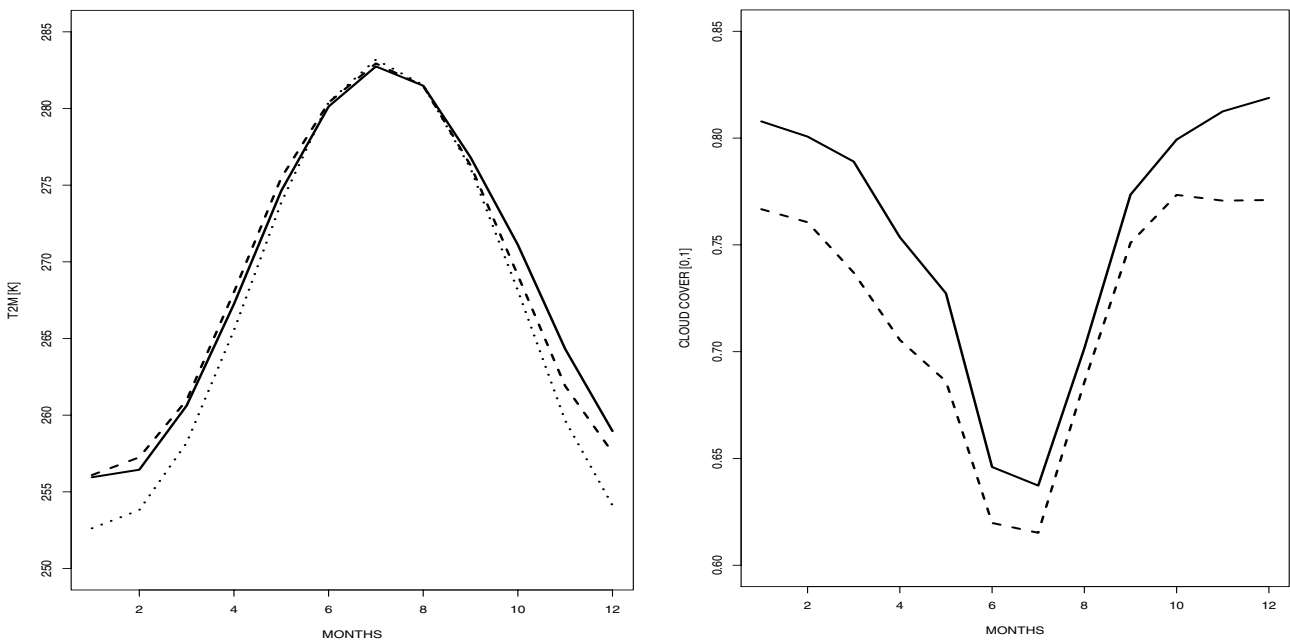


**Figure 4:** Annual cycle of mean 2-meter temperature (left) over the domain shown in Figure 2 for coupled model (solid line), stand-alone HirHam (dashed line) and ERA40 (dotted line). The right panel shows the total cloud cover from the coupled and stand-alone simulations.

**MSLP:** Figure 5 shows a time-series of monthly values of area-averaged mean sea level pressure (MSLP) for the coupled model (solid line), stand-alone HirHam (dashed line) and ERA40 (dotted line). The correlation between the curves seems quite good, but the amplitudes of the extreme peaks are generally larger in the coupled model than in the two others. The coupled model has much more freedom to depart from ERA40 than the stand-alone model due to an interactive and different surface state.

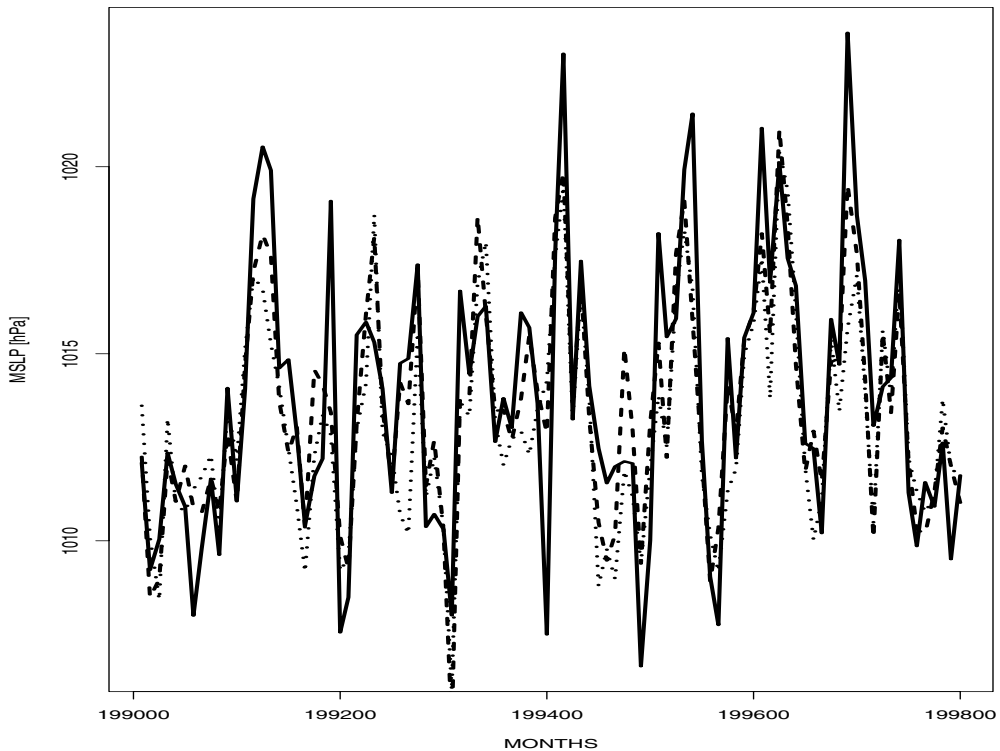


**Figure 5:** The time-evolution of the mean sea level pressure averaged over the domain for coupled model (solid line), stand-alone HirHam (dashed line) and ERA40 (dotted line).

## 7. Summary and final remarks

The technical coupling methods used in ORCM are documented, and the sub-grid interpolation methods used when fluxes are transferred from the coarse atmosphere grid to the higher resolving ice/ocean grid are described in detail in this report. We have also seen the first promising results from this system, thus still there are some unresolved items that should be improved. The most important of these are the open boundary condition in the ocean model, the runoff scheme, and tuning of the ice model to give more realistic ice thickness and volume. We think this latter point is most important for simulating stable sea ice conditions in the coupled model. The relatively simple thermodynamics in MI-IM may underestimate ice thickness because most of the ice-growth in the Arctic is under thin ice that later is ridged into

thicker ice by mechanical deformation. This process is poorly modeled in MI-IM with only one ice thickness category. The ice can be ridged in the model, and this leaves open water that refreezes fast, but once this is done the model has only one mean ice thickness. Thermodynamically, this can be quite thick, but it may still be too thin compared with observed ice volumes. In addition, MI-IM has an empirical equation for the sea ice concentration that includes critical parameters for the increase and decrease of ice concentration due to freezing and melting. These parameters have to be tuned. Because much of the problems with too little sea ice are also present without the atmosphere model, most of this issue can be solved in the coupled ice-ocean system.

Even with too little sea ice, the ORCM shows promising results in the first 10-year integration. Most of the biases compared with stand alone HirHam simulations and the ERA40 seems to be due to the strong reduction in summer sea ice extent, and the thin winter sea ice. Further analyses of the results are needed to study the system behavior further, and we know that there are remaining parts that should be addressed, but the system is working well technically and we feel confident that the steps forward to a system that gives a stable, realistic downscaling of reanalysis as ERA40 are short. The issue with too little sea ice is solvable, and the consequences of that for the whole system may be of great importance. Sea ice is a very important component of the Arctic climate system, and a coupled model is punished hard if this quantity is poorly modeled.

## Acknowledgement

Both authors are in whole (JD) or in part (MØK) supported by the Research Council of Norway under the national project RegClim (grant no. 155976/720), and the EU project GLIMPSE (EVK2-2001-00337) (MØK).

## References

- Bleck, R., C. Rooth, D. Hu, and L. T. Smith (1992) Salinity-driven thermohaline transients in a wind and thermohaline-forced isopycnic coordinate model of the North Atlantic, *J. Phys. Oceanogr.*, 22, 1486–1515.
- Christensen, J. H., O. B. Christensen, P. Lopez, E. van Meijgaard and M. Botzet (1996): The HIRHAM4, Regional Atmospheric Climate Model, Danish Meteorological Institute – Scientific Report – Copenhagen.
- Debernard J and L P Røed (2005): Simulations with a North Atlantic coupled ice-ocean model. RegClim General Technical Report 8 (this issue)
- Debernard J, Køltzow M Ø, Haugen J E and L P Røed (2003): Improvements in the sea ice module of the regional coupled atmosphere-ice-ocean model and the strategy and method for the coupling of the three spheres. RegClim General Technical Report 7, pp 59-70.

- Döscher R., Willén U., Jones C., Rutgersson A., Meier H.E.M. and U Hansson (2002): The development of the coupled ocean-atmosphere model RCAO. Rossby Centre, SMHI, S-60176 Norrköping, Sweden.
- Furevik T, Bentsen M, Drange H, Kindem L.K.T., Kvamstø N.G. and A. Sorteberg (2002): Description and Evaluation of the Bergen Climate model: ARPEGE coupled with MICOM. Revised version submitted to Climate Dynamics.
- Hunke, E., and J. Dukowicz (1997) An elastic-viscous-plastic model for sea ice dynamics, *J. Phys. Oceanogr.*, 27, 1849–1867.
- Kauffman B.G and W.G. Large (2002): The CCSM Coupler, Version 5.0, Combined User's Guide, Source Code Reference and Scientific Description. Community Climate System Model, National Center for Atmospheric Research, Boulder, CO, USA.  
<http://www.ccsm.ucar.edu/models>
- Koltzow M (2003): Observation of sea ice albedo. Research Note No. 107, Norwegian Meteorological Institute.
- Levitus S and T P Boyer (1994): Word Ocean Atlas 1994, vol. 4, *Temperature*. NOAA Atlas NESDIS. Vol. 4, 129 pp. Natl. Oceanic and Atmos. Admin., Silver Spring, Md.
- Levitus S, Burgett R and T P Boyer (1994): Word Ocean Atlas 1994, vol. 3, *Salinity*. NOAA Atlas NESDIS. Vol. 3, 111 pp. Natl. Oceanic and Atmos. Admin., Silver Spring, Md.
- Røed LP and J Debernard (2004): Description of an integrated flux and sea-ice model suitable for coupling to an ocean and atmosphere model. Met.no Report 4/2004, Norwegian Meteorological Institute.

# Simulations with a North Atlantic coupled ice-ocean model

by

*Lars Petter Røed<sup>1,2</sup>, Jens Debernard<sup>1</sup>*

<sup>1</sup>Norwegian Meteorological Institute, Oslo, Norway

<sup>2</sup>Institute of Geosciences, University of Oslo, Norway

## Abstract

Through the project RegClim (Regional Climate Development under Global Warming) a coupled ice-ocean model is developed at the Norwegian Meteorological Institute (met.no). The ice model is met.no's in house developed MI-IM code, while the ocean model is met.no's version of the multilayered Miami Isopycnic Coordinate Ocean Model (MICOM). The ice model is integrated with a flux module (coupler) that calculates all fluxes between the atmosphere and ocean based on atmospheric input data in ice covered as well as open ocean areas. The results presented is from two 30 year runs covering the Arctic Ocean, the Nordic Seas, and the Atlantic Ocean north of about 30 degree south, a domain that includes the brackish Baltic as well as the dense bottom waters of the Mediterranean Seas. The atmospheric forcing data are constructed from ECMWF's ERA40 reanalysis data. While the first run (verification run) is forced using a two year cycle covering the years 2000 and 2001, the second run uses the ten year cycle covering the years 1986 through 1995. The system is initialized with Levitus type ocean climatology and an ice cover 2 m thick and of 90% concentration in areas with temperatures less than -0.5°C. Results emanating from the experiments show that the coupled model produces a stable climate that repeats itself after about 5 years of integration. Despite the coarse resolution the model fairly well represents the northward transport of warm and saline water masses toward the Nordic Seas. The model produces steady overflows from the Nordic Seas that spreads into the Atlantic Ocean. This indicates that the model establishes an Atlantic meridional overturning circulation as part of the mean meridional northward heat transport.

## 1. Introduction

Considered are results obtained with a coupled ice-ocean model covering the North Atlantic Ocean (including the Arctic Ocean) north of 30°S. It consists of the ocean model MICOM (Bleck et al., 1992) coupled to a dynamic-thermodynamic sea-ice model (Røed and Debernard, 2004).

To refine and enhance the climate scenarios simulated by coupled global climate models (AOGCM's) it is customary today to nest a regional finer mesh atmosphere only model (ARCM) into the coarser mesh AOGCM. Such a scheme is commonly referred to as dynamic downscaling (e.g., Jones et al, 1995, Bjørge et al., 2000). The ARCMs, often being developed from NWP models, are usually equipped with a soil model that computes and thus changes the surface values over the land portion of the integration area over those produced by the AOGCM. At the same time the surface values prescribed by the AOGCM over that portion of the computational domain covered by open ocean or sea-ice is retained. One such important surface value is the albedo, which then changes in accord with the regionally (re)computed snow cover. Thus the ARCM is allowed to change the radiation conditions over land surfaces, but not over the sea-ice and ocean surfaces. This is slightly inconsistent, in particular taking into account that, e.g., 70% of the total computational domain of an ARCM used to perform a dynamical downscaling for Scandinavia is either open ocean or sea-ice covered (Bjørge et al., 2000). Thus when performing a dynamical downscaling of a global climate scenario the model used should also be allowed to recompute the surface values over ocean areas, in particular if these areas are partly ice covered part of the year.

Scandinavia borders on the Arctic, a domain commonly poorly represented in AOGCMs, and the ocean areas in its immediate vicinity are the Nordic Seas (consisting of the Greenland, Iceland and Norwegian Seas together with the adjacent North Sea and Barents Sea). These are waters that are partly ice covered year round. Given that the ratio of open ocean to ice covered areas is sensitive to the amount of warm and saline water advected toward the Nordic Seas and finally into the Arctic Ocean and the Barents Sea, it may be argued that to be consistent a model that also regionally consists of a coupled atmosphere-ice-ocean model should be employed when performing a dynamical downscaling over Scandinavia. This is the approach taken in the Norwegian national climate project RegClim (Regional Climate Development under Global Warming), where one of the overall aims is to produce scenarios

for regional climate change suitable for impact assessments. A regional coupled atmosphere-ice-ocean model is developed in the project RegClim (Debernard and Køltzow, 2005).

The present model is part of the above development, but coarser mesh version is also used to provide lateral boundary conditions to the regional coupled climate model for the following reasons. Since the sea-ice cover in the Arctic and sub-Arctic portions of the North Atlantic is sensitive to the amount of warm and saline water advected northward through the Nordic Seas, it is of imminent importance that the advection and thereby the amount of warm and salty water toward the Nordic Seas are simulated as correctly as possible too. Normally global climate models utilize mesh sizes of about one degree (e.g., Kiehl and Gent, 2004) or larger. This resolution is poor relative to the dynamical length scale in the ocean that determines such important current systems as the Gulf Stream in the North Atlantic. As argued by Hurlbert and Hogan (2000) the better the resolution the better the representation of the northward advection of warm and salty water, e.g., the Gulf Stream. Thus when using an AORCM to dynamically downscale a global climate scenario limited to an area north of about 50-55°N (Debernard and Køltzow, 2004), it is advantageous to employ an intermediate nested ice-ocean model. This is the purpose of the North Atlantic coupled ice-ocean model presented here. It is designed to act as an intermediate coupled ice-ocean model providing lateral boundary conditions to the more limited and finer mesh regional coupled atmosphere-ice-ocean model. This is accomplished by using the atmospheric forcing directly from the AOGCM, and by using the ocean temperature and salinity of the ocean components of the AOGCM as forcing at its lateral (southern) boundary.

Before the North Atlantic model can be applied in such a setting, it is important to demonstrate that it successfully advects realistic amounts of warm and salty water towards the Nordic Seas. This is the main goal of this presentation.

## **2. The ice-ocean model**

### **2.1 The ocean model component**

The ocean model component is based on a version of MICOM (the Miami Isopycnic Coordinate Ocean Model). MICOM is a three-dimensional, barotropic-baroclinic, general ocean circulation model, utilizing potential density as its vertical coordinate. Hence the vertical coordinate becomes Lagrangian, as opposed to the more common Eulerian geopotential depth. The development of MICOM is summarized in Bleck et al. (1992). It

solves the primitive equations discretized (in the horizontal) on a C-grid employing a split-explicit numerical scheme to expedite the computation of the barotropic and baroclinic modes. The particular version used here is based on the version described in Shi et al. (2001). In the present application it consists of 27 layers, of which the uppermost layer is a mixed layer. The model domain is shown in Figure 1. It includes the Baltic and the Mediterranean Seas, and hence layers are included that represents the very low salinity (brackish) Baltic water masses and the very dense bottom water of the Mediterranean Sea. The model domain extends as far south as 30°S. This is done to ensure that the warm and salty waters crossing the equator is correctly simulated.

The mixed layer interacts with the atmosphere as well as the sea ice as described in the next section. It also interacts with the interior fixed density layers through entrainment/detrainment processes when the mixed layer deepens/retreats based on the bulk formulation of Gaspar et al. (1990). The isopycnic interior layers interact mainly through hydrostatic pressure, but include a weak interlayer mixing based on the scheme suggested by McDougall and Dewar (1998).

The grid is a rotated spherical grid with the ‘North Pole’ located in the Indian Ocean at 15°N and 95°W. The mesh size is about 55 km in the ‘meridional’ direction and varying from 22 km to 55 km in the ‘zonal’ direction. At the open boundary to the south (at about 30°S) the temperature and salinity are specified according to the Levitus climatology linearly interpolated between months. About 35 of the major rivers in the domain are included and supply freshwater to the system by specifying their discharges as excess precipitation at a certain temperature (limited downwards to 0°C). A similar procedure is also used to mimic the inflow of the continuous inflow of 1.1 Sv ( $1 \text{ Sv} = 10^6 \text{ m}^3\text{s}^{-1}$ ) through the Bering Strait (Debernard and Røed, 2002).

## 2.2 The sea-ice model component

The sea-ice model is a fully dynamic-thermodynamic ice model. It consists of three layers, an ice layer, a snow layer and an open water layer. The dynamic part utilizes an elastic-viscous-plastic (EVP) rheology after Hunke and Dukowicz (1997). The advantage is that it makes the numerical scheme explicit by treating the internal stress as an unphysical prognostic variable. The thermodynamic part is based on that of Mellor and Kantha (1989) and Häkkinen and Mellor (1992). The model carries ice velocity, ice concentration, ice thickness, snow thickness, and ice thermal energy as prognostic variables. The latter allows ice frozen in one

region to be melted in another without unduly violating heat conservation (Bitz and Lipscomb, 1999, Debernard et al., 2003). Advection of ice concentration, thickness and thermal energy are all solved employing a version of the positive definite advection scheme due to Smolarkiewicz and Margolin (1998).

The ice model is integrated with a flux module that computes all energy fluxes between the atmosphere and the ocean in a conservative fashion based on a specified atmospheric input (2 m temperature and dew point temperature, cloud fraction, incoming solar radiation, precipitation, 10 m wind velocity, and mean sea level pressure) using bulk formulas (Kara et al., 2000, 2002). As such the formation of sea-ice is a way to store the surplus energy when sea-water freezes. For a more detailed description of the ice model and its integrated flux module (coupler) the reader is referred to Røed and Debernard (2004).

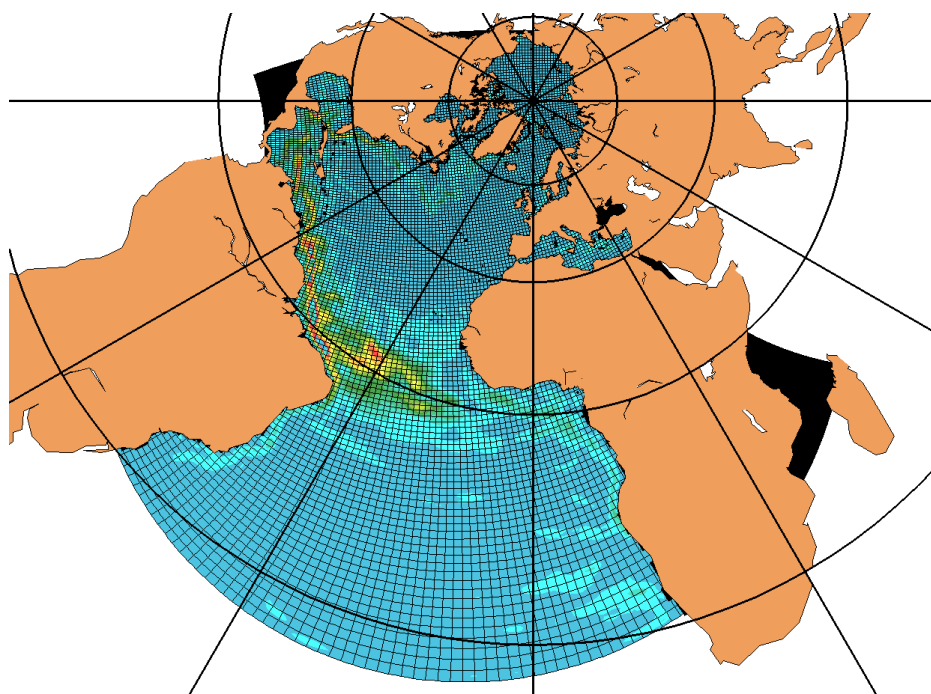


**Figure 1.** Model grid and 5 day mean mixed layer currents 1-6 March 1995-3 (year 30). Colors gives speed in intervals of 10 cm/s. Note the position of the Gulf stream (cf. Figure 6).

### 3. Model simulations and results

The ocean model is initialized with the Levitus climatology, that is, it is initially at rest with a specified distribution of temperature and salinity. Lateral gradients that give rise to internal pressure forcing therefore exists and the ocean is initially in a dynamic imbalance. Likewise

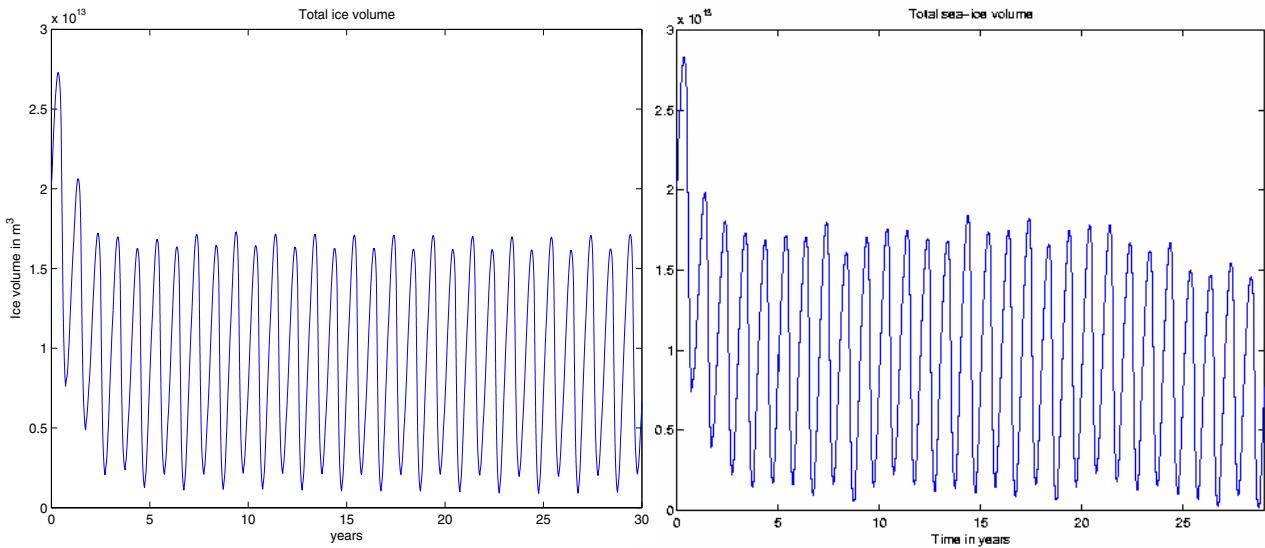


**Figure 2.** Solid curves show total Arctic ice volume (in  $10^{13} \text{ m}^3$ ). Left panel is the 30 year long verification run, while the right panel is the 30 year long validation run. Both runs were initialized with a 2 m thick ice slab and 90% ice concentration in areas where the initial sea surface temperature (SST) were less than  $-1^\circ\text{C}$ , and with a “Levitus” type ocean. The atmospheric forcing was constructed from ECMWF’s ERA40 reanalyses data. While the verification run used a repeated two year cycle consisting of the years 2000 and 2001, the validation run used a repeated 10 year cycle consisting of the years 1986 – 1995. Note the adjustment toward a stable climate in both runs is about 5 years. Furthermore the validation shows signs of a longer time period oscillation (not resolved by the 30 years run).

the sea-ice is initially at rest and is specified as an ice slab 2 m thick whenever the initial surface temperature is less than  $-0.5^\circ\text{C}$ . The initial ice concentration is 90%, while the initial snow thickness is 10 cm.

A motion is forced by applying momentum, heat and salinity fluxes at the atmosphere-ocean and atmosphere-ice interfaces. These are computed within the integrated flux module of the ice model (coupler) based on a specified atmospheric input, which also computes the fluxes at the ice-ocean interface. In the simulations reported here the atmospheric input is extracted from the ECMWF’s reanalyses data (the ERA40 data base). At the lateral southern open boundary the model is forced by specifying the temperature and salinity in accord with the mean monthly values from the Levitus hydrographic database, starting January 1 at 00UTC.

Two 30 year long model simulations are reported here. The first, here denoted the verification run, is forced by applying the two years 2000 and 2001 repeatedly 15 times in a cyclic fashion. Its purpose is to demonstrate that the model quickly reaches a stable climate (a statistical equilibrium) in which the two year cycle repeats itself. The second simulation, here denoted the validation run, is forced by applying the 10 years 1986-1995 repeatedly three times in a cyclic fashion. Besides demonstrating that the model reaches a statistical

equilibrium in this case as well, the purpose is in addition to demonstrate that the coupled ice-ocean model advects a proper amount of warm and salty water toward the Nordic Seas.

### 3.1 Ice volume and distribution

The evolution of the total ice volume in the two 30 year simulations is displayed in Figure 2. As is evident both appear to adjust to a stable climate after about five years of integration. In both cases the maximum total ice volume is about  $1.5-2.0 \cdot 10^{13}$  while the minimum volume is about  $0.1-0.3 \cdot 10^{13} \text{ m}^3$ . Details in the ice distribution and extent vary from year to year. This is displayed in Figures 3 and 4 showing the 5 day mean ice concentration and thickness distribution for the second, respectively, the third 10 year cycle for the period 1-6 April 1995 (that is, after 20 and 30 years respectively). The model simulated ice extent appears, however, not to extend far enough south along East Greenland and along the eastern coast of Canada, and also exhibits too little ice extent in summer (Figure 5) compared to observed average values for the years 1978-1987 (Gloersen et al., 1992). This indicates that there is a surplus of heat added to the system compared to observations.

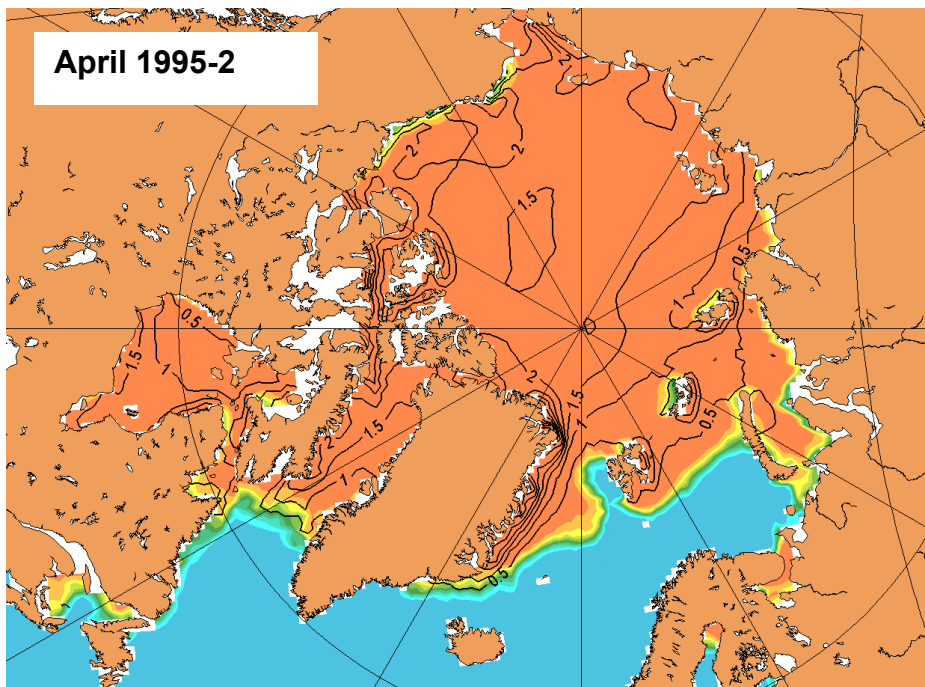


**Figure 3.** Image shows the 5 day mean ice concentration (color coded) and thickness (solid black curves) for April 1-6, 1995-2 (year 20). Contour interval is 10% for ice concentration and 0.5 m for thickness.

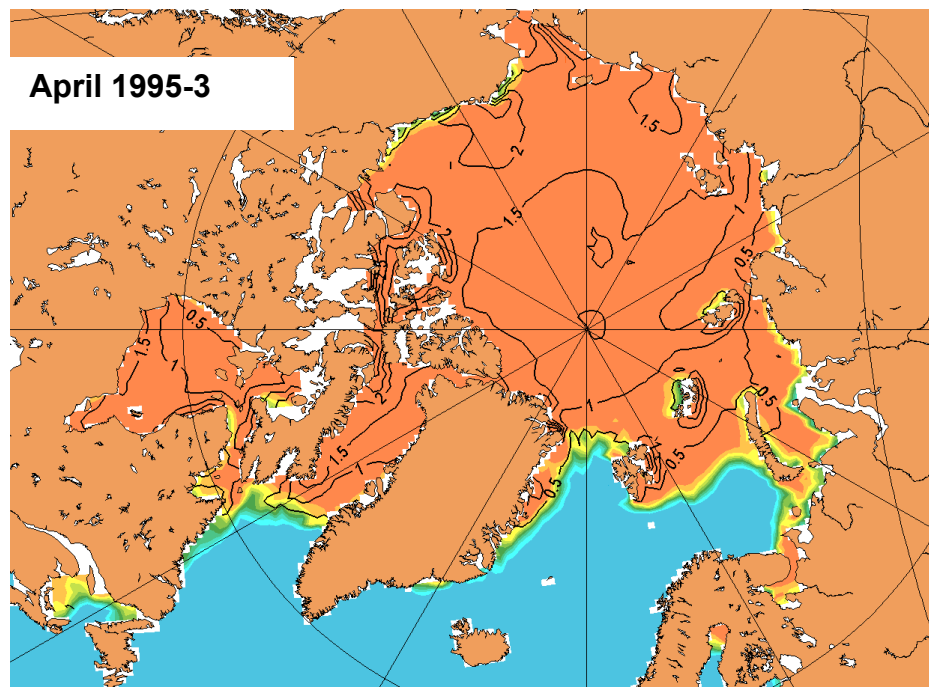


**Figure 4.** As Figure 3, but for 1995-3 (year 30).



**Figure 5.** As Figure 3, but for September 16-21, 1995-2 (year 20).

### 3.2 Ocean circulation

By far the most significant ocean circulation feature in the North Atlantic is the transport of warm and saline water from the equatorial region toward the Nordic Seas and the Arctic Ocean. An important part of this transport is the Gulf Stream exiting the Mexican Gulf

between Florida and Cuba and continuing northward along the US east coast. As it separates from the US east coast (e.g., Figure 6) it becomes unstable and sheds eddies (the so called Gulf Stream rings) to the south and north of its mean path. It is well known that coarse resolution models have difficulties in positioning the separation point of the Gulf Stream correctly. This is also evident in the present simulation by comparing the mean observed SST pattern with that produced by the model (Figure 6). The separation point is clearly shifted northwards resulting in a northward displaced Gulf Stream extension compared to the observations. This is to be expected since the present mesh size of  $1/2^\circ$  is coarse compared to the mesh size required to position the Gulf Stream and its separation from the eastern US coast correctly. Indeed the latter is shown by Hurlburt and Hogan (2000) to be  $1/64^\circ$  or better. The range and absolute values of the SST as indicated in Figure 6 compares, however, satisfactorily with the observations. This confirms that the flux parameterizations employed in the coupler embedded in MI-IM is appropriate for this region. Equally important it indicates that the amount of warm water in the modelled Gulf Stream extension is on target, a necessary requisite for the present model to satisfy its purpose.

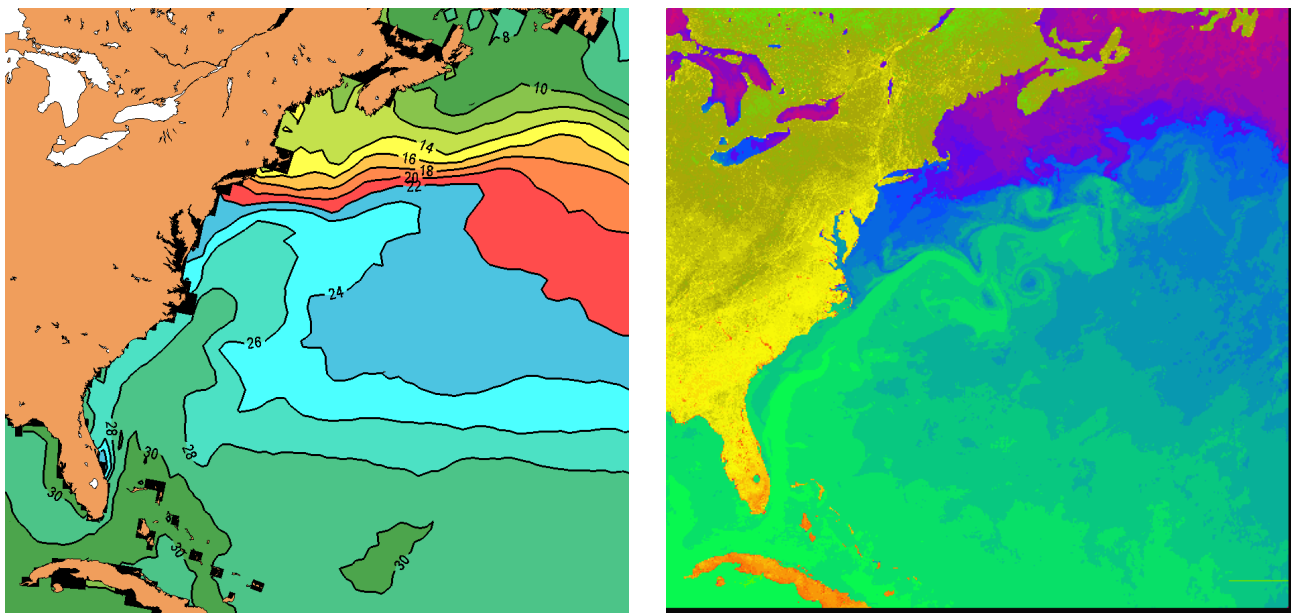


**Figure 6.** Model simulated 5 day mean mixed layer temperature 6-11 June 1995-3 (left panel) and satellite imagery of the Gulf Stream June 1984 (<http://dcz.gso.uri.edu/amy/avhrr.html>) (right panel). In the right panel the temperature in the core of the Gulf Stream ranges between  $25^\circ$  and  $28^\circ\text{C}$  (green colors). The blue-green water below the stream is about  $23^\circ\text{C}$  and the blue water off Long Island is about  $14^\circ\text{C}$ . The lilac water around Nova Scotia is about  $5^\circ\text{C}$ . Note the remarkably good comparison with the model simulated Gulf Stream in view of the coarse resolution employed ( $1/2^\circ$ ).

Another way of analysing the ocean circulation is by inspecting the formation of dense bottom water. The present application employs the canonical diapycnal mixing scheme of McDougall and Dewar (1998). Hence as time progresses the Nordic Seas bottom water, here represented by layer 25 water, crosses the Greenland-Iceland-Scotland ridge and descends into the North Atlantic with no apparent change in its density (Figures 7 and 8). The water mass represented by this layer is clearly too dense compared to observations. Thus application of an enhanced mixing able to make the densest layers to collapse, e.g., the Richardson number dependent mixing scheme described in Shi et al. (2001) or any other or enhanced mixing scheme, is necessary to inhibit the overflow water from the Nordic Seas to the North Atlantic to become too dense. The pathways taken by the overflow water is, however, correctly simulated, and as revealed by Figures 7 and 8 the model appears to produce an almost steady overflow of bottom water from the Nordic Seas to the North Atlantic through the Denmark Strait throughout the 30 year simulation of the validation run. This indicates that the model is able to establish an Atlantic meridional overturning circulation (AMOC). The AMOC in turn is of utmost importance in the northward transport of warm water.

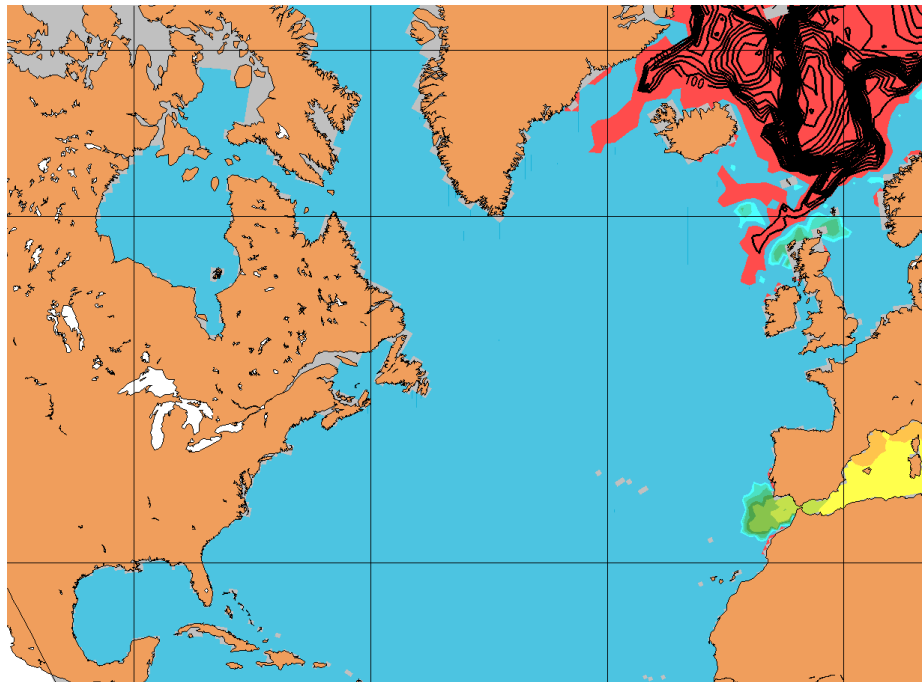


**Figure 7.** Solid curves shows the 5 day mean thickness (contour interval = 100 m) while colors shows the temperature (contour interval 2°C) of layer 25 on May 31, 1986-1 (year 1). Note the difference in temperature between the layer 25 water of the Mediterranean and that of the Nordic Seas. At this time layer 25 water, initially not present in the North Atlantic,

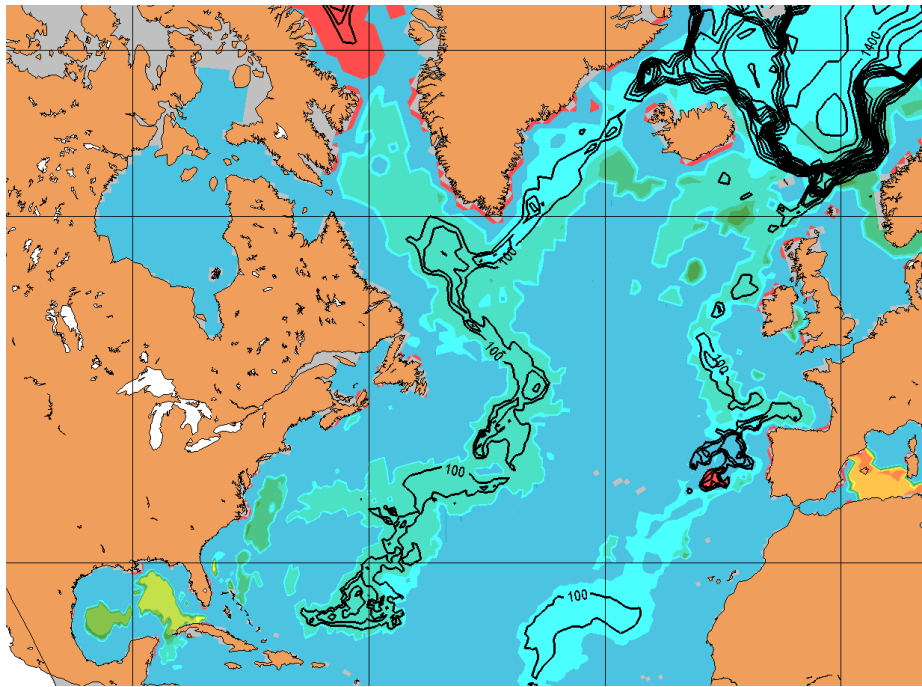


**Figure 8.** Same as Figure 7, but showing the 5 day mean for the period 1-6 December 1995-3 (year 30). Note that most of the overflow water exits through the Denmark Strait. Also noteworthy is that it position itself on the western side of the mid Atlantic Ridge.

#### 4. Conclusions and final remarks

Through the project RegClim (Regional Climate Development under Global Warming) a coupled ice-ocean model is developed at the Norwegian Meteorological Institute (*met.no*). The ice model is *met.no*'s in house developed MI-IM code, while the ocean model is *met.no*'s version of the multilayered Miami Isopycnic Coordinate Ocean Model (MICOM). Results from two 30 year simulations are considered, both commencing from the same initial conditions. The atmospheric fluxes (momentum, heat and salinity) are computed using the flux module integrated within the ice model based on atmospheric data extracted from the ECMWF's ERA40 data base. The first simulation is based on the years 2000 and 2001 repeatedly applied in a cyclic fashion 15 times, while the second is based on the ten years 1986-1995 repeatedly applied in a cyclic fashion three times. The results are analysed with a view to the models ability to reach a stable climate and its ability to transport warm and saline water from the equator region toward the Nordic Seas.

It is demonstrated that a fairly coarse resolution ( $1/2^\circ$ ) coupled ice-ocean model for the Atlantic basin domain that includes the adjacent Arctic Ocean, the Nordic Seas, the Baltic Sea, and the Mediterranean Sea is successfully developed and implemented at *met.no*. Furthermore, the two 30 years simulations performed show that the model fairly well

reproduces today's oceanic climate at this coarse resolution, and that the ice cover, mixed layer temperature and current adjusts to today's climate after about five years of integration from an unbalanced initial state. It is concluded that despite the coarse resolution employed the northward flow of warm and saline water is fairly well described. Finally it is noted that the model establishes an Atlantic meridional overturning.

The analysis also reveals several shortcomings in the results, in particular that there is too little ice coverage in the summer, and that the Atlantic fills up with too dense water. Work is now underway to remedy these shortcomings. starts to flow across the Greenland-Iceland-Scotland ridge and to descend into the abyss of the North Atlantic.

## References

- Bitz, C. M., and W. H. Lipscomb, 1999: An energy-conserving thermodynamic model of sea ice. *J. Geophys. Res.*, **104**(C7), 15,669-15,677.
- Bjørge, D., J. E. Haugen, and T. E Nordeng, 2000: Future climate in Norway; dynamical downscaling experiments within the RegClim project. DNMI Research Report No. 103, Norwegian Meteorological Institute, Oslo, Norway. [Available from the Norwegian Meteorological Institute, Box 43 Blindern, N-0313 Oslo, Norway.]
- Bleck, R., C. Rooth, D. Hu, and L. T. Smith, 1992: Salinity-driven thermocline transients in a wind- and thermohaline-forced isopycnic coordinate model of the North Atlantic. *J. Phys. Oceanogr.*, **22**, 1486-1505.
- Debernard, J., and L. P. Røed, 2002: Implementation of rivers in met.no's MICOM-version. RegClim - General Technical Report No. 6, 115-118. [Available from the Norwegian Meteorological Institute, Box 43 Blindern, N-0313 Oslo, Norway.]
- Debernard, J., and M. Ø. Køltzow, 2005: Technical documentation of the Oslo Regional Climate Model version 1.0. This volume, pp. xx-xx.
- Debernard, J., M. Ø. Køltzow, J. E. Haugen and L. P. Røed, 2003: Improvements in the sea ice module of the regional coupled atmosphere-ice-ocean model and the strategy for and method for the coupling of the three spheres. RegClim – Technical Report No. 7, 59-69. [Available from the Norwegian Meteorological Institute, Box 43 Blindern, N-0313 Oslo, Norway.]
- Gaspar, P., Y. Gregories, and J.-M. Lefevre, 1990: A simple eddy kinetic energy model for simulations of the oceanic vertical mixing: Tests at station papa and long-term upper ocean study site. *J. Geophys. Res.*, **95**, 16,179-16,193.
- Gloersen, P., W. J. Campbell, D. J. Cavalieri, J. C. Comiso, C. L. Parkinson, and H. J. Zwally, 1992: Arctic and Antarctic sea ice, 1978-1987: satellite passive-microwave observations and analysis. NASA SP-511, National Aeronautics and Space Administration, Washington D.C., 290 p.
- Häkkinen, S., and G. L. Mellor, 1992: Modeling the seasonal variability of a coupled Arctic ice-ocean system. *J. Geophys. Res.*, **97**(C12), 20,285-20,304.
- Hunke, E., and J. Dukowicz, 1997: An elastic-viscous-plastic model for sea ice dynamics. *J. Phys. Oceanogr.*, **27**, 1849-1867.
- Hurlburt, H. E., and P. J. Hogan, 2000: Impact of 1/8° and 1/64° resolution on Gulf Stream model-data comparisons in basin scale subtropical Atlantic Ocean models. *Dyn. Atmos. Oceans*, **32**, 283-329.
- Kara, B. A., P. A. Rochford, and H. E. Hurlburt, 2000: Efficient and accurate bulk parameterizations of air-sea fluxes for use in general circulation models. *J. Atmos. Ocean Tech.*, **17**, 1421-1438.
- Kara, B. A., P. A. Rochford, and H. E. Hurlburt, 2002: Air –sea flux estimates and the 1997-1998 ENSO event. *Bound.-Layer Meteor.*, **103**, 439-458.
- Kiehl, J. T., and P. R. Gent, 2004: The Community Climate System Model, Version 2. *J. Clim.*, **17**, 3666-3682
- McDougall, T. J., and W. K. Dewar, 1998: Vertical mixing, cabbeling, and thermobaricity in layered models. *J. Phys. Oceanogr.*, **28**, 1458-1480.
- Mellor, G. L., and L. Kantha, 1989: An ice-ocean coupled model. *J. Geophys. Res.*, **94**(C8), 10,937-10,954.
- Røed, L. P., and J. Debernard, 2004: Description of an integrated flux and sea-ice model suitable for coupling to an ocean and atmosphere model. *met.no report 4/2004*, 51 p, Norwegian Meteorological Institute, Oslo, Norway, ISSN 1503-8025. [Available from the Norwegian Meteorological Institute, Box 43 Blindern, N-

- 0313 Oslo, Norway.]  
Shi, X. B., L. P. Røed, and B. Hackett, 2001: Variability of the Denmark Strait overflow: A numerical study. *J. Geophys. Res.*, **106(C10)**, 22,277-22,294.  
Smolarkiewicz, P. K., and L. G. Margolin, 1998: MPDATA: A Finite-Difference Solver for Geophysical Flows. *J. Comp. Phys.*, **140**, 459-480.



## **Aspects of validation of a North Sea model**

**by**

**Bjørn Ådlandsvik**

Institute of Marine Research and Bjerknes Centre for Climate Research, Bergen

### **Abstract**

The Regional Ocean Model System (ROMS) has been set up for the North Sea in a preliminary validation study before applying the model to downscale results from global coupled atmosphere-ocean models. The period from spring 1988 to autumn 1994 has been simulated with atmospheric forcing from the NCAR/NCEP reanalysis. The oceanic forcing at the lateral boundaries and the freshwater run-off including Baltic are taken from climatology. The model reproduces the main current system with Atlantic inflow from north and a fresh coastal current. The overall results show a rapid freshening of the North Sea for the first 18 months, until a new salt balance has formed. The model results are compared to the regular coastal station Lista at the southern tip of Norway. The model reproduces the seasonal cycle and much of the interannual variability in the hydrography of the Norwegian Coastal Current. The results are encouraging for the use of ROMS as a downscaling tool for a shelf sea like the North Sea. The limiting factor seems to be the quality of the forcing data used.

## 1. Introduction

For studies of the effects of future climate change in the North Sea ecosystem, scenarios on the future marine climate are needed. The North Sea is a shallow shelf sea where fine scale topographic features and shelf processes like strong tidal mixing are important. Therefore, results from global or Atlantic scale ocean general circulation models may not be directly applicable. The volume and properties of the variable Atlantic inflow to the North Sea is a major factor for the local marine climate. This inflow is to a high degree controlled by regional atmospheric forcing. On this background we have chosen to use a state-of-the-art shelf sea model to downscale scenarios from larger scale climate models.

A necessary step before downscaling future climate scenarios is to validate the shelf model and the coupling techniques for the present climate. This report presents some of the results obtained in this direction. Emphasis is put on the mean properties and the Norwegian Coastal Current. In addition the model results have been compared to observed vertical sections. These results will be presented elsewhere.

## 2. The Regional Ocean Model System

The shelf model chosen for regionalization in the RegClim project is the Regional Ocean Model System (ROMS). This is a community model developed by Hernan Arango at Rutgers University and Alexander Shchepetkin at UCLA. The model is 3D baroclinic based on the primitive equations. The methods are explained in a series of papers by Shchepetkin and McWilliams (1998, 2003, 2005) and Ezer et al. (2002). The ROMS model uses relative high order numerical schemes including a vertical parabolic spline representation. ROMS has been designed from the ground for effective parallelisation with shared memory (OpenMP) or distributed memory (MPI) parallelisation from the same Fortran 95 code.

Vertically, the model uses a generalized sigma-coordinate system called s-coordinates (Song and Haidvogel, 1994). Compared to the standard sigma-coordinates this allows improved resolution near surface and bottom in the deeper parts of the domain. In the horizontal, general orthogonal curvilinear coordinates are used. The model uses finite differences with a time splitting between the fast 2D barotropic mode and the slower baroclinic 3D mode.

The ROMS code offers a large degree of flexibility. A wide choice of vertical mixing schemes, including the non-local KPP (Large et al., 1994) and the Generic Length Scale second order turbulence closures (Umlauf and Burchard, 2003; Warner et al., 2005). As described by Ådlandsvik and Budgell (2003), the ROMS code have been locally extended at Institute of Marine Research in certain aspects. Most important for the present work is the inclusion of an NCEP flux module, and the Flow Relaxation Scheme (FRS) at the open boundary.

### 3. Model set-up

The model domain is shown on figure 1. It uses an isotropic stretching, with resolution from 3.5 km in Kattegat to 6.5 km north west of Ireland. In the vertical there are 32 vertical levels, with increased resolution near surface and bottom.

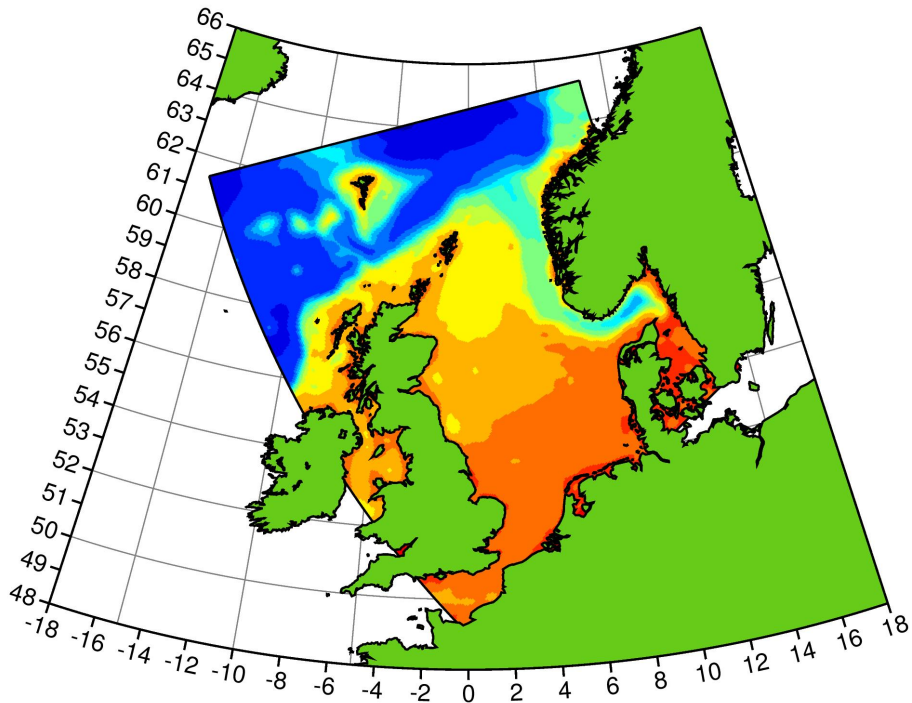


**Figure 1.** The model domain with bottom topography.

For vertical mixing the GLS formulation of the Mellor-Yamada level 2.5 turbulence closure is used. There is no explicitly imposed horizontal mixing. At the open boundaries, the 2D variables are handled with a combination of the Chapman and Flather schemes (Marchesiello et al., 2001), while the 3D variables use the FRS. The model is initialized with the monthly DNMI-IMR diagnostic climatology (Engedahl et al. 1998).

The atmospheric forcing is taken from the NCAR/NCEP reanalysis. The daily averaged fluxes corrected for model surface temperatures following an algorithm from Bentsen and Drange (2000). The fresh water forcing is done by monthly climatological river input. The mean river run-off is 13417 m<sup>3</sup>/s. This method is also used for the Baltic outflow, with a mean value of 13500 m<sup>3</sup>/s and salinity 8. The NCEP precipitation is also included. In the main run, evaporation is not included. In a second and shorter run, evaporation is computed from the latent heat parameterization.

The lateral boundary forcing consists of eight major constituents (K2, S2, M2, N2, K1, P1, O1, Q1) and the monthly DNMI-IMR climatology for the 3D fields. Both simulations start at 1 May 1988. The main run continues until 29 March 1994. The run with evaporation ends at 15 February 2000.

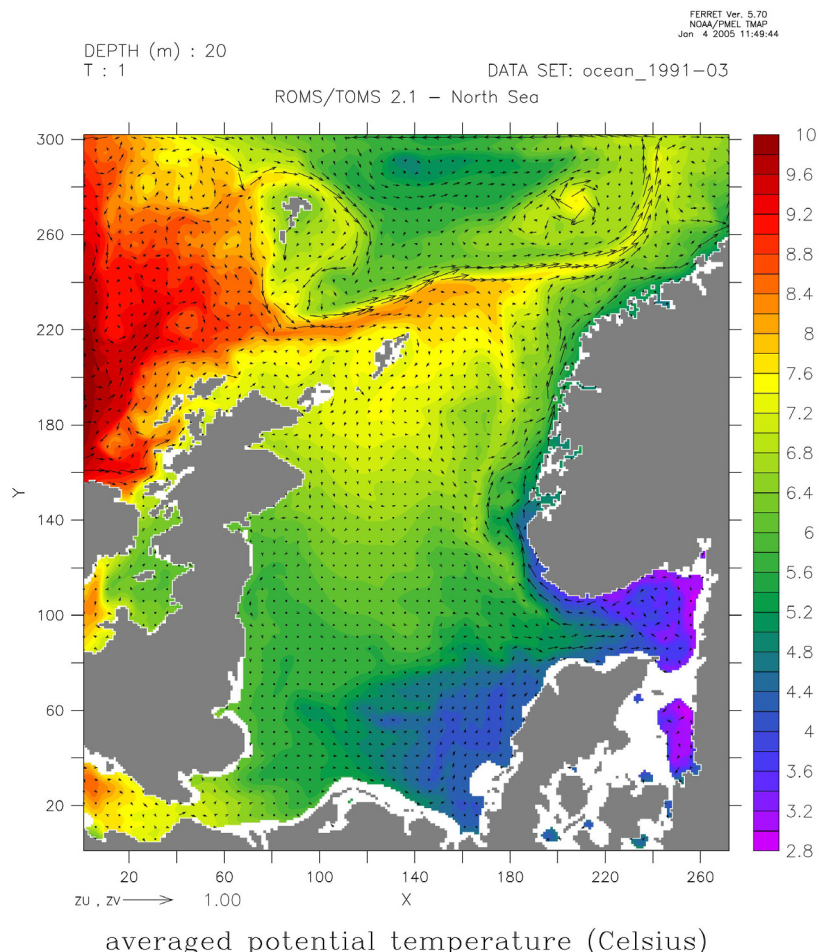


**Figure 2.** Modelled temperature and currents at 20 m, averaged over March 1990

## 4. Results

Figure 2 shows the near-surface picture of the temperature and current, averaged over the month March 1990. The warm Atlantic Water flows northwards, at both side of the Faros. These branches merge to a frontal jet following the shelf edge northwards. The inflow of Atlantic Water to the North Sea takes place in the Norwegian Trench, north east of Shetland, and between Shetland and the Orkneys. Part of this Atlantic inflow reaches Skagerrak where it meets the more brackish water from the Baltic and Kattegat. The result is the Norwegian Coastal Current, visible as a cold current along the coast of southern Norway.

The near-surface salinity fields from both simulations at 13 August 1989 is shown in Figure 3. The fields are averaged over a three-days period. Due to this shorter averaging time, the figures show more of the mesoscale activity at the front between Atlantic and Coastal waters. The left panel is taken from the main simulation, without evaporation. This field may be too fresh locally, in particular in the central parts of the southern North Sea. The simulation with evaporation is shown in the right panel. Here the values above 35.4 in the central part of the northern North Sea are unrealistic.

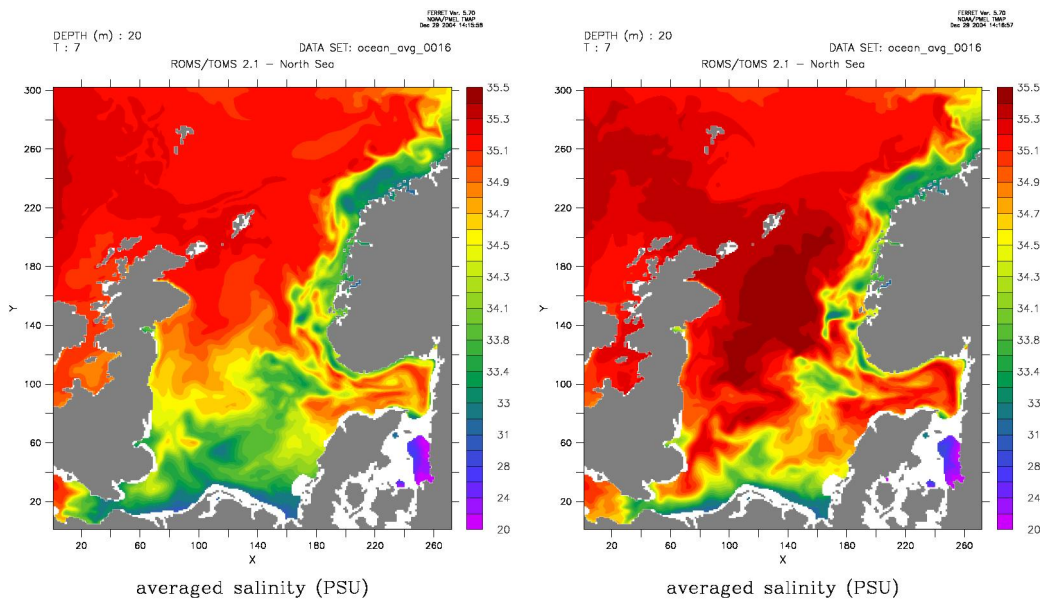


**Figure 3.** Salinity in 20 m averaged over a 3 days period centered on 13 August 1989. Left: main simulation. Right: simulation with evaporation.

For statistics the domain is limited to the North Sea. More precisely, a subdomain is limited to the west by the gridline  $x=40$  in the English Channel, and to the north by  $y=144$  between Bergen and the north-eastern tip of Scotland. Figure 4 shows the time evolution of the hydrography, averaged over this subdomain. In the main run, without evaporation, the mean

salinity drops rapidly from 34.65 to 34.25 in approximately 18 months. With an average depth of 73 m in this subdomain, this extra fresh water correspond to a layer of 0.89 m. To build up such a layer in 18 months require approximately 10000 m<sup>3</sup>/s of the fresh water runoff or equivalently 1.6 mm/day of precipitation. After the initial drop, the mean salinity fluctuates between 34.2 and 34.3. Without evaporation, the salinity increases slightly and fluctuate between 34.6 and 34.7. The mean temperature follows a seasonal cycle modulated by some interannual variability. The two runs give almost identical results for temperature.

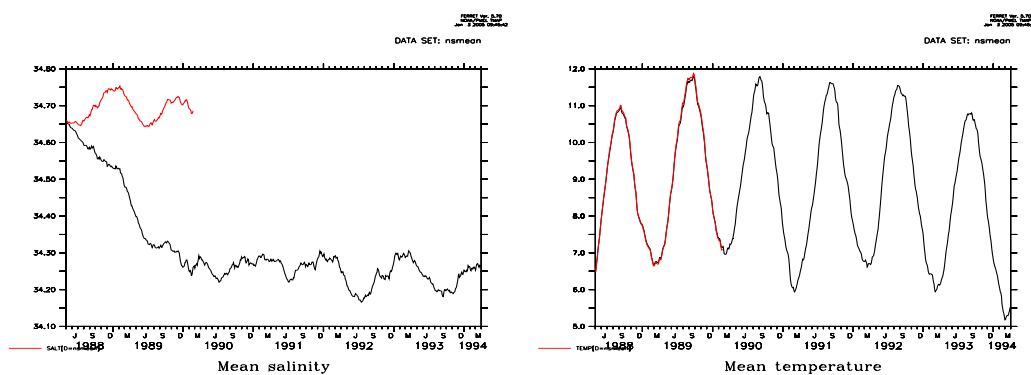


**Figure 4.** Left: Time development of the averaged salinity for the North Sea subdomain. Right: Average temperature series for the North Sea subdomain. Results from the main run is given with black colour and the evaporation run in red.

#### 4.1. Comparison with the Lista coastal station

The Institute of Marine Research (IMR) operates a set of regular coastal stations, taken approximately twice a month (Aure and Gjertsen, 2000; Norges Forskningsråd, 2004). Information and data are available on internet, <http://pegasus.nodc.no:8080/stasjoner/>. The length and regularity of these time series, make them very useful for evaluating the model generated marine climate on seasonal and interannual time scales. Here the Lista station (N 58°01' E 06°32') at the southern tip of Norway is used. In 1992 the observation method changed from water sampling to mini-CTD. Unfortunately, this change of technology had some initial problems, making the observed salinity values in 1992 and 1993 unreliable.

Figure 5 show time-depth plots of modelled and observed hydrography in the upper 100 m at Lista. The model values fit nicely in to the observed range. The seasonal cycle in the model compares well to the observations. The summer stratification is reasonable with fresh warm water down to 40-50 m as in the observations. The model does not quite reach the observed temperature maxima.

To look at the Lista station in more detail, time series at 20 and 75 m depth will be considered. For temperature, the results are presented in Figure 6. The monthly values follow the observations quite closely most of the time. In 75 meter, the model is not warm enough at the maximum in 1993 and partly in 1991 and 1992. The two different model runs give very similar results. The lower panels show the temperature series after filtering out the seasonal

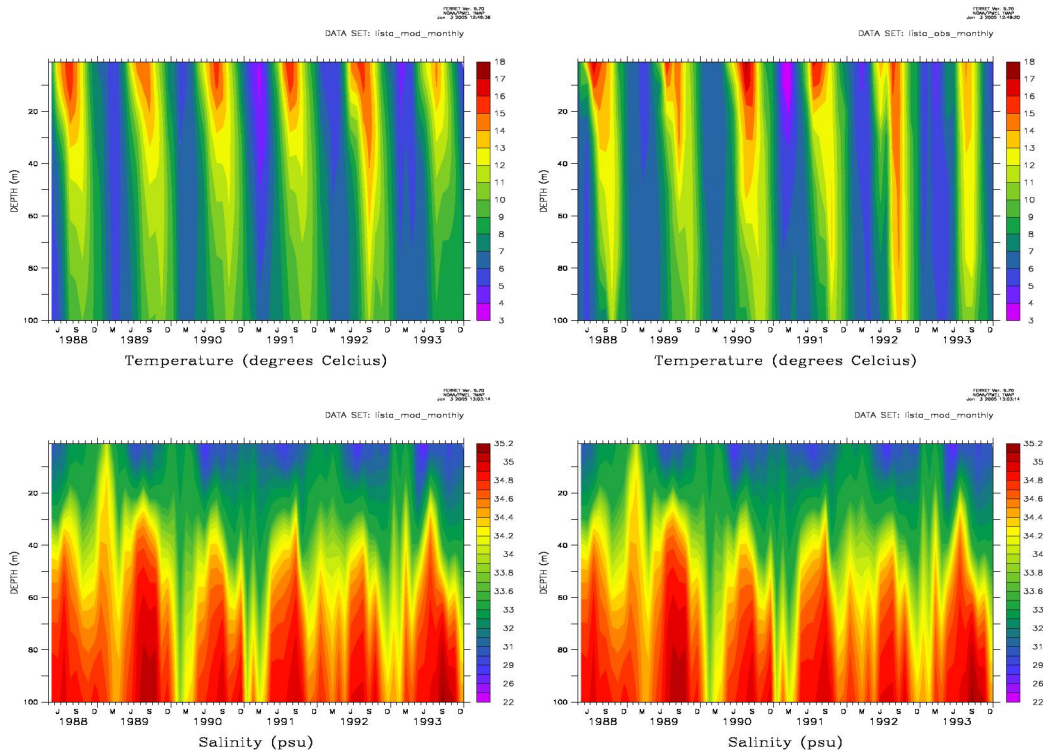


**Figure 5.** Time-depth plots of monthly averaged hydrography at the Lista station. Upper left: temperature from closest model grid point. Upper right: temperature from observations. Lower left: model salinity. Lower right: Salinity observations.

signal by a 12-month moving average. At 20 m the model temperature reflect the observed signal quite closely. At 75 m the model reproduce the warm period from 1990 to 1992, but misses the two maxima. For the evaporation run, the smoothed series become quite short, but for this period it is consistently warmer than the main run. The main run is closer to the observations for this period.

The similar salinity series are presented in Figure 7. The monthly model salinity follows more or less the upper envelope of the more fluctuating observational series. The model is not picking up the fresh events in the observations. For the deseasoned series in the lower panel,

we see that the salinity starts out too salty in the spin-up period. Thereafter there is a time window where the model agrees very well with the observed salinity levels. At the end of the series the observations can not be trusted, as mentioned above.

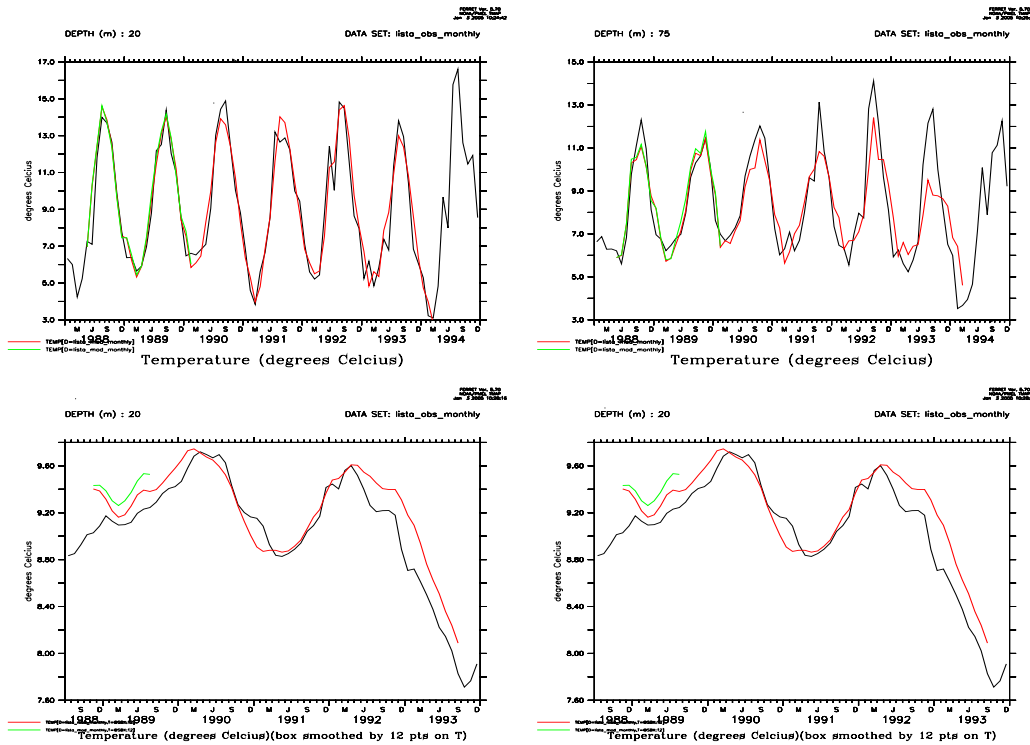


**Figure 6.** Temperature time series at Lista. Upper left: monthly averages at 20 m. Upper right: monthly values at 75 m. Lower left: temperature at 20 m smoothed with a one-year moving average. Lower right: one-year moving average of temperature at 75 m. Colour code: observations in black, main run in red and evaporation run in green.

## 5. Concluding remarks

Here two fresh water formulations have been tested. Without evaporation, the salinity decreased for a period of 18 months before settling about a lower salinity level than the climatology used in initialization. One would expect that a data based climatology have a reasonable estimate of the mean salinity. Thus the modelled mean salinity becomes too low. However, the salinity in the Coastal Current, as measured at the Lista station is well represented. A combination of too much fresh water input to the coastal current and too much mixing might account for this. Including evaporation makes the modelled mean salinity more accurate. However, locally in the Coastal Current and the northern central North Sea the salinity values become too high.

The freshwater forcing is uncertain. The run-off from the major rivers may be known. Less is known on the run-off from areas without major rivers. The NCEP precipitation over sea and the estimates of evaporation may also be uncertain. This gives some arbitrariness into the formulation of the fresh water forcing. Without any feedback from the model salinity to the forcing, balancing the fresh water is in principle impossible. Fortunately, the results indicate that the temperature field is not very sensitive to the fresh water treatment.

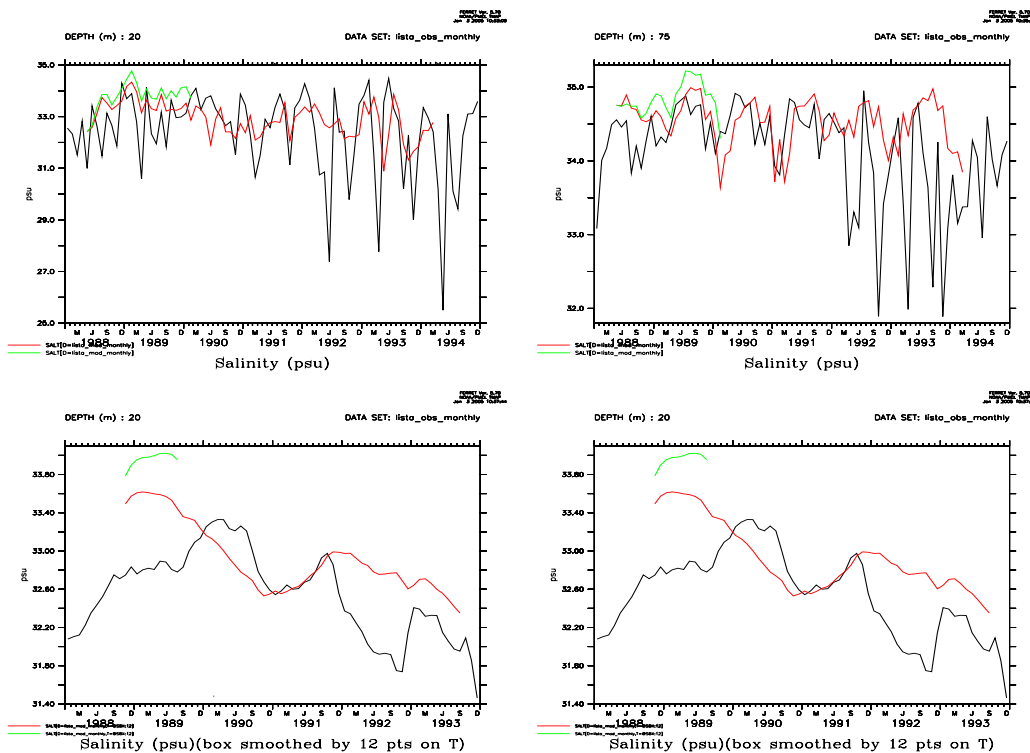


**Figure 7.** Salinity time series at Lista. Upper left: monthly averages at 20 m. Upper right: monthly values at 75 m. Lower left: one-year moving average at 20 m. Lower right: One-year moving average at 75 m. Colour code: observations in black, main run in red and evaporation run in green.

The strong fresh water forcing in the main run may be viewed as an experiment. After one and a half year this extra fresh water has been advected and mixed into the whole North Sea. Thereafter the salinity levels off because the outflowing water has become fresh enough to create a new salt balance. This experiment indicates that a spin-up time of 18 months is adequate for a shallow shelf sea like the North Sea.

The model does not pick up the fresh water events at the Lista station. These events may be due to fluctuations in the Baltic outflow which are not present in the climatological outflow

used in these simulations. The observed monthly averages might also be unrepresentative, because only one to three observations are used per month.

The model reproduces the temperature development in the Coastal Current quite well, both on seasonal and interannual scale. Since the meteorological forcing is the only non-climatological forcing in these runs, the results are consistent with the working hypothesis that regional wind forcing of the Atlantic inflow and regional heat exchange with the atmosphere are important factors for the marine climate variability in the North Sea.

The purpose of these experiments has not been to perform an optimal hindcast simulation of the North Sea. For this purpose, some improvements should be done. Based on the excess fresh water forcing in this run and the model response, the fresh water forcing should be tuned down accordingly. Interannual variability is underestimated, as large scale variability in the Atlantic is not included in the climatological forcing. This could be improved by using output from a basin scale model at the lateral boundaries. Similarly, variability in the Baltic outflow should be handled better, by using results from a Baltic model or by including the Baltic Sea in the model domain.

The overall impression is that the model is doing a good job in recreating the present climate in the North Sea with coarse forcing. The main limitation is the quality of the forcing used. The model seems to be suited for dynamic downscaling of result from global climate models.

## References

- Ådlandsvik, B. and W.P. Budgell, 2003, Adapting the Regional Ocean Model System for dynamic downscaling, RegClim General Technical Report 7, 49-57.
- Aure, J. and Gjertsen, K. 2000. Langtidsovervåkning av miljøet i norske kyst- og havområder. Report, Institute of Marine Research, Bergen, 28 pp.
- Bentsen, M. and H. Drange, 2000, Parameterizing surface fluxes in ocean models using the NCEP/NCAR reanalysis data. RegClim General Technical Report 4, 149-158.
- Engedahl, H., B. Ådlandsvik, and E.A. Martinsen, 1998. Production of monthly mean climatological archives of salinity, temperature, current and sea level for the Nordic Seas, *J. Mar. Syst.*, 14, 1-26.
- Ezer, T., H.G. Arango and A.F. Shchepetkin, 2002. Developments in terrain-following ocean models: intercomparisons of numerical aspects, *Ocean Modelling*, 4, 249-267.

- Large, W.G., J.C. McWilliams, and S.C. Doney, 1994. A review and model with a nonlocal boundary layer parameterization. *Rev. Geophys.* 32, pp. 363–403
- Marchesiello, P., J.C. McWilliams, and A.F. Shchepetkin, 2001. Open boundary conditions for long-term integration of regional ocean models, *Ocean Modelling*, 3, 1-20.
- Norges Forskningsråd 2004, Lange tidsserier for miljøovervåkning og forskning, report no. 3, Viktige marine dataserier, Oslo, 53 pp.
- Shchepetkin, A.F. and J.C. McWilliams, 1998. Quasi-monotone advection schemes based on explicit locally adaptive dissipation, *Monthly Weather Rev.*, 126, 1541-1580
- Shchepetkin, A.F. and J.C. McWilliams, 2003. A Method for Computing Horizontal Pressure-Gradient Force in an Oceanic Model with a Non-Aligned Vertical Coordinate, *J. Geophys. Res.*, 108, 1-34
- Shchepetkin, A.F. and J.C. McWilliams, 2005. The regional oceanic modeling system (ROMS): a split-explicit, free-surface, topography-following-coordinate oceanic model, *Ocean Modelling*, in press
- Song, Y.T. and D.B. Haidvogel, 1994. A semi-implicit ocean circulation model using a generalized topography-following coordinate system, *J. Comput. Phys.*, 115, 228-244
- Umlauf, L. and Burchard, H., 2003. A generic length-scale equation for geophysical turbulence models. *J. Marine Res.* 61, 235–265
- Warner, J.C., C.R. Sherwood, H.G. Arango, and R.P. Signell, 2005, Performance of four turbulence closure models implemented using a generic length scale method, *Ocean Modelling*, 8, 81-113



# The effect of internal variability on anthropogenic climate projections

**Asgeir Sorteberg**

Bjerknes Centre for Climate Research, University of Bergen, Norway

**Nils Gunnar Kvamstø**

Geophysical Institute, University of Bergen, Norway

## **Abstract**

An ensemble of climate change simulations is presented, with special emphasis on the spread among the different member. Using a single model ensemble, the spread in the climate change estimates may be interpreted as the effect of internal variability. As expected, the areas of significant changes increased with the strength of the CO<sub>2</sub> forcing. For temperature this change was rapid in the absence of other external forcings 90% of the global area showed a significant change in 20-year averaged annual temperature around year 30. The global fraction for precipitation at the same time was around 30% which increased to 60% around doubling of CO<sub>2</sub>. The reduction of the spread by averaging over a longer period was investigated. A increase in averaging period from 15 to 30 years reduced the annual and seasonal grid point temperature spread by around 20% in most areas. The impact on the precipitation spread was about two third of that. This might provide some information on the design (resolution versus length of time period) of regional climate simulations. Analysis on the number of ensemble members needed to sample internal variability indicate that to require the same level of certainty for a Arctic temperature change as a tropical or subtropical the number of ensemble members should be increased by a factor of 5 to 6.

## 1. Introduction

Simulation of future climate change encompasses a wide range of uncertainties. Some are related to uncertainties in future external forcings like solar variability and emission of greenhouse gases and particles, while others are related to our understanding of the climate system and uncertainties due to internal climate variability. Thus, the spread among model results may both be due to real intermodel differences (parameterisations, level of sophistication, resolution), but also due to insufficient sampling of the natural internal variability of the climate system, which will add ‘noise’ to the climate signal imposed by changes in the external forcings.

As computer capacity has increased the use of multiple realizations for more reliable estimates of the anthropogenic influence on future climate has become more common. These ensembles are either produced by a number of different models or a single model with perturbed model physics or perturbed initial conditions.

In this study we attempt to quantify the uncertainties related to insufficient sampling of internal variability using a single model with perturbed initial conditions. This uncertainty is depending on several factors. The length of the temporal averaging (averaging the results over a longer time period will smooth out natural variability), and the spatial averaging (averaging over a larger area may reduce the natural variability). Thus we expect zonal means to be less influenced by natural variability than gridpoint values. In addition the strength of the external forcing and how strongly the external forcing is acting on the chosen meteorological parameter is important (eg. a stronger CO<sub>2</sub> increase will reduce the relative influence of the natural variability on the result and natural variability may be more important for meteorological parameters that are less affected by increased CO<sub>2</sub>). As the amount of spatial or geographical averaging increases we expect the climate signal to be better defined, however this is on the expense of the geographical and temporal information content of the simulations. In this paper we do not cover the effect of spatial averaging on the signal and noise, but focus on the effect of temporal averaging and the strength of the external forcing. We believe an investigation into the changes in signal and noise behaviour might provide insight into how to best design global and regional climate change simulations and aid choices regarding the question of the number of ensemble members versus the complexity and therefore computationally cost of running the model.

The methodology and experimental setup is given in section 2. Section 3 discusses the changes in the models signal and noise with temporal averaging and strength of the external

forcing while section 4 discusses the implication of this for the number of ensemble members needed to significantly detect a climate change. Section 5 discusses the single model spread (which represents natural variability) versus the multimodel spread (which represents both natural variability and real model differences).

## 2. Methodology and experimental setup

An ensemble (consisting of 5 members) of CMIP2 (1% increase in CO<sub>2</sub> per year) simulation with the coupled Bergen Climate Model (BCM) (Furevik et al., 2004) has been performed. The Bergen BCM consists of the atmospheric model ARPEGE/IFS together with a global version of the ocean model MICOM (including a dynamic-thermodynamic sea-ice model). The coupling between the two models is done with the software package OASIS. The atmosphere model has a linear T<sub>L</sub>63 (2.8°) resolution with 31 vertical levels. MICOM has an approximately 2.4° resolution with 24 isopycnal vertical levels. Key quantities regarding climatic means and variability of the control integration have been evaluated against available observations in Furevik et al. (2004).

Evaluation of the variability and the stability of AMOC and other oceanic variability in the BCM and in the ocean only model run with daily forcing from NCEP/NCAR reanalysis (Kalnay et.al., 1996) has been investigated in a series of papers (Bentsen et al., 2002; Gao et al., 2003; Nilsen et al., 2003; Dutay et al., 2002). In general the model's Atlantic Meridional Overturning Circulation (AMOC) strength and variability is realistic with the AMOC being among the less sensitive to both a CO<sub>2</sub> increase (10-15% AMOC reduction at doubling of CO<sub>2</sub>) and to freshwater perturbations (Otterå et al., 2003; 2004a; 2004b).

The initial conditions for the CMIP2 members have been taken from 300-year control integration; see figure 1. The true state of the AMOC, which is a good measure of the poleward oceanic heat transport, is not exactly known and each experiment has been initialized in different phases of the AMOC to span the natural variability (maximum difference in AMOC initial state between the different members was around 3 Sverdrups) of the AMOC. The simulations are integrated for 80 years until doubling of CO<sub>2</sub> is reached. By systematically choose different initial states of the ocean heat transport we ensure that the spread among the different members are not underestimated as might be the case if only the atmospheric state is perturbed. Results indicate that the AMOC has a ‘memory’ of one to two decades (Collins et al., 2005), thus the initial state of the AMOC is assumed to directly influence the simulation during the first few decades. However, the initial state may have

indirect effects on the simulations for a longer time since it might affect the initiation or enhance/reduce the strength of other feedbacks in the system.

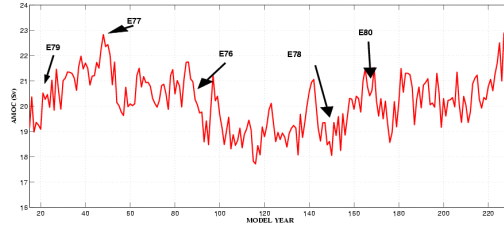


**Figure 1:** The AMOC of the control simulation and the start of the five CMIP2 members.

### 3. Analysis methods

In a linear framework the temperature of the control and climate change simulation at a certain time may be written as a function of the unperturbed mean control integration ( $\overline{T_{cntrl}}$ ), plus a deterministic anthropogenic signal ( $T_f$ ) and internal variability under the control ( $T'_{cntrl}$ ) and climate change scenario ( $T'_{cmip2}$ ), respectively

$$T_{cntrl} = \overline{T_{cntrl}} + T'_{cntrl} \quad (1)$$

$$T_{cmip2} = \overline{T_{cntrl}} + T_f + T'_{cmip2} \quad (2)$$

Thus, difference in temperature between the control and climate change simulation at a certain time can be represented as:

$$\Delta T = (T_{cmip2} - T_{cntrl}) = T_f + (T'_{cmip2} - T'_{cntrl}) \quad (3)$$

For an ensemble of simulations  $T_f$  is the deterministic (anthropogenic) signal which we want to detect and give a certain confidence, while  $(T'_{cmip2} - T'_{cntrl})$  represent the random (internal variability) component of the simulated climate change for a certain time period.

The ensemble mean temperature change ( $\{\Delta T\}$ ) may then be written as:

$$\{\Delta T\} = T_f + \{(T'_{cmip2} - T'_{cntrl})\} \quad (4)$$

where  $\{ \}$  indicates averaging over the ensemble members. We assume that the  $\{\Delta T\}$  estimate from the  $n$  number of ensemble members is an unbiased estimate of the models ‘true’  $\{\Delta T\}$ , that the ensemble members are independent and that there is no covariability between the forced component and the temperature change variability. Thus, an unbiased estimate of the variance of the ensemble means change ( $\sigma_{\Delta T}^2$ ) is:

$$\sigma_{\Delta T}^2 = \frac{\sum_{i=1}^n (\Delta T - \{\Delta T\})^2}{n-1} = \frac{\sum_{i=1}^n [(T'_{cmip2} - T'_{cntrl}) - (\bar{T}'_{cmip2} - \bar{T}'_{cntrl})]^2}{n-1} \quad (5)$$

which has a uncertainty that can be estimated using the chi-square relationship between the estimated variance of the ensemble mean change ( $\sigma_{\Delta T}^2$ ) and the true variance ( $\sigma_{\Delta T, TRUE}^2$ ):

$$\frac{(n-1)\sigma_{\Delta T}^2}{\chi_{\alpha/2}^2} < \sigma_{\Delta T, TRUE}^2 < \frac{(n-1)\sigma_{\Delta T}^2}{\chi_{(1-\alpha/2)}^2} \quad (6)$$

where  $\chi_{\alpha/2}^2$  and  $\chi_{(1-\alpha/2)}^2$  are properties of the chi-square distribution.

As the variance ( $\sigma_{\Delta T}^2$ ) only depend on the internal variability of the control and climate change simulation, this is a measure of the climatic *noise*. From the above expression it is clear that the natural variability *noise* is a function of the spatial and temporal averaging of both the control and climate change simulations. In this paper the climate change ( $\Delta T$ ) is calculated as the difference between the temperature in the climate change simulation for a given time period and the mean temperature of the control integration over the 80 years of the climate change simulation. Thus,  $T'_{cntrl} < T'_{cmip}$  and the variance of the ensemble mean change ( $\sigma_{\Delta T}^2$ ) should be interpreted mainly as variance related to natural variability within the climate change simulations.

The signal-to-noise ratio is given as the absolute value of the ratio of the ensemble mean change over the standard deviation of the ensemble mean change:

$$\frac{S}{N} = abs\left(\frac{\{\Delta T\}}{\sigma_{\Delta T}}\right) \quad (7)$$

Assuming that the temperature changes of the ensemble members are normal distributed, we may calculate the  $100(1-\alpha)$  % confidence interval for the *true* ensemble mean change given a infinite number of ensemble members ( $\{\Delta T\}_{TRUE}$ ) using the Student's t-test:

$$\{\Delta T\} - t_{\alpha/2} \frac{\sigma_{\Delta T}}{\sqrt{n}} < \{\Delta T\}_{TRUE} < \{\Delta T\} + t_{\alpha/2} \frac{\sigma_{\Delta T}}{\sqrt{n}} \quad (8)$$

where  $t_{\alpha/2}$  is a property of the t-distribution.

Rearranging the above equation gives an estimate of the number of ensemble members required to calculate the climate change within a certain threshold ( $\pm E$ ):

$$n = \left( \frac{t_{\alpha/2} \sigma_{\Delta T}}{E} \right)^2 \quad (9)$$

#### 4. The BCM ensembles mean response and signal-to-noise ratio

It seems fair to assume that the relative effect of natural variability on the climate change results will decline with the strength of the external forcing and to the extent the changes in external forcing influence the weather parameter we are interested in. Thus, in our 1% CO<sub>2</sub> increase per year simulations, we expect the signal-to-noise ratio to increase with time during the integrations and be higher for weather parameters which is more strongly influenced by the changes in external forcing. Figure 2 shows the ensemble mean BCM annual temperature and precipitation change (equation 4), the standard deviation among the different members (equation 5) and the signal-to-noise ratio (equation 7) based on averages over year 60-80 when the external forcing it is relatively strong (a doubling of CO<sub>2</sub>). As with many other coupled models the BCM has a temperature change signature showing an Arctic climate change amplification (Figure 2a) and a particularly pronounced amplification over the Arctic ocean due to reduction of the sea ice. This is also the area showing the largest spread among the ensemble members (Figure 2c). Hence, in contrast to popular belief, even though the Arctic may have a large sensitivity to anthropogenic greenhouse gas changes its large internal variability does make it hard to attribute any climate variability to a particular external cause.

The BCM simulations indicate part of the tropics as having the largest signal-to-noise ratio for temperature and therefore (given a case with a globally equal distribution of observations) the place where one easiest could attribute a climate change to human influence (Figure 2e). The picture is different for precipitation where the strongest changes are in the tropical areas, with a fairly pronounced intensification of the wintertime Hadley cell circulation (Figure 2f). In the tropics the spread among the different members (Figure 2d) follows the amplitude of the mean change. Surprisingly, the Arctic is the area of the largest signal-to-noise ratio for precipitation (Figure 2f). However, the signal-to-noise ratio is generally smaller than for temperature worldwide.

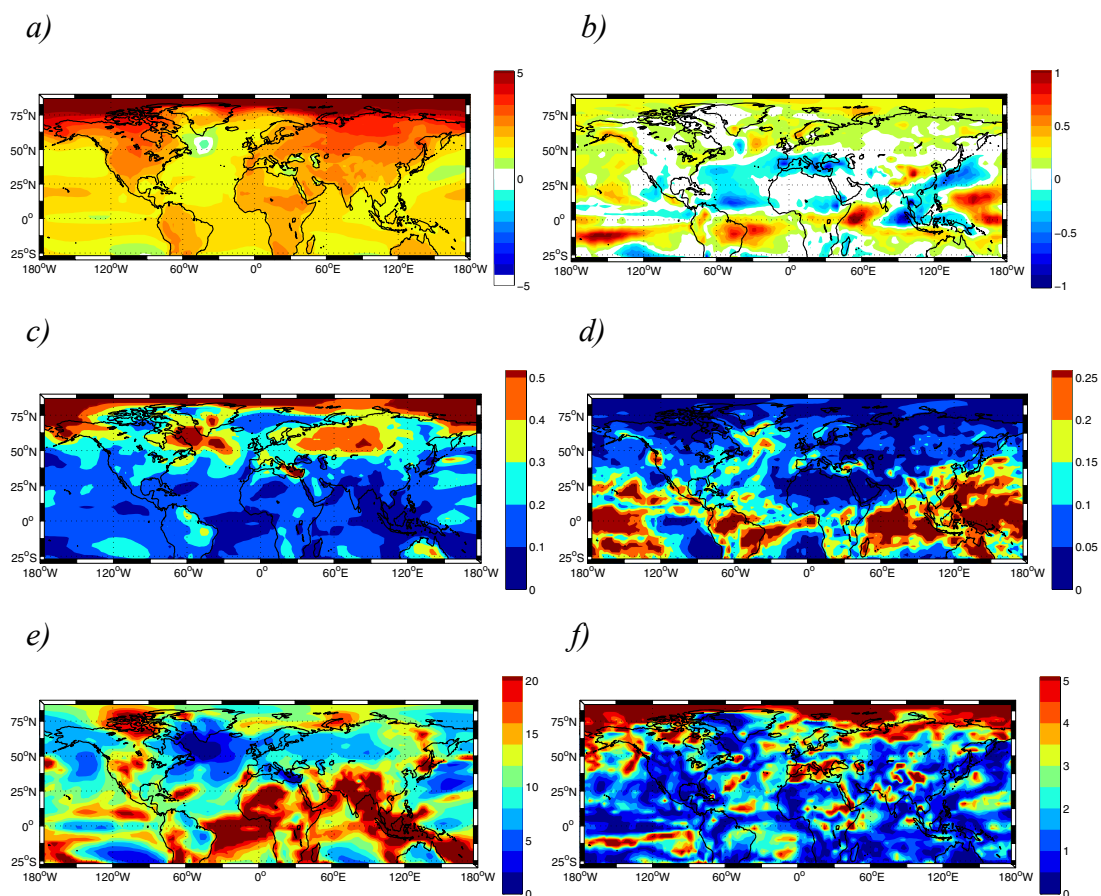
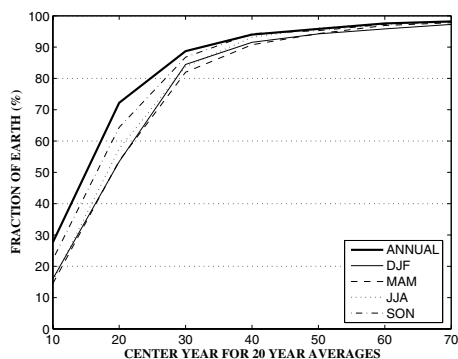


**Figure 2:** Ensemble mean change (a,b), standard deviation between the ensemble members of the change(c,d) and the signal-to-noise ratio (e,f) for 20-year averages of annual temperature (a,c,e) and precipitation (b,d,f) during doubling of CO<sub>2</sub> (year 61-80).

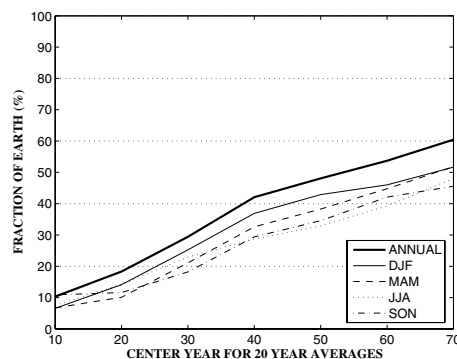
## 5. The changes in signal-to-noise ratio as a function of averaging time and external forcing

Figure 3 shows the increase in fraction of the earth's area where a 20-year ensemble mean temperature and precipitation change are significantly different from zero (using equation 8) at the 95% level. While it is possible to detect a significant change in the 20 year averaged annual mean temperature in over 70% of the earth's area around year 20 (mean over year 10 to 30) the area of significant precipitation changes is less than 20% and increasing rather slowly with the strength of the external forcing to 60% around doubling of CO<sub>2</sub>. Not surprisingly the fraction of the earth experiencing significantly seasonal changes is lower than for the annual changes. During weak forcing, the temperature change signal seems most robust during autumn and winter for precipitation. The much lower fraction with significant precipitation changes compared to temperature is reflecting both the strong internal variability of precipitation and the weaker influence of increased CO<sub>2</sub> levels on precipitation. The actual geographical areas where the results show statistical significant changes around doubling of CO<sub>2</sub> is given by the areas having a signal-to-noise ratio above 2 in Figure 2e,f.

a.)



b.)



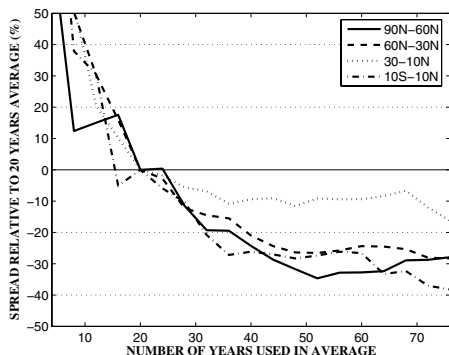
**Figure 3:** Fraction of global area which have a 95% significant change in the 20-year averaged ensemble mean of temperature (a) and precipitation (b) as a function of simulation time (ie. The strength of the external forcing).

As computer power still is a limiting factor when climate simulations are performed, there is a trade-off between the complexity and resolution of the model and the simulation length. Most regional downscaling simulations are performed over time slices of 15-30 years (IPCC, 2001),

an important quantity is therefore how much the noise due to internal variability can be reduced when the length of the simulation is increased and the result can be averaged over a longer time period. Figure 4 shows the gain in increasing the averaging period relative to using a 20-year period. The changes were calculated by comparing the mean grid point spread among the different ensemble members (given by the ensemble standard deviation (equation 5) in selected zonal bands when different number of years is used in the averaging. All averages are centered on year 40 (e.g. If number of years used in averages is 10 the mean is the average from year 35 to 45. If the number of years are 20 it's the average from year 30 to 50 etc.).

For annual temperatures the spread for the 30-year average is reduced with around 20% in the Arctic, mid-latitude and tropical area and 10% for the subtropical area compared to the 20 year average, while for averaging times beyond 40-50 years the spread remains fairly constant (Figure 4a). The gain in reducing the precipitation spread when increasing the number of years used in the averaging is less. A reduction of 20% is not reached before the number of years is increased from 20 to over 40 (Figure 4b).

a.)



b.)

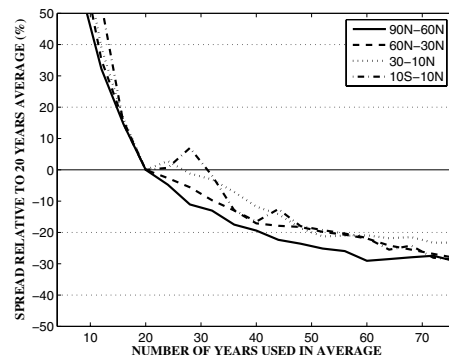


**Figure 4:** The mean grid point spread (spread given by the ensemble standard deviation) in annual temperature (a) and precipitation (b) changes among the different ensemble members relative to using a 20 years average (%) as a function of the number of years used in the average. All calculations centered on year 40.

## 6. The number of ensemble members needed to sufficiently sample natural variability

The fact that different areas exhibit different strength of the internal variability implies that in order to gain the same uncertainty range, the number of ensemble members needed to average out the internal variability will be different in different regions. An approximate number of ensemble members needed to estimate the ensemble mean change at a certain confidence level is given by equation 9. This number is a function of the chosen level of accuracy we allow and the models variance of the ensemble mean which will vary for different models and the amount of temporal and spatial averaging used before the variance is calculated. As seen in Figure 3 the areas where we can detect significant changes are small when the number of ensemble members is small and the external forcing is weak. To estimate the approximate number of ensemble members we need to provide a grid point change result within a certain threshold  $\pm E$  we have used equation 9 and calculated the median number of ensemble members needed to calculate the annual mean temperature and precipitation change in grid square within  $\pm 0.2\text{K}$  and  $\pm 0.1\text{mm/day}$ , respectively. Figure 5 shows the results for 20-year averaged annual ensemble mean changes in different zonal bands and during different strength of the CO<sub>2</sub> forcing. As  $n \propto \sigma_{AT}^2$  the geographical distribution is similar to Figure 2c,d. For temperature (Figure 5a) the two most prominent features is the larger number of ensemble members needed as we go northward and the fact that the number of members needed is quite insensitive to the strength of the CO<sub>2</sub> forcing. The first point pinpoints the larger internal variability of the mid latitudes (possibly related to variability in storm tracks) and especially in the Arctic (possibly related to ice albedo and heat transport feedbacks). Thus, given the geographical distribution of the internal variability in the BCM, to gain the same level of certainty in the Arctic as in the tropics and subtropics the number of ensemble member must be increased by a factor of 5-6. For precipitation the result are reversed. The tropical areas have a much stronger internal variability and therefore require a larger number of ensemble members.

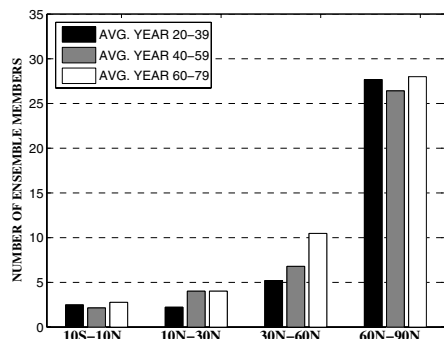
Given the fact that we have only 5 members the uncertainty in the calculation of the ensemble variance and therefore the number of ensemble members needed are large and should only be interpreted as indicative values.

Bearing in mind the uncertainties, the results indicate that the number of members needed is quite insensitive to the strength of the CO<sub>2</sub> forcing. This is consistent with our linear framework, where the variance of the ensemble mean change is only a function of the internal

variability (equation 5). In addition this indicates that the amplitude of the internal variability is not significantly changed by the increased CO<sub>2</sub> forcing. For the Arctic this last point may be somewhat surprising. Intuitively, a reduced ice and snow extent should lead to a reduced strength of the ice and snow albedo feedbacks and therefore reduced the internal variability. To test this one of the members was continued until 10 times CO<sub>2</sub> was reached. The results showed that the internal variability of the Arctic was gradually reduced. Thus, in the case of the Arctic areas, the argument that the CO<sub>2</sub> forcing does not influence the internal variability probably only holds for a moderate increase in the CO<sub>2</sub> forcing.

Note the  $E^2$  dependence in the estimation of the ensemble numbers (equation 9), thus if the thresholds  $E$  was reduced with a factor 2 the number of ensemble member needed would increase by a factor 4.

a.)



b.)

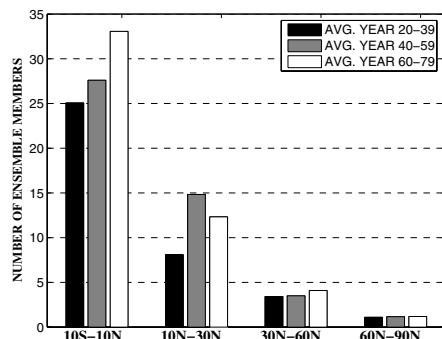
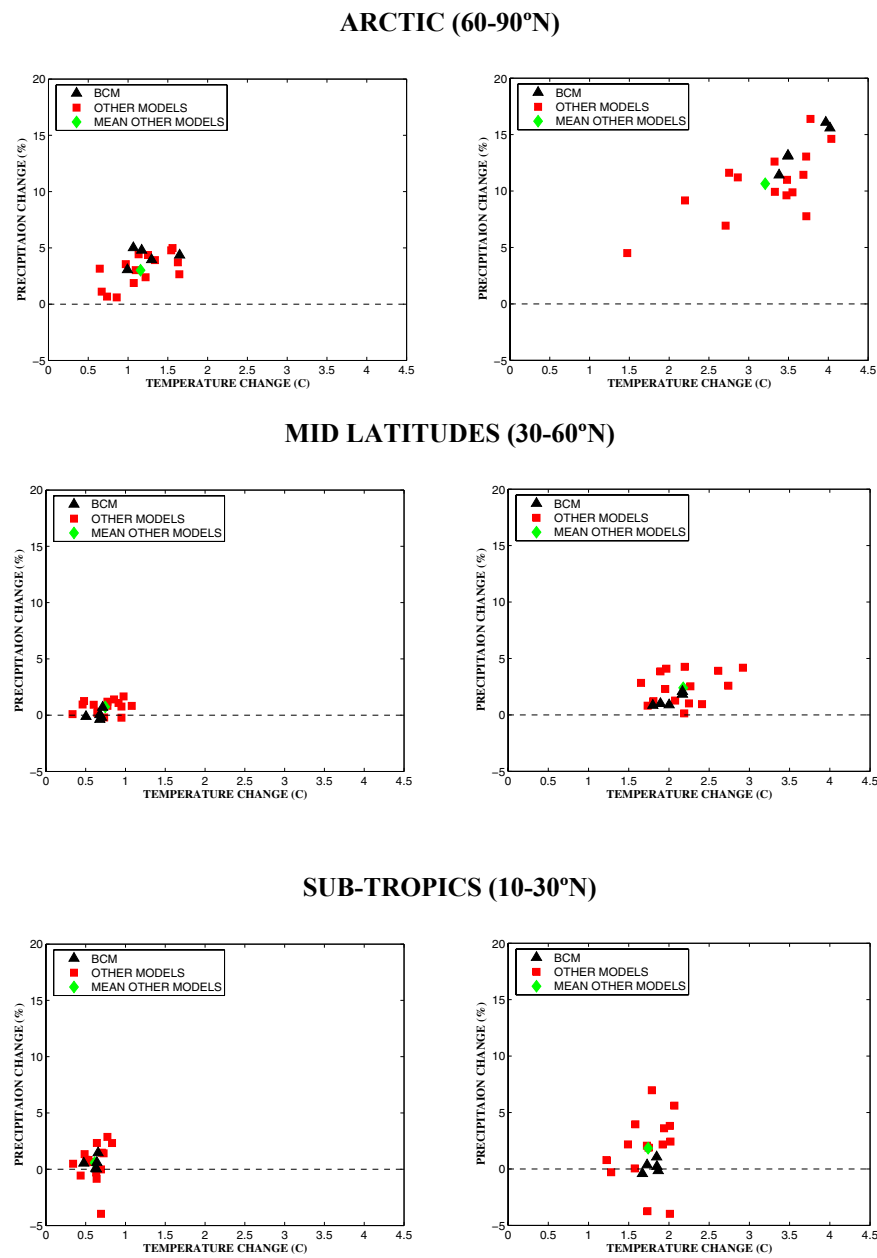


**Figure 5:** Median number of ensemble members needed to 95% confidently detect an annual mean gridpoint change in temperature(left) and precipitation (right) within  $\pm 0.2\text{K}$  and  $\pm 0.1\text{mm/day}$  in different areas. The number of ensemble members needed are calculated based on 20-year averages, for a weak (black), medium (grey) and strong (white) CO<sub>2</sub> forcing.

## 7. The single model ensemble spread versus a multimodel ensemble spread

The spread in result among different models may both be due to real intermodel differences, but also due to insufficient sampling of the internal variability of the climate system. By investigating the spread of the one model ensemble to the spread of a multimodel ensemble running the same 1% per year CO<sub>2</sub> increase scenario, we may get knowledge of how much of the multimodel spread that can be attributed to insufficient sampling of internal variability. Figure 6 provides the precipitation and temperature change for the 5 BCM members and for 15 other models averaged over year 20-39 and 60-79, weak and strong CO<sub>2</sub>

forcing, respectively. With the exception of the Arctic, the BCM simulations are generally lower than the multimodel ensemble mean when it comes to precipitation changes and fairly close to the mean for temperature.



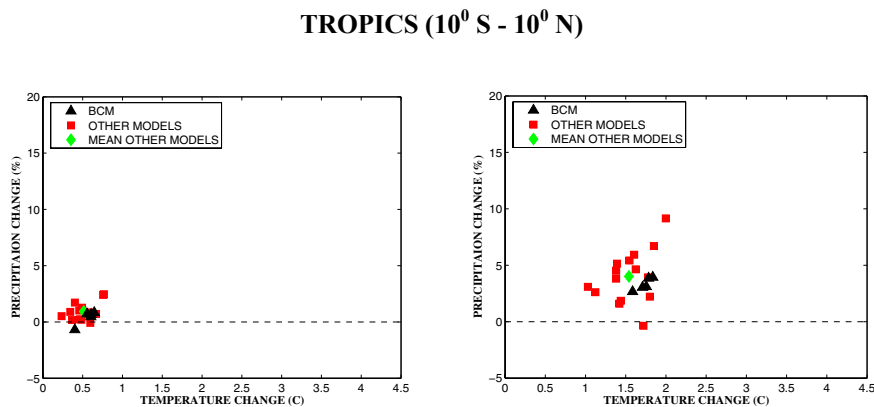


**Figure 6:** Mean area averaged temperature and precipitation changes in the different BCM members (triangle) and from 15 other coupled models (squares) during doubling of weak (20-year averages over year 20-39) and strong (20-year averages over year 60-79) CO<sub>2</sub> forcing.

Evident is also the spread among the different BCM members, which in some cases especially during the weak CO<sub>2</sub> forcing case (Figure 6a, c, e), is a substantial fraction of the multimodel spread even when the data is averaged over the respective areas. As we go down to grid point values the ratio between the BCM spread and multimodel ensemble spread is increased. The average grid point ratio between the single model and multimodel spread using 20-year averages are shown in Figure 7 (using the standard deviation of the ensemble changes as a measure of the spread). Surprisingly, the spread among the different BCM members during weak forcing is above 50% and 70% of the multimodel spread in all areas for temperature and precipitation, respectively. For temperature the largest ratio is in the Arctic, reflecting the strong internal variability in this area. The ratio is more equally distributed for precipitation. As the CO<sub>2</sub> forcing strengthens (year 60-79) the ratio drops to around 20-30% for temperature and 35-55% for precipitation. Due to the fact that this calculations are based on grid point means the fraction of the spread due to internal variability is larger than the IPCC (2001) reported values for global means. IPCC (2001), building on the indirect estimates of Raisanen (2001), reported that for annual values approximately 10% of the temperature and 30% of the precipitation spread was due to internal variability at time of doubling of CO<sub>2</sub>. Similar estimates using the BCM ensemble are 14% and 24%, for temperature and precipitation, respectively.

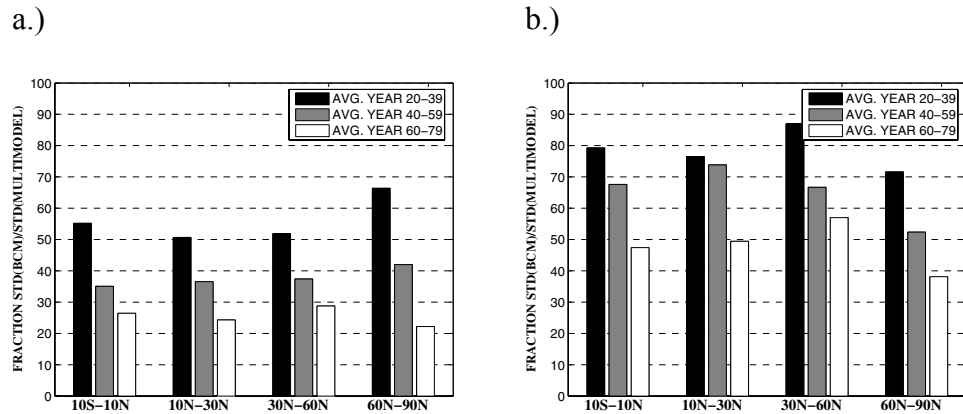


**Figure 7:** Mean difference (%) in the grid square spread of temperature (left) and precipitation (right) for the BCM ensemble spread versus the multimodel spread ( $\text{std}(\text{BCM})/\text{std}(\text{multimodel})$ ). The spread are calculated using equation 5 and based on 20-year averages for weak (black), medium (grey) and strong (white)  $\text{CO}_2$  forcing.

## 8. Discussion and conclusions

Using a single model ensemble, the spread in the climate change estimates among the different members may be interpreted as the effect of internal variability. The ensemble was run with a simplified 1%  $\text{CO}_2$  per year increase and the different members were initialized in different phases of the Atlantic Meridional Overturning Circulation to make sure that the initial state of the ocean heat transport spanned the models internal variability. Our analysis has focused on the spread on grid point scale. Due to the relative few members we have mainly focused on the mean grid point behavior in different regions.

In the framework of normal distributions the signal-to-noise ratio given by the ensemble mean change divided by the standard deviation of the changes from the different members is directly related to the area of significant changes. As expected the area of significant changes increased with the strength of the  $\text{CO}_2$  forcing. For temperature this change was rapid in the absence of other external forcings 90% of the global area showed a significant change in 20-year averaged annual temperature around year 30. The global fraction for precipitation at the same time was around 30% which increased to 60% around doubling of  $\text{CO}_2$ . By increasing the number of years used in the averaging the grid point spread reduced in all areas studied. This was especially the case for temperature, where a increase in averaging period from 15 to 30 years reduced the annual and seasonal grid point spread by around 20% in most areas. The impact on the precipitation spread was about two third of that. This might provide some information on the design (resolution versus length of time period) of regional climate

simulations. Analysis on the number of ensemble members needed to sample internal variability indicate that to require the same level of certainty for a Arctic temperature change as a tropical or subtropical the number of ensemble members should be increased by a factor of 5 to 6 and vice versa for precipitation.

## References

- Bentsen, M., H. Drange, T. Furevik and T. Zhou (2004), Variability of the Atlantic thermohaline circulation in an isopycnic coordinate OGCM, *Clim. Dynam. In Press*
- Collins M., Botzet, A. Carril, H. Drange, A. Jouzeau, M. Latif, O.H. Otteraa, H. Pohlmann, A. Sorteberg, R. Sutton, L. Terray (2005), Interannual to Decadal Climate Predictability: A Multi-Perfect-Model-Ensemble. *J. of Climate, submitted*.
- Dutay, J.-C., J.L. Bullister, S.C. Doney, J.C. Orr, R. Najjar, K. Caldeira, J.-M. Champin, H. Drange, M. Follows, Y. Gao, N. Gruber, M.W. Hecht, A. Ishida, F. Joos, K. Lindsay, G. Madec, E. Maier-Reimer, J.C. Marshall, R.J. Matear, P. Monfray, G.-K. Plattner, J. Sarmiento, R. Schlitzer, R. Slater, I.J. Totterdell, M.-F. Weirig, Y. Yamanaka, and A. Yool (2002), Evaluation of ocean model ventilation with CFC-11: comparison of 13 global ocean models. *Ocean Modelling, 4, 89-120*
- Furevik T., Bentsen, M., Drange, H., Kindem, I.K.T., Kvamstø, N.G., and Sorteberg, A. (2003): Description and Validation of the Bergen Climate Model: ARPEGE coupled with MICOM, *Climate Dynamics, No. 21, pp. 27-51, 2003*
- Gao, Y., H. Drange and M. Bentsen (2003), Effects of diapycnal and isopycnal mixing on the ventilation of CFCs in the North Atlantic in an isopycnic coordinate OGCM, *Tellus, 55B, 837-854*.
- IPCC, (2001): Climate Change 2001. The scientific basis. Eds. J. T. Houghton, Y. Ding, M. Nogua, D. Griggs, P. Vander Linden, K. Maskell, Cambridge Univ. Press., Cambridge, U.K.
- Kalnay, E., M. Kanamitsu, R. Kistler, W. Collins, D. Deaven, L. Gandin, M. Iredell, S. Saha, G. White, J. Woolen, Y. Zhu, M. Chelliah, W. Ebisuzaki, W. Higgins, J. Janowiak, K. C. Mo, C. Ropelewski, J. Wang, A. Leetma, R. Reynolds, R. Jenne, and D. Joseph, 1996: The NCEP/NCAR 40-year reanalysis project. *Bulletine of Amer. Meteorol. Soc., 77, 437-471*.
- Nilsen, J. E. Ø., Y. Gao, H. Drange, T. Furevik and M. Bentsen (2003): Simulated North Atlantic-Nordic Seas water mass exchanges in an isopycnic coordinate OGCM, *Geophys. Res. Lett., 30, 1536*
- Otterå, O. H., H. Drange, M. Bentsen, N. G. Kvamstø and D. Jiang (2003): The sensitivity of the present day Atlantic meriodinal overturning circulation to anomalous freshwater input, *Geophysical Research Letters, Vol. 30, No. 17, pp. 3-1-3-4*.
- Otterå, O. H. and H. Drange (2004a): A possible coupling between the Arctic fresh water, the Arctic sea ice cover and the North Atlantic Drift. A case study. *Advances in Atmospheric Sciences, Vol. 21, No. 5, pp. 784-801*.
- Otterå, O. H. H. Drange, M. Bentsen, N. G. Kvamstø and D. Jiang (2004b): Transient response of enhanced freshwater to the Nordic Seas-Arctic Ocean in the Bergen Climate Model, *Tellus, Vol. 56, pp. 342-361*
- Raisanen J. (2001). Co<sub>2</sub>-induced climate change in CMIP2 experiments. Quantification of agreement and role of internal variability. *J. of Climate, 14, 2088-2104*.



# **Calculated feedback effects of climate change caused by anthropogenic aerosols**

by

**Trond Iversen, Jón Egill Kristjánsson, Alf Kirkevåg, and Øyvind Seland**

Department of Geosciences, University of Oslo, Norway.

## **Abstract**

Two twin experiments with CCM-Oslo coupled to a slab ocean have been performed to estimate the feedback effects of climate change due to the indirect effect of sulphate and black carbon aerosols. Each twin consists of one simulation with emissions of natural aerosols and precursors, and one with both natural and anthropogenic emissions (for year 2000). The first twin uses prescribed aerosol concentrations, enabling dynamic response of the indirect effect (geophysical feedback). The second twin calculates aerosol concentrations on-line with other variables, enabling two-way interactions between the aerosol processes and dynamics (chemical feedback). The chemical feedback is calculated as the difference between the indirect effects in twin 2 and twin 1. We use data from the last 20 of a total of 30 years, after the model has reached a quasi equilibrium.

In both experiments we find a widespread cooling, especially in the northern hemisphere, and a southward displacement of the inter-tropical convergence zone, similar to e.g. Rotstayn and Lohmann (2002). These effects are reduced by the chemical feedback, despite a 17% increase in sulphate burdens globally. These somewhat surprising results may be explained as a combination of several effects. Most of the increase in sulphate is produced in cloud droplets, and thus contributes very little to new CCN. Furthermore, enhanced levels of sulphate from gas phase production mainly occur in regions where clouds are not particularly sensitive to CCN amounts. Finally, clouds in the upper tropical troposphere, which enhance the greenhouse effect through their trapping of heat from below, become more abundant with chemical feedback included.

## 1. Introduction

Depending on their chemical composition, sizes and shapes, aerosol particles may scatter or absorb solar radiation and act as nuclei for condensation of water vapour and for freezing of water droplets. Availability of cloud condensation (CCN) and ice nuclei (IN) is responsible for the realized water vapour super-saturations in the troposphere.

Human activity inadvertently produces aerosol particles. Production mechanisms include combustion of fossil fuels and biomass, leading to submicron particles containing sulphate, nitrate, black carbon and particulate organic matter. These compounds typically reside up to a week in the troposphere and the mixing ratios have considerable gradients. Depending on their composition as a function of size and shape, particles may scatter or absorb solar radiation and act as CCN. Anthropogenic changes in these properties may directly produce radiative forcing, or indirectly through changes in cloud properties. Considerable attention has been paid to the potential climate influence of anthropogenic particles (e.g. Charlson *et al.*, 1987; Wigley, 1989; Charlson *et al.* 1991; Kiehl and Briegleb, 1993). There is considerable uncertainty associated with its quantification, and in particular the indirect effect (Houghton *et al.*, 2001).

First principle calculations of aerosol-climate interactions are computationally impossible due to the complex processes involved. The chemical and physical processes that influence aerosols need to be parameterized in climate models. Climate scenario runs with prescribed aerosol forcing without feedback have proven successful for historical climate periods (Mitchell *et al.*, 1995; Delworth and Knutson, 2000), and simplified aerosol forcing has been included in future climate projections (e.g. Roeckner *et al.*, 1999). Several atmospheric GCMs calculate two-way interactions between parameterized aerosol properties and meteorological conditions (e.g. Kiehl *et al.*, 2000; Chin *et al.* 2000; Koch, 2001; Iversen *et al.*, 2001; Kirkevåg and Iversen, 2002, Kristjánsson, 2002). However, the response of the climate system also implies changes in geophysical parameters such as sea-surface temperatures (SST) and sea-ice cover. Equilibrium climate simulations with atmospheric GCMs coupled to “slab ocean” models for the upper mixed layer, provide first-order estimates of such changes. Rotstayn *et al.* (2000) used prescribed sulphate concentration (*off-line*) whilst Williams *et al.* (2001) and Rotstayn and Lohmann (2002) calculated sulphate as a part of the model (*on-line*). A southward shift of rainfall was found in the Tropics and a strong sea-ice albedo feedback in the Arctic. In a recent paper by Feichter *et al.* (2004), a qualitatively different response to

greenhouse gas and aerosol forcing was demonstrated, this being largely due to the suppression of the hydrological cycle by the cooling induced by the aerosol indirect effect.

The present paper discusses the indirect effects studied in an atmospheric GCM (CCM-Oslo) coupled to a slab ocean model. The experiments allow separate discussions of the response in atmospheric dynamics, sea-surface temperature (SST), and sea-ice (*the geophysical feedback*) on one hand, and the response in aerosol processes responsible for indirect forcing (*the chemical feed-back*) on the other.

## 2. Two twin experiments

CCM-Oslo is a well documented extension of the NCAR CCM3.2 global atmospheric model with resolution T42L18. It contains a prognostic cloud water scheme (Rasch and Kristjánsson, 1998), and calculates aerosol concentrations and interactions with radiation and clouds (Iversen and Seland, 2002, 2003; Kirkevåg and Iversen, 2002; Kristjánsson, 2002). Primary marine (sea-salt) and continental (soil dust) aerosols are prescribed. Sulphate and BC are calculated from emissions estimated for the year 2000 (Penner *et al.*, 2001). Aerosols are allocated to production mechanisms, which enables estimated size-distributions and mixing states. Tables for optical parameters and CCN concentrations are used to quantify interactions with radiation and clouds. Recently, improvements have been made to the aerosol life-cycle scheme, including the introduction of organic carbon as a prognostic variable, but this study uses the previous version of the aerosol scheme.

A series of 30 year equilibrium runs have been made with CCM-Oslo coupled to a slab ocean. Data from years 11-30 during equilibrium are used for analysis. Two twin experiments are made. *Twin 1* uses monthly aerosols prescribed from the atmospheric model alone; thus the geophysical response is calculated off-line. In the first member of the twin, the anthropogenic contribution of the aerosol emissions is removed whilst the second uses all emissions. *Twin 2* uses the same two sets of emissions, but in this case the aerosols are calculated on-line with the geophysical variables. Anthropogenic increments are obtained by taking differences between members 2 and 1 for each twin. Twin 1 only produces geophysical feedbacks whilst twin 2 produces the combined geophysical and chemical feedbacks. Greenhouse gases are kept at the level of year 2000 throughout. The anthropogenic aerosols are sulphate and black carbon (BC). Of these two components only sulphate has a potential indirect climate effect of any significance.

### 3. Geophysical feedback

Table 1 shows global budget numbers for sulphur components in the model. The numbers for Twin 1 are for the prescribed budgets introduced off-line with the geophysical fields in the model. The numbers are similar to those obtained by many other global models of this type, although the burdens and lifetimes are on the lower side. This is because the model version used here does not include direct vertical transport in deep convective clouds (Iversen and Selander, 2004). The indirect anthropogenic aerosol forcing of sulphate and black carbon has been estimated as the sum of short-wave and long-wave radiative cloud forcing taken over the first year of the off-line experiment (Twin 1). In this way a top-of-the-atmosphere radiative quasi-forcing by both indirect effects (the droplet radius effect and the cloud life-time effect) is estimated to  $-1.55 \text{ Wm}^{-2}$ . There are huge regional contrasts. The long-wave forcing adds to zero globally.

**Table 1.** Global budget parameters for the production of airborne particulate sulphate.

	SO <sub>x</sub> <sup>a</sup> source (TgS/a)	SO <sub>2</sub> dep. (%)	SO <sub>4</sub> -prod.		SO <sub>2</sub>		SO <sub>4</sub> source (TgS/a)	SO <sub>4</sub>		SO <sub>4</sub>	
			Aq. (%)	Gas. (%)	burden (TsS)	T <sup>b</sup> (days)		wetdep. (%)	burden (TgS)	T <sup>b</sup> (days)	
<b>Twin 1:</b> aerosols off-line											
Natural emissions	22.0	45.2	44.1	10.3	0.07	1.1	12.0	82	0.11	3.3	
Total emissions	90.4	40.7	44.8	13.2	0.37	1.5	54.0	85	0.51	3.4	
Anthropogenic increment	68.4	39.3	45.0	14.1	0.30	1.6	42.0	86	0.40	3.5	
<b>Twin 2:</b> aerosols on-line											
Natural emissions	22.0	45.0	43.5	11.1	0.07	1.2	12.1	82	0.12	3.5	
Total emissions	90.4	37.7	47.3	13.4	0.38	1.6	56.5	81	0.60	3.8	
Anthropogenic Increment	68.4	35.3	48.5	14.1	0.31	1.7	44.4	81	0.48	3.9	
<b>Difference Twin 2 - Twin 1</b>											
Anthropogenic Increment	0.0	-4.0	+3.5	0.0	+0.01	+0.1	+2.4	-5	+0.08	+0.4	

<sup>a</sup>SO<sub>x</sub> source are emissions of SO<sub>2</sub> and Sulphate plus SO<sub>2</sub> produced by oxidation of DMS. <sup>b</sup>T are turnover times.

Fig. 1 shows the 20-year equilibrium climate response of the indirect forcing by anthropogenic sulphate and BC. Shown are average anthropogenic changes in 2m temperature, daily precipitation, and fractional cloudiness. Surface cooling is widespread in the northern hemisphere with maximum (more than 3K) in the Arctic. At southern extra-tropical latitudes the cooling amounts to ca. 1K. In the tropics there are patches with a slight warming ( $<0.5\text{K}$ ), due to changes in cloudiness. Global cooling matches the negative forcing with a global feedback parameter (top of the atmosphere forcing per 2m temperature response) of  $1.34\text{W}/(\text{m}^2\text{K})$ . The feedback is positive at high latitudes due to increased extension of sea-ice and snow cover as the atmosphere cools.

Considerable precipitation changes are seen in the tropics, and the inter-tropical convergence zone is displaced southwards in many regions. This is in agreement with other model results and to some extent also with measured changes during the 20<sup>th</sup> century (Rotstyn and Lohmann, 2002). This response is believed to be linked to the asymmetric cooling of the two hemispheres due to more anthropogenic aerosols in the northern hemisphere. The cloud response is closely related to the precipitation, in particular in the Tropics. Although being a small impact, there is a net reduction of total cloudiness due to the indirect effect. The reduction is found in the middle subtropical troposphere; other areas experience increased cloudiness.

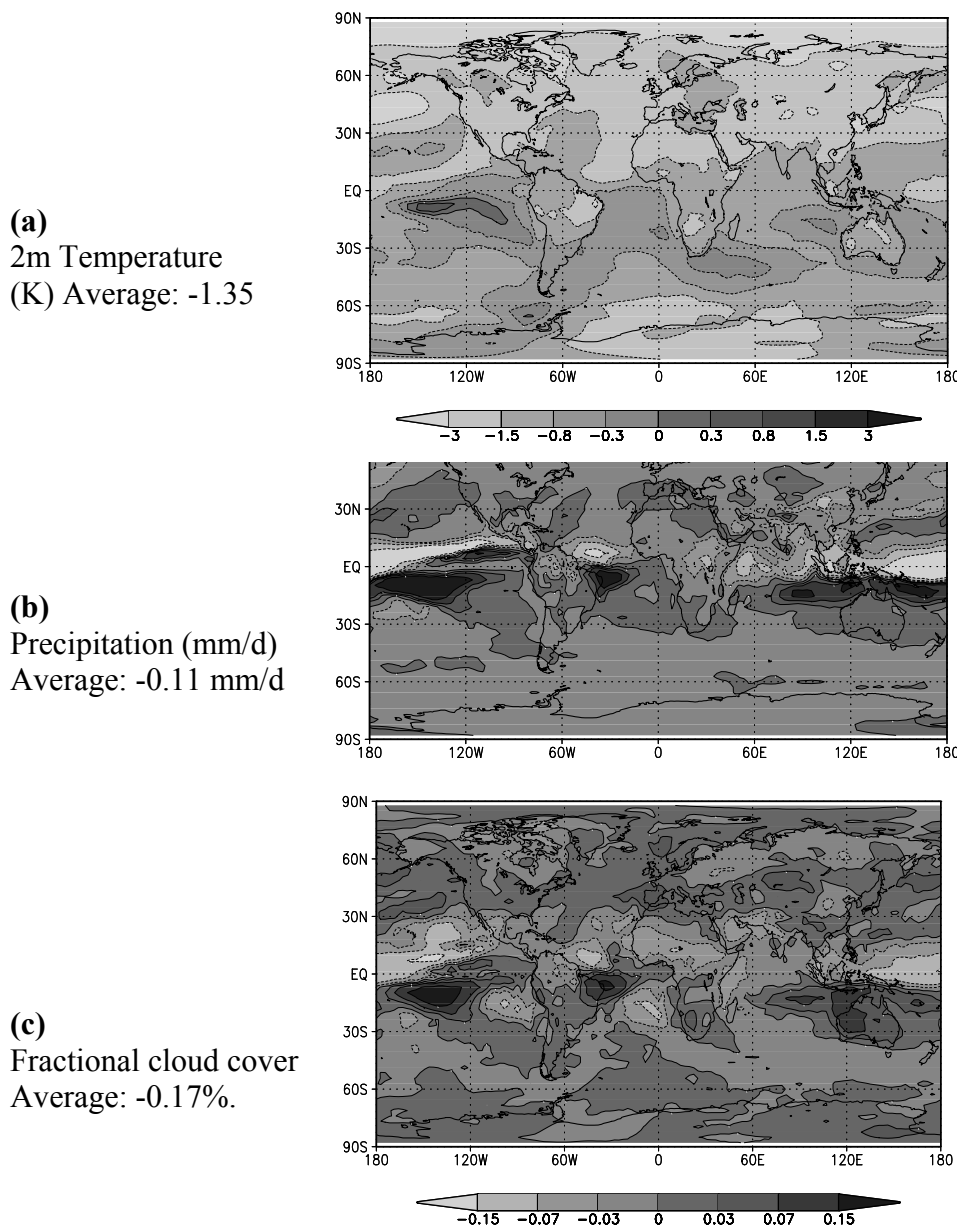


**Figure 1.** Calculated increments in selected equilibrium geophysical variables due to indirect effects of anthropogenic sulphate and black carbon.

#### 4. Chemical feedback

Differences between corresponding variables calculated in twin 2 and twin 1 are estimates of the chemical feedback of the indirect effects of aerosols. Fig. 2 shows the effect of chemical feedback on the same variables as in Fig. 1, and the patterns in Fig. 2 are to a large extent the opposite of those in Fig. 1. This means that the chemical feedback reduces the indirect climate effects in our calculations: the NH cooling is reduced and the displacement of tropical precipitation and associated clouds are partly reversed. Exceptions are the enhanced cooling in the three major emission regions of the NH and enhanced cloudiness in Europe. The indirect effect is far from cancelled, but the global feedback parameter is increased with  $0.11\text{W}/(\text{m}^2\text{K})$ , i.e. 8%. Fig. 3 shows that the chemical feedback increases the amount of sulphate almost everywhere except in some tropical regions influenced by the reversed displacement of tropical rainfall. The global burden increases with approximately 17%.

Increased sulphate and reduced indirect effect is a paradox, since sulphate is responsible for the model's indirect effect in the first place. From Table 1 it is seen that the chemical feedback causes less efficient  $\text{SO}_2$  removal and that more of it is transformed to sulphate by oxidation in cloud droplets. In addition to enhanced production, sulphate is less efficiently scavenged by precipitation. Reduced scavenging is consistent with the indirect effect causing precipitation decrease in a cooler climate. The chemical feedback also produces slightly increased cloudiness globally, but in particular over the emissions in Europe (Fig. 2c).

Why does the indirect effect decrease with increased sulphate burden? First, sulphate produced in cloud droplets will to a small extent (if any) contribute to new CCN. Second, Fig. 4 shows that increased levels of sulphate produced in gas phase due to chemical feedback are obtained in the lower troposphere between  $0^\circ$  and  $15^\circ\text{S}$ . This is close to regions of heavy convective precipitation but little cloudiness. Figs. 2c and 3 also confirm that the sulphate change is anti-correlated with cloud cover changes (except in Europe). Hence the enhanced sulphate levels, which may produce new CCN, occur in regions where clouds are not particularly sensitive to CCN amounts.

The chemical feedback causes reduced cooling since clouds in the upper tropical troposphere become more abundant (Fig. 4). This leads to an enhanced trapping of heat through reduction of outgoing longwave radiation. The 20-year averaged global long-wave cloud forcing is

$+0.21\text{W/m}^2$  whilst the short-wave is only  $-0.14\text{ W/m}^2$ . Thus the net change is positive ( $+0.07\text{ W/m}^2$ ) despite enhanced sulphate burden. The feedback on the direct effect remains to be estimated.

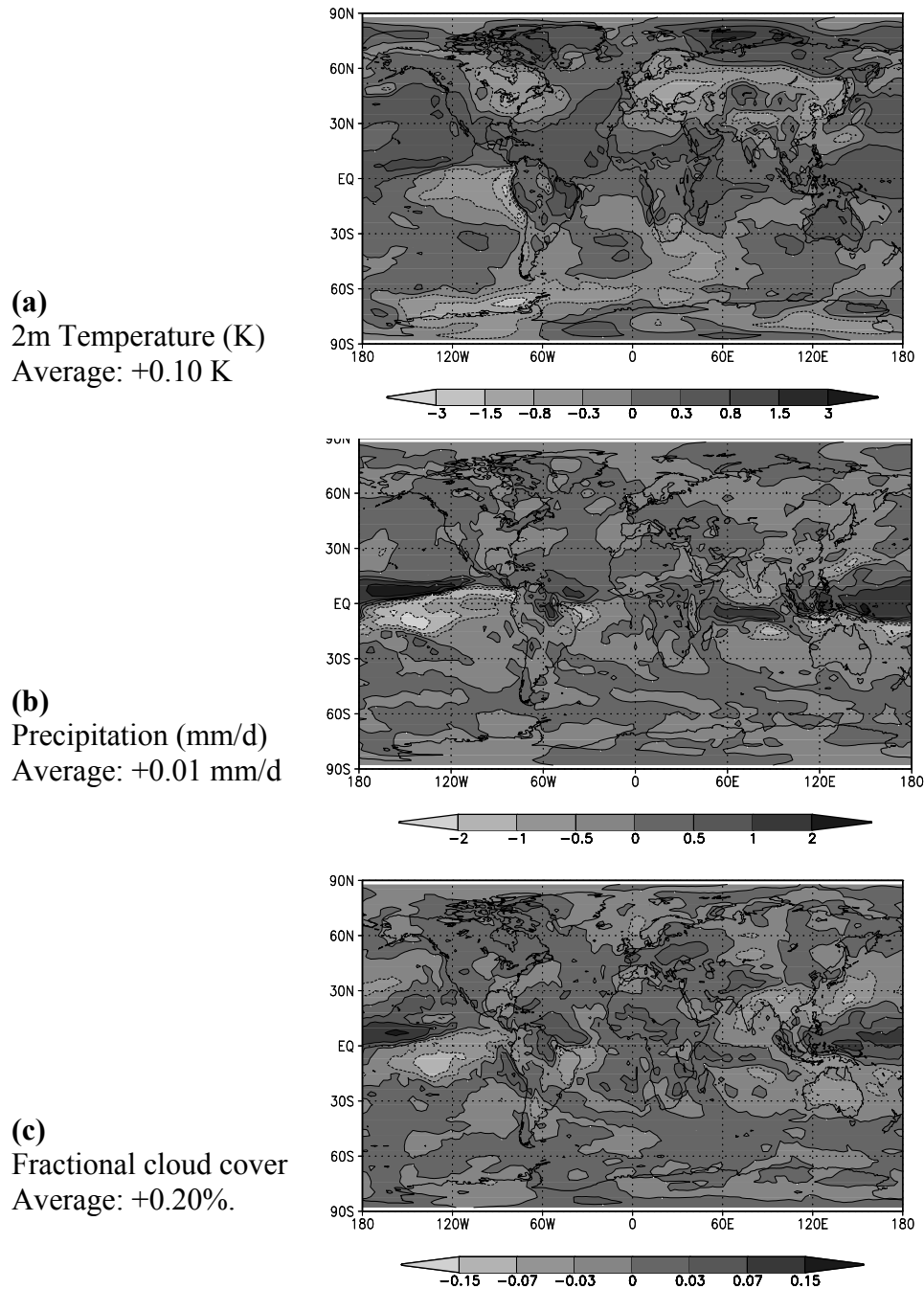


**Figure 2.** Difference between on-line and off-line calculated increments in selected equilibrium variables due to indirect effects of anthropogenic sulphate and black carbon.

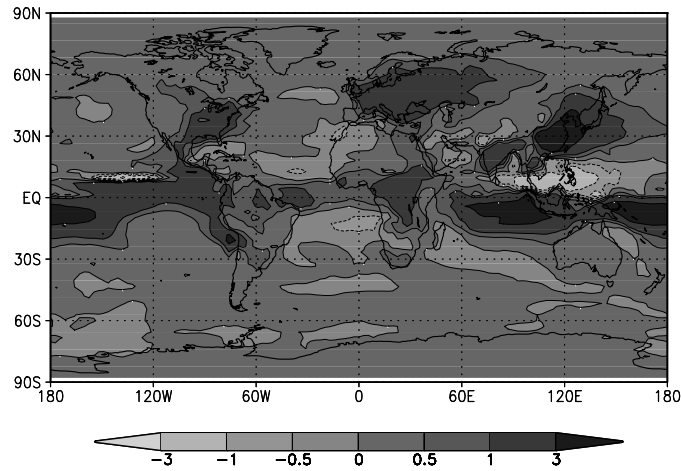


**Figure 3.** Difference between on-line and off-line calculated sulphate ( $\text{mg}/\text{m}^2$ ) at equilibrium due to indirect effects of sulphate and black carbon. Average:  $+0.50 \text{ mg}/\text{m}^2$ .

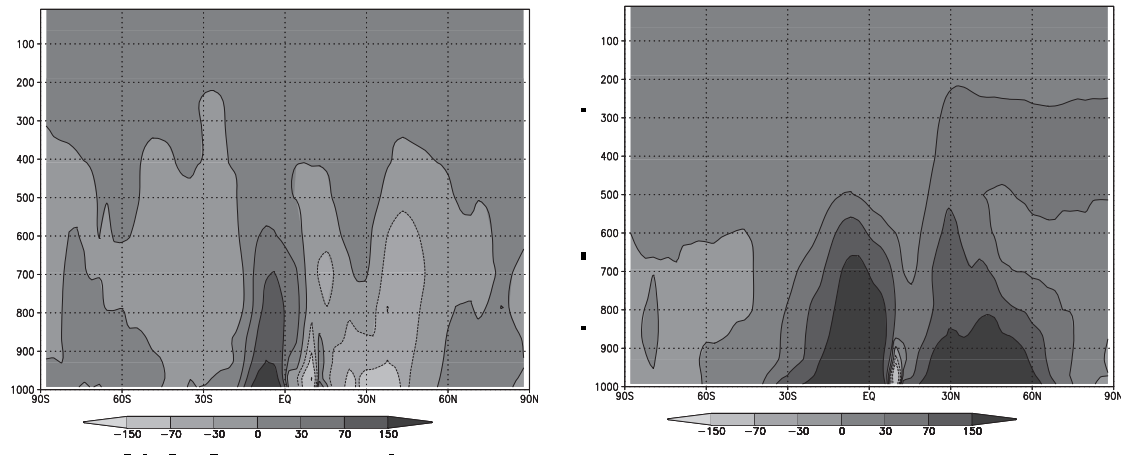
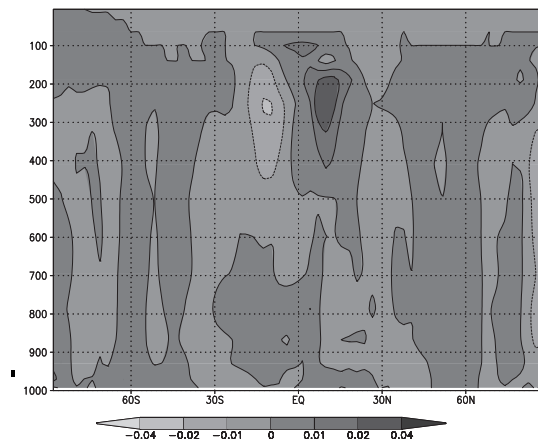


**Figure 4.** Zonal averages of differences between on-line and off-line equilibrium calculations of:

- (above left) sulphate produced in clear air ( $\text{ng}(\text{SO}_4)/\text{kg}(\text{air})$ );
- (above right) sulphate produced in cloud droplets ( $\text{ng}(\text{SO}_4)/\text{kg}(\text{air})$ );
- (below right) fractional cloudiness.



## Acknowledgements

This work is partly financed by the Research Council of Norway (RegClim and AerOzClim). Computational costs are covered by a grant from the Research Council's Programme for Supercomputing. IPCC-emissions were provided by J. Penner. Thanks are due to J. Debernard at met.no in connection with the set-up of the slab-ocean model code. We gratefully acknowledge co-operation with P. J. Rasch, and S. Ghan.

## References

- Charlson, R.J., Lovelock, J.E, Andreae, M.O., Warren, S.W., 1987: Oceanic phytoplankton, atmospheric sulphur, cloud albedo and climate. *Nature*, **326**, 655-661.
- Charlson, R.J., Langner, J., Rodhe, H., Leovy, C.B. and Warren, S.G., 1991: Perturbation of the northern hemisphere radiative balance by backscattering from anthropogenic sulphate aerosols. *Tellus*, **43AB**, 152-163.
- Chin, M., Rood, R. B., Lin, S.-J., Müller, J-F., and Thompson, A. M., 2000: Atmospheric sulfur cycle simulated in the global model GOCART: Model description and global properties. *J Geophys. Res.* **105**, 24,671-24,687.
- Delworth, T.L. and Knutson, T.R., 2000: Simulation of early 20th century global warming. *Science*, **287**, 2246-2250.
- Feichter, J., Roeckner, E., and Lohmann, U., 2004: Nonlinear aspects of the climate response to greenhouse gas and aerosol forcing. *J. Climate*, **17**, 2384-2398.
- Houghton, J.T., Ding, Y., Griggs, D.J., Noguer, M. van der Linden, P.J., Dai, X., Maskell, K., and Johnson, C.A. (eds.), 2001: *Climate Change 2001: The Scientific Basis*. Contribution of Working Group I to the Third Assessment Report of the Intergovernmental Panel of Climate Change. Cambridge University Press, 881 pp.
- Iversen, T., Kirkevåg, A., Kristjánsson, J.E. and Seland, Ø., 2001: Climate effects of sulphate and black carbon estimated in a global climate model. In: *Air Pollution Modeling and Its Application XIV, Gryning and Schiermeier (Eds.)*. 335-342. Kluwer Academic/Plenum, New York.
- Iversen, T., and Seland, Ø., 2002: A scheme for process-tagged SO<sub>4</sub> and BC aerosols in NCAR CCM3: Validation and sensitivity to cloud processes. *J. Geophys. Res.*, **107** (D24), 4751, 10.1029/2001JD000885.
- Iversen, T., and Seland, Ø., 2003: Correction to "A scheme for process-tagged SO<sub>4</sub> and BC aerosols in NCAR CCM3: Validation and sensitivity to cloud processes." *J. Geophys. Res.*, **108** (D16), 4502, 10.1029/2003JD003840.

- Iversen, T. and Seland, Ø., 2004: The role of cumulus parameterisation in global and regional sulphur transport. In: *Air Pollution Modeling and Its Application XVI, Borrego and Incecik (Eds.)*. 225-233. Kluwer Academic/Plenum, New York.
- Kiehl, J.T. and Briegleb, B.P., 1993: The relative roles of sulfate aerosols and greenhouse gases in climate forcing. *Science*, **260**, 311-314.
- Kiehl, J. T., Schneider, T. L., Rasch, P. J., Barth, M. C., and Wong, J., 2000: Radiative forcing due to sulfate aerosols from simulations with the NCAR Community Climate Model (CCM3). *J. Geophys. Res.*, **105**, 1441-1457.
- Kirkevåg, A., and Iversen, T., 2002. Global direct radiative forcing by process-parameterized aerosol optical properties. *J. Geophys. Res.*, **107**, (D20) 10.1029/2001D000886.
- Kristjánsson, J. E., 2002. Studies of the aerosol indirect effect from sulfate and black carbon aerosols. *J. Geophys. Res.* **107**, 10.1029/2001JD000887.
- Koch, D., 2001: Transport and direct radiative forcing of carbonaceous and sulphate aerosols in the GISS GCM. *J Geophys. Res.* **106**, 20,311-20,332.
- Mitchell, J.F.B., Johns T.C., Gregory, J.M. and Tett, F.B. (1995): Climate response to increasing levels of greenhouse gases and sulphate aerosols. *Nature*, 376, 501-504.
- Penner, J. E., Andreae, M., Annegarn, H., Barrie, L., Feichter, J., Hegg, D., Jayaraman, A., Leaitch, R., Murphy, D., Nganga, J., and Pitari, G., 2001. Aerosols, their direct and indirect effects. Chapter 5 (pp. 289-348) in: *Climate change 2001: The scientific basis*. Contribution of working group I to the Third Assessment Report of the Intergovernmental Panel on Climate Change. Cambridge University Press.
- Rasch, P.J., and Kristjánsson, J.E., 1998: A comparison of the CCM3 model climate using diagnosed and predicted condensate parameterisations. *J. Climate*, **11**, 1587- 1614.
- Roeckner, E., Bengtsson, L., Feichter, J., Lelieveld, J., Rodhe, H., 1999: Transient climate change simulations with a coupled atmosphere-ocean GCM including the tropospheric sulfur cycle. *J. Clim.*, **12**, 3004-3032.
- Rotstayn, L.D., Ryan, B.F., and Penner, J.E., 2000: Precipitation changes in a GCM resulting from the indirect effects of anthropogenic aerosols. *Geophys. Res. Lett.*, **27**, 3045-3048.
- Rotstayn, L. D., and Lohmann, U., 2002. Tropical rainfall trends and the indirect aerosol effect. *J. Climate*, **15**, 2103-2116.
- Williams, K. D., Jones, A., Roberts, D. L., Senior, C. A., and Woodage, M. J., 2001. The response of the climate system to the indirect effects of anthropogenic sulfate aerosol. *Climate Dyn.*, **17**, 845-856.
- Wigley, T.M.L., 1989: Possible climate change due to SO<sub>2</sub>-derived cloud condensation nuclei. *Nature*, **339**, 365-367.